THE UNIVERSITY OF CALGARY

PRECISE GPS/INS POSITIONING FOR A HIGHWAY INVENTORY SYSTEM

BY

DARIUSZ LAPUCHA

A THESIS

SUBMITTED TO THE FACULTY OF GRADUATE STUDIES

IN PARTIAL FULFILLMENT OF THE REQUIREMENTS FOR THE

DEGREE OF MASTER OF SCIENCE IN ENGINEERING

DEPARTMENT OF SURVEYING ENGINEERING

CALGARY, ALBERTA

DECEMBER, 1990

ISBN 0-315-67011-8

THE UNIVERSITY OF CALGARY

FACULTY OF GRADUATE STUDIES

The undersigned certify that they have read, and recommend to the Faculty of Graduate Studies for acceptance, a thesis entitled "Precise GPS/INS Positioning for a Highway Inventory System" submitted by Dariusz Lapucha in partial fulfillment of the requirements for the degree of Master of Science in Engineering.

K.P. Schwarz

Supervisor, Dr K.P. Schwarz
Department of Surveying Engineering

Dr G. Lachapelle
Department of Surveying Engineering

Dr E. J. Krakiwsky
Department of Surveying Engineering

Dr A. A. Jeje
Department of Chemical & Petroleum Engineering

Date: December 13, 1990

ABSTRACT

This thesis describes the successful development of a precise positioning component for the Mobile Highway Inventory System, used by Alberta Transportation for the monitoring of highways. The prototype system integrates differential GPS and a strapdown inertial system, via the software module GPIN. It has been extensively tested in the field and reached operational status in the course of this research. The program package GPIN correlates the two data streams by a decentralized Kalman filter. The analysis of results shows that the positioning accuracy of the system is in the 5-10 cm range. The slope can be obtained to 0.1% and curvature to better than 0.1 degrees per 40 m. The thesis gives background on both GPS and INS positioning, error estimation and GPS/INS data integration. The GPS/INS prototype and software package are then described and results of field tests are analyzed.

ACKNOWLEDGEMENTS

I wish to express my deep gratitude to my supervisor, Dr. Klaus-Peter Schwarz, for his continuous support and encouragement throughout the course of my graduate studies.

I would also like to thank my colleagues from the GPS/INS team for their invaluable help at different stages of the research. Mrs. E. Cannon is gratefully acknowledged for making her GPS kinematic software available and for her willingness to discuss GPS data problems. Mr. H. Martell is thanked for sharing his extensive expertise in inertial positioning and surveying. His help was indispensable in conducting the tests. Special thanks go to Dr. M. Wei for his excellent advice and his contribution to the project. Graduate students from the Department are also thanked for their participation in test measurements. Mrs. E. Cannon, Mr. H. Martell and Mr. F. Sigouin-Allan are gratefully acknowledged for proofreading the manuscript.

Financial support for this research was obtained through a contract with Alberta Transportation and the Helmut Moritz scholarship fund. Graduate Teaching Assistantships of The University of Calgary helped to support my stay in Canada.

Thanks go to my home institution in Poland, the Space Research Centre, for the support of the author's graduate study by providing travel funds and granting a leave of absence. I am also very grateful to my wife Natasza and my son Mateusz, for their sacrifice during our long separation.

TABLE OF CONTENTS

PREFACE ii

ABSTRACT iii

ACKNOWLEDGEMENTS iv

TABLE OF CONTENTS v

LIST OF TABLES viii

LIST OF FIGURES ix

LIST OF PHOTOGRAPHS xi

NOTATION xii

Chapter

1 Introduction 1

1.1 Background 1

1.2 Mobile Highway Inwentory System 6

1.3 Objective of the Research and Outline of the Thesis 9

2 GPS Positioning 11

2.1 General Description and Principle 11

2.2 GPS Observation Model 16

2.3 GPS Observation Differencing 19

2.4 Advances in GPS Kinematic Techniques 22

3 INS Positioning 28

3.1 General Description and Principle 28

3.2 Strapdown INS Mechanization 34

3.2.1 Computation Frame 36

3.2.2 Transformation of Body Sensed Angular Rates 37

3.2.3 Transformation of Body Sensed Acceleration 40

3.2.4 Navigation Output 41

3.3 Alignment 44

4 Error Analysis 46

4.1 State Space Approach 46

4.2 Kalman Filtering 49

4.3 Linearization 53

4.4 INS Error State and Dynamics Matrix 55

4.4.1 Misalignment Error Equations 56

4.4.2 Position Error Equations 56

4.4.3 Velocity Error Equations 56

4.4.4 Gyro Drifts and Accelerometer Biases Error Equations 57

4.5 GPS Error State and Dynamics Matrix 59

5 GPS/INS Integration 62

5.1 Complementary Role of GPS and INS 59

5.2 Cycle Slip Detection and Correction 65

5.3 Integration Strategies 67

5.4 Offset Correction 70

6 Implementation 72

6.1 GPS/INS Prototype 72

6.1.1 Inertial Strapdown System 73

6.1.2 GPS Receiver 75

6.1.3 Data Acquisition System 75

6.1.4 Antenna Lever Arm 77

6.2 Attitude Parameters for Slope and Curvature 78

6.3 Software Development 80

7 Field Tests And Results 87

7.1 Establishment of Test Network 87

7.2 General Description of Tests 89

7.3 1989 Tests and Results 91

7.3.1 Position Accuracy 92

7.3.2 Attitude Analysis 95

7.4 1990 Tests and Results 101

7.5 Testing of Bridging Interval and Cycle Slip Detection and Correction 105

7.5.1 Bridging Interval 105

7.5.2 Cycle Slip Detection and Correction 108

8 Conclusions and Recommendations 116

References 122

LIST OF TABLES

1.1 Current and Proposed Accuracy of the Mobile Inventory System 5

6.1 Characteristics of GPS/INS Components 76

7.1 Accuracy of Horizontal Curvature 100

7.2 Spectral Densities Chosen 108

7.3 Cycle Slip Detection and Correction- Case A 110

7.4 Cycle Slip Detection and Correction- Case B 111

7.5 Biases in Computed Coordinates 111

7.6 New Possible Ambiguities for Cases A and B 112

7.7 Combination Pattern for Five Satellites 113

LIST OF FIGURES

1.1 Current Alberta Transportation MHIS 6

2.1 Absolute GPS Positioning 13

2.2 Relative GPS Positioning 15

2.3 Single Differencing between Stations 19

2.4 Double Differencing between Stations and Satellites 21

2.5 GPS Relative Kinematic Positioning 24

3.1 Strapdown INS Mechanization Flowchart 43

4.1 Dynamics Matrix for a 15-state INS Kalman Filter 58

5.1 Integrated GPS/INS Relative Positioning 64

5.2 Cycle Slip Detection and Correction Flowchart 66

5.3 GPS/INS Filter Flowchart 69

6.1 GPS/INS Prototype Scheme 73

6.2a Radius of Vertical Curvature 79

6.2b Radius of Horizontal Curvature 79

6.3 Degree of Curve 80

6.4 GPS/INS Software Package Flowchart 81

6.5a GPIN Program Flowchart - Static Part 83

6.5b GPIN Program Flowchart - Dynamic Part 84

6.6 Time Tagging of GPS and INS Measurements 85

7.1 Sketch of Field Test Area 88

7.2 Accuracy of the Integrated System at the Static Control Coordinates for October 11 93

7.3 Accuracy of the Integrated System at the Static Control Coordinates for October 12 93

7.4 Height Computed on October 11 and Difference in Computed Heights between October 11 and 12 95

7.5 Slope Computed on October 11 and Difference in Computed Slopes between October 11 and 12..... 95

7.6 Slope vs Distance 96

7.7 Roll vs Distance..... 97

7.8 Mean Error of Roll vs Distance..... 97

7.9 Pitch vs Distance 98

7.10 Mean Error of Pitch vs Distance 98

7.11 Azimuth vs Distance 99

7.10 Mean Error of Azimuth vs Distance 99

7.13 Accuracy of the Integrated System at the Static Control Coordinates for May 3 103

7.14 Accuracy of the Integrated System at the Static Control Coordinates for May 4 103

7.15 Comparison of Height Profile for May 3..... 104

7.16 Comparison of Height Profile for May 4..... 105

7.17 Difference between INS Predicted and GPS Filtered Coordinates for a Four Seconds Interval..... 106

7.18 RMS Position Error of Free-Mode INS vs Bridging Interval 107

7.19 Results of Ambiguity Search - Case A..... 114

7.20 Results of Ambiguity Search - Case B 114

LIST OF PHOTOGRAPHS.

1.1 Installation of MHIS Instrumentation..... 8

6.1 LTN 90-100 Strapdown System 74

6.2 GPS Receiver and Compaq 386..... 74

6.3 GPS Antenna Lever Arm 77

6.4 Centering the GPS Antenna over the Point..... 78

NOTATION

1. CONVENTIONS

1.1. Vectors and matrices are typed in boldface.

1.2. Vectors are represented by lower case letters.

1.3. Matrices are represented by upper case letters.

1.4. "Vector" means coordinates of a vector. A superscript will be used if necessary to indicate the particular coordinate frame in which the vector is represented, e.g.

$$\mathbf{r}^b = [r_x^b, r_y^b, r_z^b]^T .$$

1.5. Rotation matrices **R** are specified by two indices so that the transformation from frame b to frame c is given by

$$\mathbf{r}^c = \mathbf{R}_b^c \mathbf{r}^b$$

1.6. Angular velocity of frame c with respect to frame i, coordinatized in frame b is described by

$$\boldsymbol{\omega}_{ic}^b = [\omega_x, \omega_y, \omega_z]^T$$

or by the corresponding skew-symmetric matrix

$$\boldsymbol{\Omega}_{ic}^b = \begin{pmatrix} 0 & -\omega_z & \omega_y \\ \omega_z & 0 & -\omega_x \\ -\omega_y & \omega_x & 0 \end{pmatrix}.$$

1.7. The following symbols specify an arbitrary quantity x:

x	true value
$\bar{x}$	measured value
$\tilde{x}$	approximate value

$E\{x\}$	expected value
δx	perturbation in x
Δx	difference in x
$\dot{x}$	first order derivative of x with respect to time
x_k	value at epoch k
$\mathbf{x}^T$	transpose of $\mathbf{x}$

1.8. The vector product is represented by $\times$.

2. COORDINATE FRAMES

Body, (b)

origin: at centre of accelerometer proof masses, assumed to be identical with centre of rotation of rotated sensor unit

x-axis: right

y-axis: forward

z-axis: upward

Earth-fixed, (e)

origin: centre of mass of the Earth

x-axis: orthogonal to z-axis, in mean Greenwich meridional plane

y-axis: completes right-handed system

z-axis: direction of mean spin axis of the Earth

Operational Inertial, (i)

origin: centre of mass of the Earth

x-axis: pointing towards mean vernal equinox

y-axis: completes right-handed system

z-axis: direction of mean spin axis of the Earth

Local-level, (n)

origin: as in (b)

x-axis: east direction on ellipsoid

y-axis: north direction on ellipsoid

z-axis: upward direction of ellipsoidal normal

Wander , (w)

origin: as in (b)

x-axis: rotated from the east towards the north in the tangent plane by an angle α (meridian convergence)

y-axis: orthogonal to the x-axis in the level plane

z-axis: upward direction of ellipsoidal normal

3. LIST OF SYMBOLS

Symbol	Description
A	azimuth
$\mathbf{A}$	design matrix
$\mathbf{b}$	accelerometer bias

$\mathbf{C}_x$	covariance matrix of state vector
c	speed of light
$\mathbf{d}$	gyro bias
$\mathbf{e}$	observation error
$\mathbf{F}$	dynamics matrix
$\mathbf{f}$	specific force
f	carrier beat frequency
$\mathbf{G}$	coefficient matrix of the random forcing functions
g	gravity (magnitude)
$\mathbf{g}$	gravity vector
h	ellipsoidal height
$\mathbf{I}$	identity matrix
p	pitch
r	roll
r_M	meridional radius of curvature
r_N	prime radius of curvature
$\mathbf{Q}$	power spectral density matrix
$\mathbf{u}$	system input
v	horizontal velocity
$\mathbf{x}$	state vector
$\mathbf{l}$	vector of the measurements
α	wander azimuth
β	parameter of Markov processes
Δ	single difference
$\nabla\Delta$	double difference
γ	normal gravity

λ	geodetic longitude
ρ	distance; pseudorange
Φ	transition matrix
ϕ	geodetic latitude
Φ	carrier phase observation

Chapter 1

Introduction

1.1 Background

Kinematic positioning, with high technology systems like the Global Positioning System (GPS) and Inertial Navigation Systems (INS), is fast becoming an operational survey method, competitive with traditional ones. The term kinematic positioning indicates that position measurements are done from a moving vehicle. This has the advantage that surveys can be performed much faster and therefore more economically. Both GPS and INS methods do not require intervisibility between points and are weather independent. In addition to the traditional surveying activities, the new systems open up completely new areas of activity for geodesists. These include precise navigation, automatic vehicle location and tracking, and airborne geophysical exploration.

Inertial Navigation Systems, originally developed for aircraft and ship navigation, were adapted for use in surveying to meet specific purposes and requirements (Schwarz, 1983). Specific measurement methods utilizing Zero Velocity Updates, as well as data processing techniques like Kalman filtering and smoothing, were developed to

significantly improve the positional accuracy of navigation systems, typically from the 1 nm h^{-1} (nautical mile per hour) range to the submetre level. The surveying INS systems have been used successfully in a wide range of applications including typical geodetic control (Wong, 1988), cadastral surveying (Forsberg, 1990), pipeline profiling (Porter et al, 1990), determination of hoist skip and mine shaft trajectory (Martell et al, 1990).

High accuracy relative kinematic positioning using GPS carrier phase measurements has been an area of extensive development in recent years. The method, proposed and tested by (Remondi, 1985), has been successfully applied for geodetic control (Cannon, 1990), (Goad, 1990a) hydrographic surveying (Lachapelle et al, 1988) and tested for use in airborne photogrammetry (Mader, 1986; Baustert et al, 1989). In anticipation of the full satellite constellation, GPS is becoming a recognized surveying method of high potential. Considerable research effort of different groups has gone into the development of new algorithms and solutions to improve data analysis performance. Further progress was made by advances in receiver technology, which resulted in improved receiver reliability as well as reduced cost and size. However, certain GPS limitations remain unresolved such as loss of lock due to physical obstructions or a data rate which is too slow for some applications, as discussed in (Lachapelle and Schwarz, 1989).

With the integration of a GPS receiver and an INS, the individual system limitations can be overcome thus exploiting the capabilities of each positioning system. Although GPS provides very accurate

positions (e.g. Cannon,1987; Schwarz et al,1989), the accuracy of the velocity is limited and vehicle attitude is usually not available. In comparison, INS can give very accurate position, velocity and attitude information over short time intervals. If the system is regularly updated with accurate external positions (Wong et al,1988), this accuracy can be maintained over long time spans. Thus, the two systems are complementary since GPS can be used to update the inertial system which can then provide accurate velocities and attitudes. The position output of the INS can be also used for the solution of the cycle slip problem in the GPS carrier phase data.

The idea of integrating of GPS and INS has been around for several years. Various simulation studies have indicated its potential for high-precision positioning (Hein et al, 1988; Loomis and Geier, 1990), airborne photogrammetry (Goldfarb, 1987) and vector gravimetry (Knickmeyer, 1990). However, aside from military applications, few integrated systems, actually have been implemented, due to the complexity of the resulting system. Medium accuracy positioning results at the metre level were first reported by (Wong et al, 1988). Recently, high-accuracy results at the decimetre level were achieved in airborne mode (Cannon and Schwarz, 1990) as well as in land mode (Lapucha et al, 1990).

Conventional mapping usually involves the position determination of selected ground points which are characteristic of the terrain, and simple interpolation between the selected points. In this approach, some short wavelength terrain features are neglected in the generalization process. While this approach is appropriate for

many applications, it does not satisfy all requirements. For highway and airport runway maintenance , the short term features are very important because they can be used to identify potential danger spots. Visual inspection cannot always detect the problem. An effective solution can be provided by a system which is capable of detecting relevant discontinuities using sufficiently accurate near-continuous profiling. Profiling must be performed in a reasonable time frame so as not to interfere with on-going traffic and operations. The GPS/INS integrated system is an ideal candidate for such a role. Its high-rate output is ideally suited for fast, on-line analysis using modern computer data bases and digital terrain models. Survey time can be reduced dramatically comparing to conventional survey because the system has to be driven along a highway at normal cruise speed.

The work described in this thesis has been done as part of The University of Calgary's research on developing a precise positioning component for the Mobile Highway Inventory System (MHIS). This video-logging system is used to monitor highways and is operated by Alberta Transportation. It is an interesting example of a modern kinematic system, and will be further described in the sequel. One of the system's operational requirements is a knowledge of position, velocity and attitude. The low accuracy of its current positioning component , listed in the first column of Table 1.1, limits the use of data from MHIS to qualitative analysis. In response to the need for more accurate positioning requirements, The University of Calgary proposed the use of a GPS/INS system. An integrated GPS/INS system offers potential improvement in determination of position, velocity,

slope and curvature. Table 1.1 gives the current geometric accuracies of the MHIS, the future accuracies using the integrated GPS/INS, and the accuracy requirements of a future highly precise road survey system.

	CURRENT MHIS ACCURACY	**REQUIRED MHIS ACCURACY**	**FUTURE SURVEY SYSTEM ACCURACY**
Position	±1 m over 1 km	±0.3 m over 1 km	±0.05 m over 1 km
Speed	<±5 km h^{-1}	±0.4 km h^{-1}	N/A
Slope	±1% of grade	±0.5% of grade	±0.1% of grade
Azimuth	±2 deg	±0.2 deg	±0.2 deg
Curvature	±2 deg per 40 m	±0.2 deg per 40 m	±0.2 deg per 40 m

Table 1.1: Current and Proposed Accuracy of the Mobile Inventory System

The improvement in using an integrated system is significant for all parameters, increasing the accuracy by at least 50% in all cases. Through the introduction of a GPS/INS positioning system into the MHIS, improved geometric integrity can be achieved, thereby increasing the potential uses of the MHIS data. This system can also be refined for use as a general road survey system. A road survey system would require even further increase in accuracy over the MHIS, especially in the position component.

1.2 Mobile Highway Inventory System

Alberta Transportation is responsible for the operation and maintenance of over 13,000 km of primary highways and 14,000 km of secondary roads throughout Alberta (Ross, 1983). Due to the high cost of maintaining up to date records of the physical features and characteristics of these roads by traditional means, Alberta Transportation developed the Mobile Highway Inventory System. Operational since the summer of 1983, the MHIS is an integration of various technologies mounted in a customized van. The main data collection instruments are a video-log system which records a continuous image of the road, a digital inventory system which captures all roadway events (e.g. signs, guard-rails, etc.) and a geometric data collection system which captures all vehicle trajectory information.

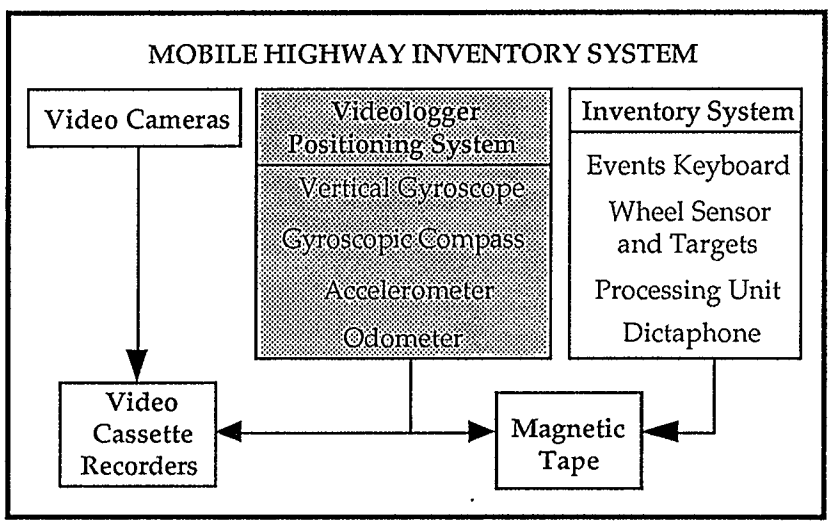

Figure1.1: Current Alberta Transportation MHIS

Figure 1.1 shows a schematic of the Alberta Transportation MHIS instrumentation currently in use. There are two color video systems installed in the van, each giving a different view of the roadway. One camera is pointed to give a general overview of the roadway, while the other is inclined to view the actual road surface. Two 3/4" video cassette recorders record the data. The digital inventory system is made up of a Tenn-II Inventory system and a Techwest videologger. The roadway works are recorded in the Tenn-II system using a control keyboard located in the front of the van (Alberta Transportation, 1983). The Techwest system collects trajectory information such as distance, grade, curvature, roughness and direction. The instruments used for geometric data collection are a compass, a vertical gyroscope, an odometer and an accelerometer. Data from these instruments is automatically transmitted to the video recorder for superimposition on the video image as shown in Figure 1. Improvement of the MHIS positioning system, represented by the shaded area in Figure 1.1, has been the aim of the research at The University of Calgary.

Photo 1.1 shows the positioning instrumentation as it is installed in the MHIS van. The vertical gyroscope and accelerometers are located beneath the video monitor. Adjacent to these instruments is the gyroscopic compass, followed by the video recorders.Data post-processing is performed in the office. The main tasks are data editing and reformatting so the video and inventory data can be used by various departments throughout Alberta Transportation. By maintaining an accurate inventory, the need for field checks is greatly

reduced, thus increasing cost-effectiveness. Such a system can be used in a number of applications, ranging from safety inspections to analysing re-surfacing requirements.

Photo 1.1: Installation of MHIS Instrumentation

Each road section is driven three times, once for sensor calibration, and the other two times for data collection in each direction. The MHIS van is operated for about 6 months of the year due to weather restrictions. Approximately 200-300 km of road are surveyed per day, covering about 1/3 of the province per year. This rate restricts the resurveying of a particular stretch of road to a three year cycle.

The current use of the MHIS within Alberta Transportation is mainly for qualitative analysis, e.g. the location of signs and guard-rails or the condition of the pavement surface. The cost-effectiveness of the system could be considerably improved, by providing more accurate geometric information which would also allow quantitative analysis.

1.3 Objective of the Research and Outline of the Thesis

The primary objective of this thesis is the development and testing of a GPS/INS positioning component for the Mobile Highway Inventory System. A secondary objective is the assessment of the GPS/INS system for high-precision road surveying. The emphasis of the thesis is on GPS/INS software development, data processing and field testing. A software package, that processes data from differential GPS and a strapdown inertial system INS will be developed including the design of a GPS/INS Kalman filter. The focus is thus on the applied rather than the theoretical aspects of the method. In the mathematical description emphasis is therefore placed on physical insight, basic concepts and key problems of practical importance.

A general description of positioning with GPS is given in Chapter 2. The fundamental GPS observables are introduced and discussed. Advances in GPS kinematic positioning are reviewed. In Chapter 3, general concepts of INS positioning are outlined. The specific navigation model for strapdown INS is developed giving the relation between measured INS observables and navigation quantities like position, velocity and attitude. In Chapter 4 the framework for

dynamic parameter estimation using GPS and INS measurements is outlined. The error model for both GPS and INS is given. The complementary role of GPS and INS measurements and integration strategies are discussed in Chapter 5. The next two chapters are oriented towards implementation. Hardware and software components of the system are described in Chapter 6. A description of the field tests and analysis of results is included in Chapter 7. In the same chapter, the cycle slip detection and correction is analysed in detail. In the last Chapter 8, conclusions are drawn and recommendations for further research are made.

Chapter 2

GPS Positioning

GPS satellite techniques can be used for various kinematic positioning applications. Different GPS observables and processing methods can be used depending upon accuracies required and applications envisaged. The fundamental choices are between absolute and differential positioning, use of pseudo-range or carrier phase and selection of GPS differencing methods. The purpose of this chapter is to assess the GPS observables and the methods that can be applied to reach sub-metre accuracy in kinematic mode.

The basic concepts of GPS positioning are first reviewed in this chapter. The mathematical model, that gives the relationship between the GPS observables and the unknown parameters, is presented. Observation differencing, the fundamental concept in GPS positioning, is examined. Finally recent developments in GPS kinematic techniques are discussed with view to advances and limitations.

2.1 General Description and Principle

The GPS is a satellite based radio positioning system designed for accurate real time navigation. It uses radio signals from a

constellation of earth orbiting satellites to determine the three-dimensional position of user receivers. The 1993 GPS constellation is scheduled to consist of 21 satellites and 3 active spares orbiting the earth in 12 hour orbits at a height of 20 000 km in six orbital planes. At that time, at least four satellites will be available to a user at any time and anywhere on the globe.

The GPS satellites continuously broadcast spread spectrum signals on two frequencies L1 - 1575.42 MHz and L2 - 1227.60 MHz respectively. These frequencies are respectively 154 and 120 times the fundamental frequency of 10.23 MHz. The frequencies selected for the system have properties well suited for all-weather precise navigation, namely minimal attenuation due to the atmosphere and virtually straight line-of-sight propagation (Lachapelle, 1990). The use of these two fundamental frequencies enables ionospheric effects to be computed and removed from GPS observations. The L1 carrier is modulated with the precise P code, the coarse acquisition C/A code and the navigation message. The L2 signal is modulated with P code and the navigation message only. Both types of code allow to determine the time and position but with different precision. The precision is dependent on the resolution of each code, which is a direct function of the chipping rate of the pseudo-random codes emitted by the GPS satellites. The C/A code, which is open for civilian users, has a chipping rate of 1 msec (10^{-6} sec), with an associated wavelength of 300 m. The P code, which is mainly designated for military users, has a chipping rate of 0.1 msec, with an associated wavelength of 30 m. The actual code measurement can be resolved to

about 0.3 to 1 % of these code length. Therefore the resolution of the C/A and P codes is 1 to 3 m and 10 to 30 cm, respectively (Lachapelle, 1990).

The concept of positioning with GPS is based on simultaneous ranging to at least four GPS satellites to determine the unknown coordinates of the point (see Fig. 2.1). From a geometric point of view, a unique solution can be obtained if distances from at least three satellites - with known coordinates in some reference frame, are measured. The satellite coordinates at a given instant of signal transmission, which are required for the solution, are computed from ephemeris data transmitted in satellite signals. The algorithm for these computations is well known and is given in (Wells et al, 1986). The reference datum for GPS positioning is the earth fixed geocentric reference system WGS 84, for which parameters are given in (Wells et al, 1986). Since GPS satellite observations are not pure ranges but are affected by instrumental biases, especially timing errors, a minimum of four satellites are necessary (Fig. 2.1).

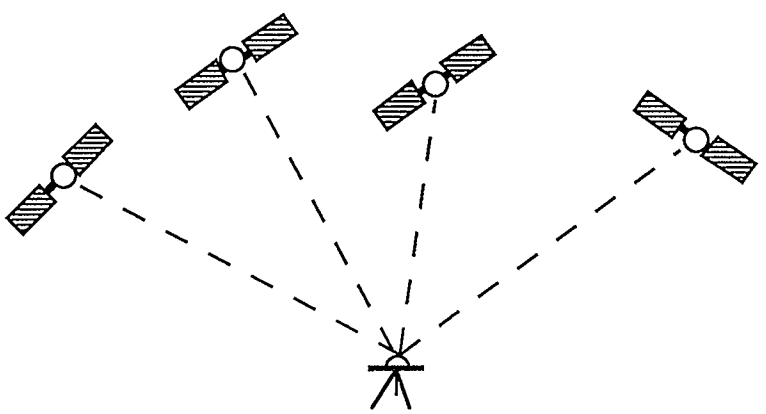

Fig. 2.1: Absolute GPS Positioning

The determination of point position coordinates - single point positioning, is affected by many errors. Some of the most significant errors are satellite orbit, clock as well as signal propagation delays. Satellite orbit errors are caused by the inaccuracy of ephemeris prediction by the GPS control segment. Presently, another error factor is the deliberate degradation of broadcast ephemeris accuracy as well as clock dithering by the owner of the GPS system. These deliberate degradations are termed Selective Availability - SA and have been introduced to restrict precise real-time navigation to a specific group of users. A significant part of the satellite clock error is eliminated by using the clock correction information that is sent in the satellite message. Signal propagation errors are caused by the change in signal travel time when the signals from GPS satellites pass through ionosphere and troposphere. The ionosphere induced range errors can be removed using double frequency P-code measurements. Troposphere induced errors can be partly removed by applying the tropospheric correction computed on the basis of meteorological measurements and existing troposphere models (Goad and Goodman, 1974).

Differential GPS positioning, in surveying usually called relative positioning, can significantly reduce these types of errors. It exploits the fact, that these errors are highly correlated for the stations within a certain area. Typically this area is about 50-60 km in diameter in high-accuracy surveying applications and up to 400 km in lower accuracy differential positioning applications. There are various differential techniques to achieve this accuracies, e.g. differencing of

observations or applying differential corrections. Implementation of the differential concept requires at least two receivers: one placed at a known master station and a second placed at a remote station (Fig. 2.2).

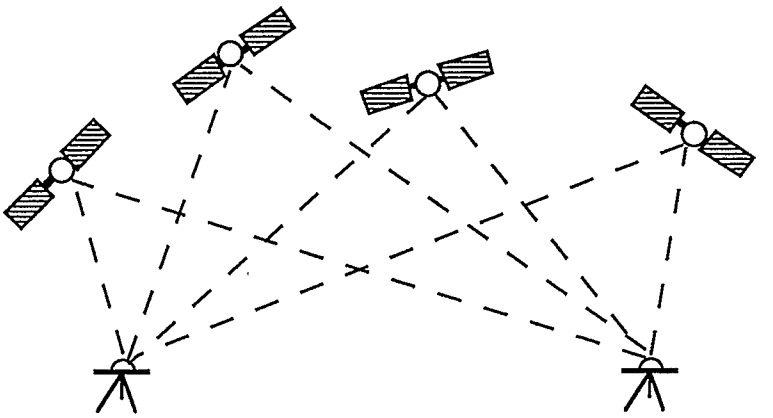

Fig. 2.2: Relative GPS Positioning

The bias in the measured range, which influences almost equally the determination of position at both points, can be taken into account in two ways. One is to calculate a differential correction by comparing the observed and predicted ranges at the master station and applying this correction to the solution determined at the remote station. Another way is the computation of differences of GPS observations recorded simultaneously at two stations thereby cancelling the common errors. Both methods give similar results, effectively determining the relative position of the remote station with respect to the fixed station more accurately. The first method is often used in real-time applications, because of the limited volume of data to be transmitted. The second method involves simultaneous processing of observation data from both receivers and is usually used in post-mission mode.

2.2 GPS Observation Model

In simplified terms, there are two basic observation types available from GPS, namely pseudo-range and carrier phase observations. Both observations give the same geometric information, namely range, but with different accuracies and biases. Pseudo-range observations have noise at the metre level for C/A code and submetre level for P code, while the noise of phase observations is below the centimetre level. The precision of phase observations results from the receiver capability to reconstruct the L1 and L2 carrier wavelengths (19 cm and 24 cm, respectively), with 1 % accuracy. This gives a precision of about 2 mm of the carrier phase for both frequencies.

Pseudorange, sometimes called code observation, is the time delay between the transmission and the reception time of the satellite signal, which is obtained by determining the time shift necessary to match the received pseudorandom sequence with an internally generated matching sequence. The term "pseudorange" implies that the range between the receiver and satellite is not exact but is contaminated by clock errors of both satellite and receiver clocks and by atmospherically induced signal delays. The distance between the satellite and receiver is computed by multiplying the time delay by the speed of light.

The model equation for a pseudo-range, p, is (Wells et al, 1986)

$$p = \rho + c(dt-dT) + d_{ion} + d_{trop} + \varepsilon_p , \qquad (2.1)$$

where ρ is the range between the station and a satellite,

dT is the receiver clock error,

dt is the satellite clock error,

d_{ion}, d_{trop} are the ionospheric and tropospheric corrections, respectively,

c is the speed of light,

and ε_p is the pseudorange noise.

The carrier phase is the difference between the carrier signal generated by the receiver oscillator and the Doppler shifted carrier signal coming from the GPS satellite. The carrier phase is integrated in time to count the number of satellite signal wavelengths as they arrive at the receiver antenna. The accumulated cycles are directly related to the change of range between satellite and receiver antenna phase centre. The phase measurement is biased by the the initial epoch cycle ambiguity which remains constant if phase lock is maintained.

The model equation for carrier phase, Φ, is (Wells et al, 1986)

$$\Phi = (f/c)\rho + f(dt - dT) - (f/c)(-d_{ion} + d_{trop}) + N + \varepsilon_\Phi , \qquad (2.2)$$

where ρ, dt, dT, d_{ion}, d_{trop}, c (as defined above),

N is the carrier phase cycle ambiguity,

ε_Φ is the carrier phase noise,

and f is the frequency of the carrier signal.

The equations (2.1) and (2.2) clearly show that the two GPS observables have the same information content. The geometric term ρ, appearing in both equations, is dependent upon the unknown receiver point coordinates. These coordinates can be determined using well known estimation techniques. With the exception of the initial ambiguity, the observation noise and the propagation effects, the model terms in the two observables are equivalent after rescaling. On the other hand, both measurements are different in nature. The pseudorange is an instantaneous observation, which is in principle independent of the past measurements, whereas the carrier phase measurement is continuous and dependent on the tracking history. In fact, these two GPS observations can be combined, in the so called phase-smoothed pseudorange. In this concept (Hatch, 1982) and (Lachapelle et al, 1986), the change of phase over time is added to the initial pseudorange to get an estimate of the current pseudorange observation. The resulting new observable has reduced noise, enabling position determination to be more accurate. Another advantage of this approach is the significant reduction of multipath effects that affect carrier phase observations much less than pseudo-range observations.

Phase rate or Doppler phase rate is another GPS observable that is available as output from some of the GPS receivers. It is simply the time derivative, denoted by $(\dot{\ })$, of the phase. It can be used for determination of receiver velocity. The model equation for phase rate $\dot{\Phi}$ is

$$\dot{\Phi} = (f/c)\dot{\rho} + (f/c)(-\dot{d}_{ion} + \dot{d}_{trop}) + \varepsilon_{\dot{\Phi}} . \qquad (2.3)$$

Equation (2.3) is derived by differentiating the basic equation(2.2).

2.3 GPS Observation Differencing

The basic GPS model equations 2.1 and 2.2 contain bias terms related to satellite clock, receiver clock, orbit and atmospheric errors. Since they cannot be extracted from observations, they have to be accounted for in the mathematical model. There are two ways to deal with them. One way, is to model them as unknowns and solve for them as well as the unknown coordinates in the estimation process. This is the so-called undifferenced approach (Goad, 1985a). The second method uses differencing of observations and is preferred because it reduces the computation burden. Differencing of simultaneous observations usually results in the cancellation of common biases. Both methods, differenced and undifferenced, are mathematically equivalent (Lindlohr and Wells, 1985), (Schaffrin and Grafarend, 1986) as long as the respective covariance matrices, that result from the differencing transformation, are taken into account.

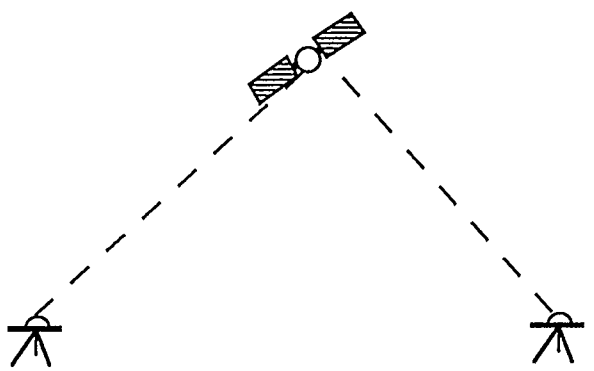

Fig. 2.3: Single Differencing between Stations

Differencing of phase observations between two receivers (Fig. 2.3) results in the elimination of terms related to satellite clock instabilities as well as in reducing the orbital errors and propagation effects.

The model equation for the single difference phase observable is

$$\Delta\Phi = (f/c)\Delta\rho + \Delta N + \Delta dT + \varepsilon_{\Delta\Phi} , \qquad (2.4)$$

where Δ is the single difference between stations and satellites,

$\Delta\Phi$ is the observed carrier phase single difference,

$\Delta\rho$ is the single difference of ranges from stations to satellites,

ΔdT is the relative receiver clock offset,

ΔN is the single difference ambiguity,

and $\varepsilon_{\Delta\Phi}$ is the measurement noise.

The single difference observable contains residual effects of orbital and atmospheric errors that can be neglected for stations separated by less than 30 km under normal atmospheric conditions and were omitted in model equation (2.4) in view of required sub-decimetre accuracy. The main problem with the use of single differences is the instability of the receiver clock oscillator. Therefore the relative receiver clock unknown ΔdT has to be modelled for every observation epoch. To avoid such processing problems, double differencing between receivers and between satellites is used as

shown in Fig. 2.4. Differencing between satellites eliminates the receiver-dependent clock terms and leaves only geometric and ambiguity parameters.

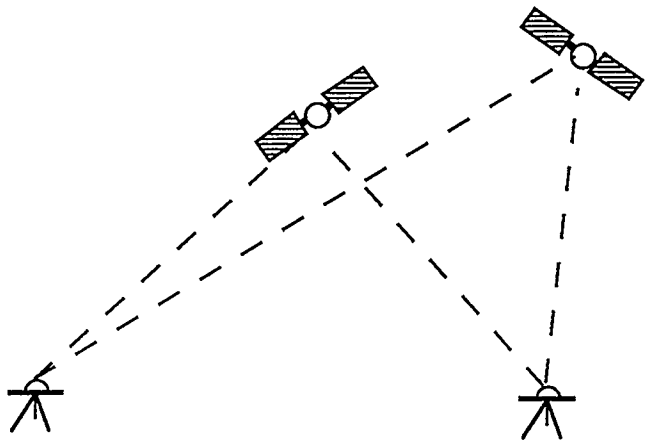

Fig. 2.4: Double Differencing between Stations and Satellites

The phase observation equation for double differences, developed from equation (2.4) is then very simple, namely:

$$\nabla\Delta\Phi = \nabla\Delta\rho + \nabla\Delta N + \varepsilon_{\nabla\Delta\Phi}\,, \tag{2.5}$$

where $\nabla\Delta$ is the double difference between stations and satellites,

$\nabla\Delta\Phi$ is the observed carrier phase double difference,

$\nabla\Delta\rho$ is the double difference of ranges from stations to satellites,

$\nabla\Delta N$ is the double difference ambiguity,

and $\varepsilon_{\nabla\Delta\Phi}$ is the measurement noise.

The phase double difference can be regarded as the best GPS observable for most survey applications. It is a function of familiar geometric terms, the range double difference $\nabla\Delta\rho$, and the ambiguity parameters. Practically, all other GPS errors are canceled out in the differencing process. Since the ambiguity parameter remains constant, unless loss of lock occurs, the change in a double difference is directly related to a change in geometry of the system receiver - the observed satellites. Another advantage of the double difference GPS observable is that it allows to optimally exploit the integer nature of the ambiguity parameter. In fact, double differencing is the most common technique in static GPS applications (Bock et al, 1986; Beutler et al, 1987) as well as kinematic applications (Cannon and Schwarz, 1989; Loomis, 1989; Goad, 1990a). It is used in this study as the basic GPS observable as well.

The same principle of differencing can be applied to pseudo-range observations resulting in very similar equations, which are not listed here.

2.4 Advances in GPS Kinematic Techniques

Kinematic positioning, that is the determination of the position and velocity of a moving vehicle along its trajectory, was a fundamental objective of GPS design and development. It is required in ship, air and land navigation. Pseudo-range observations or differential pseudo-range were used exclusively for this task in the early stages of GPS development. The second fundamental GPS observable, carrier phase,

was primarily used for high-precision static surveying (Remondi, 1984). The pseudo-range is better suited for kinematic positioning than carrier phase. It is instaneous in nature and so is the determined position. Pseudo-range positioning does not have the problem of initial ambiguity resolution and cumulative error which the carrier phase has. However, accuracy is a limiting factor. The absolute position of a moving receiver can be determined with an accuracy of 20 to 100 metres for most users with C/A code receivers (Lachapelle and Schwarz, 1989). The size of the error is largely dependent on whether or not Selective Availability is on. The pseudo-range differential method reduces some of the errors correlated between stations, as discussed earlier, and can be used in applications, where a 5 to 15 metre level of accuracy is required. These applications include hydrography, exploration geophysics, harbour and canal ship navigation. Nevertheless, this level of accuracy limits the use of pure C/A pseudorange observations to specific applications. A wider range of applications for pure pseudo-range positioning can be expected when cheaper P-code receivers become commercially available and can be used.

The advantage of using carrier phase to aid pseudo-range kinematic positioning was recognized early (Hatch, 1982), as mentioned briefly in Chapter 2.2. This method allows one to use a lower cost C/A receiver and to combine phase and pseudorange to generate filtered ranges which reach the accuracy of P-code pseudoranges (Goad, 1990b). The method has the potential for metre level accuracy and can be used in wider variety of applications.

Another conceptual breakthrough was the use of the precise static GPS relative positioning method in dynamic applications (Remondi, 1985). The idea was based on the simple fact that as long as the initial ambiguity has been resolved and is constant, the differenced carrier phase provides high accuracy relative position changes determined with respect to a receiver placed at a fixed location (Fig. 2.5). The method preserves the properties of the differenced carrier phase observables in the static case, i.e. elimination of common errors for measurements made by receivers simultaneously tracking the same satellites.

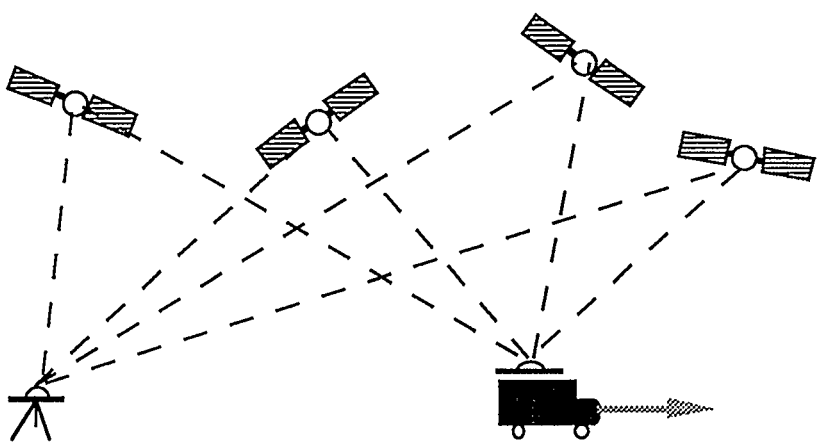

Fig. 2.5: GPS Relative Kinematic Positioning

Every GPS phase difference can be used in principle. In practice, for most implementations, double differencing is used (Cannon and Schwarz, 1989), (Loomis, 1989), (Goad, 1990a). Examining the model equation (2.5) for double difference reveals immediately the advantage of this observable for kinematic positioning. If integer ambiguity parameters $\nabla\Delta N$ are known, then there are only three unknown parameters to solve for, namely the coordinates of the rover station in

the $\nabla\Delta\rho$ term. Thus 3 independent double difference equations are necessary and therefore a minimum 4 satellites have to be observed. Based on this principle, different processing methods were developed for specific applications, with various vehicle dynamics and hardware configurations. These methods employ various estimation methods that are discussed in (Schwarz et al, 1989). All of them have to address the problem of ambiguity resolution, i.e. determination of carrier phase ambiguity. In the following, only pure kinematic techniques are discussed that do not include any form of intermediate static positioning.

Common to all approach is the determination of the ambiguity at the beginning of a survey and its use during the kinematic part as a constant correction. Of course, this is based on the fundamental assumption that phase lock is maintained. One possibility of ambiguity determination is to place the roving receiver at a known location and solve for the unknown ambiguity parameters $\nabla\Delta N$ using collected static observations. Another one is to place it at any location and solve simultaneously for the initial baseline vector and ambiguities. Practical experience (Cannon, 1990) as well as simulation studies (Frei and Beutler, 1989) show that optimal occupying time to resolve the initial baseline and ambiguity for short baselines, is around 10 min. Another common technique, which results in a time saving, is antenna swapping (Remondi, 1988). When using the integrated GPS/INS system, the inertial system has to be aligned initially for at least 10 minutes. The first method of simultaneously determining the initial vector and the ambiguity has been used in the tests described later.

The fundamental requirement of phase lock is difficult to meet in a production environment. The carrier phase observation is a continuous measurement as opposed to pseudo-range. The actual phase reading is dependent on past measurements. Any interruption in satellite tracking causes a "cycle slip" which is a discontinuity in the carrier phase measurement resulting in a change in the integer ambiguity. The interruption can be caused by the masking of the satellite by buildings and trees, by atmospheric disturbances such as high ionospheric activity, or by an electronic obstruction within the tracking bandwidth.

Cycle slip fixing, ie. determining the new value of the ambiguity, requires redundant information. This information can originate either from an external source or from the GPS system itself. The possibility of cycle slip fixing using the position information from an inertial system is one of the primary advantages of a GPS/INS system and is discussed in Chapters 5 and 7. External information can come from any other positioning system that is capable of providing position with 10 cm accuracy. Presently the availability of signals from other satellite positioning systems like the Soviet GLONASS system or the commercial STARFIX system might help to reduce the influence of shadowing effects.

Ambiguity resolution during motion using the GPS system alone is now an area of active research in the GPS community. One obvious source of redundant information are cycle slip free observations that can be used to fix the disturbed observations. This requires one redundant satellite observation for each cycle slip and therefore has

limited use in the case of multiple cycle slips. Recently, (Hwang, 1990) presented results for ambiguity resolution "on the fly", even without initial static ambiguity resolution, with seven satellites in view. Another method for cycle slip correction is to use pseudo-range data to get an approximate value for the new ambiguity and refine it in Kalman filter while going along (Wong et al, 1988; Cannon and Schwarz, 1989). This method does not give the same accuracy as for cycle slip free data. The use of more precise P-code receivers would help to increase the accuracy of this method.

Various techniques have been proposed for double frequency receivers (Goad, 1985b; Bastos and Landau, 1988). They are based on checking the known ratio between measurements on different frequencies. They are not discussed in detail herein because only single frequency C/A code receivers were available for this research.

Chapter 3

INS Positioning

Inertial Navigation Systems are widely used in kinematic positioning. Their operation is based on gyroscopic control of the measurement frame orientation and integration of measured accelerations to determine position and velocity changes. Their theory of operation is based on the second law of Newton, but formulated for practical purposes in rotating systems. The purpose of this chapter is to present the INS observation model with special emphasis on the strapdown INS, used in this research.

In this chapter, the basic concepts of inertial positioning and the underlying physical laws are reviewed. Various inertial systems are briefly examined. The body of the chapter is devoted to the presentation of INS strapdown mechanization, i.e. formulation of the strapdown observation model. Finally, the major features of the alignment procedure are described.

3.1 General Description and Principle

An Inertial Navigation System (INS) consists of a platform with two sensor triads, one composed of accelerometers and the other of

gyroscopes. The accelerometer triad measures specific force along three orthogonal axes. The gyroscope triad senses the angular velocity of the platform with respect to inertial space and thus in principle determines the orientation changes of the chosen measurement frame.

The basic theory underlying inertial navigation is that of classical mechanics. Assuming that the measurement frame is inertial, the measured specific force can be expressed by

$$\mathbf{f}(t) = \mathbf{a}(t) - \mathbf{g}(t) , \tag{3.1}$$

where t is time,

$\mathbf{f}$ is the vector of specific force,

$\mathbf{a}$ is the vector of vehicle accelerations relative to an inertial frame of reference,

and $\mathbf{g}$ is the vector of gravitational accelerations.

The above equation is the well known second law of Newton, valid in an inertial system, written for unit mass and is fundamental in a study of inertial geodesy. It is not possible to separate gravitational acceleration $\mathbf{g}$ and vehicle accelerations $\mathbf{a}$. The knowledge of either quantity is necessary for the solution of the problem of positioning or alternately gravimetry. If vehicle acceleration $\mathbf{a}$ is known, the gravity vector $\mathbf{g}$ can be determined. Vehicle acceleration can be obtained, for instance, by differentiating GPS derived velocities or by stopping the vehicle. This is the principle of gravity vector determination using

integrated GPS/INS (Schwarz, 1987; Knickmeyer, 1990) or by zero velocity updates. In the discussion presented here, knowledge of the vector **g** is generally assumed. Integrating vehicle acceleration **a** twice with respect to time results in velocity and position changes, i.e.

$$\mathbf{v}(t) = \mathbf{v}(t_o) + \int_{t_o}^{t} \mathbf{a}(t)\, dt\,, \tag{3.2}$$

$$\mathbf{r}(t) = \mathbf{r}(t_o) + \int_{t_o}^{t} \mathbf{v}(t)\, dt\,, \tag{3.3}$$

where t_o is initial time,

and $\mathbf{r}, \mathbf{v}$ position and velocity vector respectively.

Integration is usually performed in a reference frame, which is in principle determined by user requirements.This, of course, implies that the reference system, at any instance of time, has a known orientation with respect to an inertial frame. The relative orientation of the measurement frame with respect to the reference frame is determined by the gyro triad. The manner, in which the gyros control the sensor platform distinguishes different platform designs. In general terms, there are three groups of inertial systems: space-stabilized, local level and strapdown systems. In the first two, the so-called gimballed systems, gyros keep a platform in a prescribed orientation via feed-back torquing commands. In the space-stabilized system, the orthogonal axes of the platform are kept in a fixed orientation with respect to an inertial frame. In the local-level system, the measurement frame is aligned to the local ellipsoidal frame. The

platform's Z-axis coincides with the local normal of the reference ellipsoid while the secondary axis is pointed towards North. Strapdown systems do not physically instrument a reference frame. The sensors are fixed to the platform and therefore experience all rotational and translational vehicle movements with respect to inertial space. The gyros monitor, almost continuously, the sensor platform rotation with respect to an inertial frame. These rotations are taken into account at a high rate by an on-board computer. The specific forces are then transformed to the chosen computation frame via the computed transformation matrix.

In practice two problems have to be addressed when computing kinematic acceleration **a** from (3.1), to be used in equations (3.2) and (3.3). First, the measurement frame and the computational reference frame, used in the integration, differ. The accelerometer output is referenced to the specific platform axes mechanized for the particular system under consideration while the computational frame is generally in some way Earth referenced. The specific force, measured for instance in the body frame b, has thus to be first transformed to the computational frame, denoted by c. The same applies to the gravity vector **g**, which is given in an Earth-centred frame and has to be transformed to the computational frame. The transformations are given by the following equations:

$$\mathbf{f}^{c} = \mathbf{R}_{b}^{c}\,\mathbf{f}^{b}\,, \tag{3.4}$$

$$\mathbf{g}^{c} = \mathbf{R}_{e}^{c}\,\mathbf{g}\,, \tag{3.5}$$

where $\mathbf{R}_b^c$ is body to computation frame transformation matrix,

$\mathbf{R}_e^c$ is earth to computation frame transformation matrix,

and $\mathbf{f}^b$ is measured specific force.

The transformation matrix $\mathbf{R}_b^c$ is computed from the measured orientation changes in the measurement frame as determined by the gyro system. The transformation matrix $\mathbf{R}_e^c$ is well known for the computational systems that are in use.

Secondly, these computational frames usually are not inertial because they rotate with respect to inertial space. Only, gimballed space-stable systems have gyro-stabilized platforms aligned to an inertial frame. In practice , in most inertial navigation systems, the measurement frame rotates with respect to an inertial frame. Gimballed local-level systems have their measurement frames aligned with local astronomic frames, thus their measurement frame experiences the rotation of the earth as well as the rotational movement with respect to the centre of the earth. In strapdown systems, the measurement frame is fixed to the vehicle body and hence experiences all vehicle movements. In this case the fundamental law of Newton, valid in an inertial frame of reference, has to be modified to take into account the accelerations of the reference frame with respect to inertial space. Kinematic acceleration, in the chosen computational frame, can thus be written as

$$\mathbf{a}^c = \mathbf{R}_b^c \mathbf{f}^b + \mathbf{a}_{ic} - \mathbf{R}_e^c \mathbf{g}, \tag{3.6}$$

where $\mathbf{a}^c$ is vector of acceleration relative to reference frame,
and $\mathbf{a}_{ic}$ is the resultant vector of inertial accelerations.

The inertial accelerations $\mathbf{a}_{ic}$, sometimes called forces of inertia, are fictitious accelerations due to the rotation of the non-inertial measurement frame with respect to the inertial frame. They are the well known centripetal, Corriolis and tangential accelerations.

Equation (3.6) describes the general relationship between accelerometer output and kinematic acceleration, in any frame, which is used for the computation of position and velocity. The choice of computational frames is determined by platform mechanization for gimballed systems - inertial or local level, while for strapdown systems, it is arbitrary in principle and depends on the application. The transformation matrix $\mathbf{R}_b^c$ is continuously computed from the gyro output of strapdown systems. The gimballed systems have their matrix $\mathbf{R}_b^c$ driven to zero, through the gyro feed-back loop, while remaining misalignments are determined from calibration.

In surveying, gimballed systems have been traditionally used because they usually contain more precise sensors than the strapdown systems. However, the new generation of strapdown systems with ring-laser gyros (RLG) has a similar level of sensor accuracy as the conventional systems, but for much a lower price. The RLG's have high rate capacity, wide dynamic range and no rotating parts. In comparison to traditional systems, strapdown inertial surveying systems SISS have advantages in terms of higher reliability, smaller maintenance requirements, high output rate and high accuracy

attitude parameters (Schwarz et al,1990). Strapdown inertial systems are ideal candidates for an integration of GPS and INS because they provide accelerations and angular velocities. They are therefore well suited for an application like the one discussed in this study.

The integrated velocities and coordinates of an INS contain systematic errors that grow with time (Britting,1971). These errors can be estimated when external measurements are available. Any observable that can be expressed as a linear function of the systematic errors of the INS may be used as a control measurement. Examples of such observables are velocities and coordinates. During a land survey, vehicle stops provide an important source of velocity information, the so-called zero velocity updates. Of course this method is not feasible if the INS is continuously in motion. In this case GPS can provide control information for limiting the error growth of an INS.

3.2 Strapdown INS Mechanization

Mechanization is the process of transforming of specific force measured by accelerometers and angular rates measured by gyros into the navigation parameters velocity, position and attitude. A strapdown unit senses specific force in the body frame, which is a near-orthogonal frame fixed to the vehicle and defined by the sensitive axes of the accelerometers. It also measures angular velocity between the body frame and the inertial frame. Major steps in the derivation of the navigation equations are the choice of the reference frame for computations, the determination of the measurement frame rotation

with respect to the computation frame and the transformation of measured accelerations to the computation frame. Finally integration is performed in the computation frame to get position, velocity and the updated appropriate transformation matrices. The updated transformation matrices are computed from numerical integration of the fundamental differential equation

$$\dot{\mathbf{R}}_b^c = \mathbf{R}_b^c \, \Omega_{cb}^b \, , \tag{3.7}$$

where Ω_{cb}^c is the skew symmetric form of the vector of angular velocities of the body frame b with respect to the computational frame c, coordinatized in the computational frame c.

Equations (3.6) and (3.7) can be cast into the fundamental set of differential equations that transform inertial measurements to position, velocity and attitude with respect to the computational frame by

$$\begin{pmatrix} \dot{\mathbf{r}}^c \\ \dot{\mathbf{v}}^c \\ \dot{\mathbf{R}}_b^c \end{pmatrix} = \begin{pmatrix} \mathbf{v}^c \\ \mathbf{R}_b^c \, \mathbf{f}^b + \mathbf{a}_{ic} - \mathbf{R}_e^c \, \mathbf{g} \\ \mathbf{R}_b^c \, \Omega_{cb}^b \end{pmatrix} . \tag{3.8}$$

The above equations describe in general form the mechanization equations for a strapdown system and will be developed for a specific computational frame. In the following, only the main points of the

derivation are given. For a more detailed development see (Wong, 1988).

3.2.1 Computation Frame

The choice of the computation frame for a strapdown INS is arbitrary in principle. One of the possible choices is an earth-centred Cartesian frame. The output in this frame is given in terms of Cartesian geocentric coordinates. The choice of such a frame has advantages in terms of simple mechanization and speed of calculation (Wei and Schwarz, 1990b). For the application discussed here, it is advantageous to perform the integration in a local-level frame or the closely related wander-azimuth frame. The advantages of such a representation for a strapdown mechanization are the following:

- The geographic coordinates (ϕ,λ,h) are obtained directly from the mechanization.
- The attitude of the body with respect to the local-level frame (roll, pitch, azimuth) is given directly.

Both sets of parameters are of direct interest in trajectory determination applications.

The actual reference frame, used in this particular research, is the wander frame. The wander frame is similar to the local level frame, except that the Y-axis is not slaved to the North direction. Thus the main difference between these two frames is meridian convergence. Implementation of the wander azimuth system allows one to avoid problems due to large rotations at high latitudes

necessary to maintain the orientation of the local-level frame, whenever it moves along a parallel.

The mechanization process, described below, is given in schematic form in Figure 3.1 on page 43.

3.2.2 Transformation of Body Sensed Angular Rates

The gyro measurement data are integrated to establish the computational frame, provided the initial orientation is given. The transformation matrices, describing the relationship of the measurement frame with respect to the computational and inertial frames, include body to wander transformation matrix $\mathbf{R}_b^w$ and wander to earth transformation matrix $\mathbf{R}_w^e$.

In the first step the measured body rates of the SISS, $\tilde{\omega}_{ib}^b$ are compensated by the drift $\mathbf{d}$ determined in the calibration, namely:

$$\omega_{ib}^b = \tilde{\omega}_{ib}^b - \mathbf{d} \quad . \tag{3.9}$$

The rotations ω_{iw}^b of the wander frame with respect to the inertial frame coordinatized in the body frame have to be removed from the measured angular velocities before integration by

$$\omega_{wb}^b = \omega_{ib}^b - \omega_{iw}^b \quad . \tag{3.10}$$

The angular velocity of the wander frame with respect to the inertial frame ω_{iw}^b can be expressed using the wander to body transformation matrix $\mathbf{R}_w^b$ and the angular velocity of the wander frame Ω_{iw}^w, namely:

$$\Omega_{iw}^{b} = \mathbf{R}_{w}^{b}\,\Omega_{iw}^{w}\,. \tag{3.11}$$

The angular velocity of the wander frame with respect to the inertial frame ω_{iw}^{w}, expressed in the wander frame is caused by rotational movements of the SISS with respect to the Earth frame and by rotation of the Earth itself. It can be expressed by

$$\omega_{iw}^{w} = \omega_{ie}^{w} + \omega_{ew}^{w}\,. \tag{3.12}$$

The wander Earth rate ω_{iw}^{w} can be computed, transforming the well-known formula for the Earth rate ω_{ie}^{n} , expressed in the local level frame (Wong, 1982), to the wander frame

$$\Omega_{ie}^{w} = \mathbf{R}_{n}^{w}\,\Omega_{ie}^{n}\,, \tag{3.13}$$

where

$$\omega_{ie}^{n} = \begin{pmatrix} 0 \\ \omega_e \cos\phi \\ \omega_e \sin\phi \end{pmatrix}, \tag{3.14}$$

thus yielding

$$\omega_{ie}^{w} = \begin{pmatrix} \omega_e \sin\alpha\cos\phi \\ \omega_e \cos\alpha\cos\phi \\ \omega_e \sin\phi \end{pmatrix}. \tag{3.15}$$

Vehicle rate can be computed in a similar way through simple substitutions, namely:

$$\Omega_{ew}^{w} = \mathbf{R}_{n}^{w}\,\Omega_{ew}^{n} = \mathbf{R}_{n}^{w}\,(\,\Omega_{en}^{n} + \Omega_{nw}^{n}\,), \tag{3.16}$$

thus giving the formula in terms of angular velocities in the wander frame

$$\omega_{ew}^{w} = \begin{pmatrix} \dfrac{\cos\alpha(-\sin\alpha v_x^w - \cos\alpha v_w^x)}{R_1+h} + \dfrac{\sin\alpha(-\cos\alpha v_x^w - \sin\alpha v_w^x)}{R_2+h} \\ \dfrac{-\sin\alpha(-\sin\alpha v_x^w - \cos\alpha v_w^x)}{R_1+h} + \dfrac{\cos\alpha(-\cos\alpha v_x^w - \sin\alpha v_w^x)}{R_2+h} \\ 0 \end{pmatrix} . \quad (3.17)$$

Substituting the angular rate ω_{ew}^{w} back into equation (3.12) and using equations (3.11) and (3.10), the angular velocity of the wander frame with respect to the body frame ω_{bw}^{b} can be computed. Consequently the two basic transformation matrices $\mathbf{R}_b^w$ and $\mathbf{R}_w^e$ can be updated by solving the differential equations

$$\dot{\mathbf{R}}_b^w = \mathbf{R}_b^w \, \Omega_{wb}^{b} , \quad (3.18)$$

$$\dot{\mathbf{R}}_w^e = \mathbf{R}_w^e \, \Omega_{ew}^{w} . \quad (3.19)$$

Different numerical methods are applied for the solution of the above equations. The integration of the second equation (3.19) may be performed at a much lower rate than integration of equation (3.18), mainly because geographic coordinates ϕ,λ and vehicle velocity do not change fast in low dynamic applications. Quaternion integration must be performed for the solution of the first equation (3.18), at a rate compatible with attitude changes. The updated quaternions are then used to derive the direction cosine matrix $\mathbf{R}_b^w$. For details see (Van Bronkhorst, 1978; Wong, 1988). The matrix $\mathbf{R}_b^w$ is used to transform

acceleration measurements from the body frame to the wander frame and to derive the Euler angles - pitch, roll and azimuth. These are then used with the navigation variables to compute various system outputs. The second equation (3.19) is solved in first order approximation as

$$\mathbf{R}_w^e = \mathbf{R}_w^e (\mathbf{I} + \Omega_{ew}^w) \Delta t , \tag{3.20}$$

where Δt denotes the interval between SISS measurements.

3.2.3 Transformation of Body Sensed Acceleration

The measured specific force $\tilde{\mathbf{f}}^b$ is corrected for accelerometer biases determined in the calibration process by

$$\mathbf{f}^b = \tilde{\mathbf{f}}^b - \mathbf{b} . \tag{3.21}$$

In order to get vehicle acceleration $\mathbf{a}^w$ in the wander frame, the effect of frame rotation must be removed from $\mathbf{f}^b$. The non-vehicle accelerations include Coriolis, tangential and centrifugal accelerations. Equation (3.6) expressed in the wander frame has the form:

$$\mathbf{a}^w = \mathbf{R}_b^w \mathbf{f}^b - (2\omega_{ie}^w + \omega_{ew}^w) \times \mathbf{v}^w + \gamma^w , \tag{3.22}$$

where the first term gives specific force, the second Coriolis acceleration and the third the combined effect of gravitational and centrifugal acceleration. The last term can be approximated by the

normal gravity vector, whose Z-component is given by the well-known formula of Somigliana (Heiskanen and Moritz, 1967).

3.2.4 Navigation Output

Velocity in the wander frame can then be computed directly as

$$\mathbf{v}^{w} = \mathbf{v}^{w} + \mathbf{a}^{w}\Delta t \,, \tag{3.23}$$

where the velocity on the right-hand side is obtained from measurements at the previous epoch and accelerations during Δt, the measurement interval. The ellipsoidal heights are computed directly from the vertical component of velocity v_z^w in the wander frame as

$$h = h + v_z^w \Delta t \quad . \tag{3.24}$$

The computed height can be fed back for computation of a more accurate value of normal gravity. Refined transformation matrices $\mathbf{R}_b^w$ and $\mathbf{R}_w^e$ can be recomputed from equations (3.10) to (3.20), using the current wander velocity (3.23). Both of these matrices contain navigation parameters of interest.

The latitude ϕ, longitude λ and wander angle α can computed from the elements of the matrix $\mathbf{R}_w^e$, that is,

$$\phi = \sin^{-1}\left(\mathbf{R}_w^e(3,3) \right) \,, \tag{3.25}$$

$$\lambda = \tan^{-1}\left(\frac{\mathbf{R}_w^e(2,3)}{\mathbf{R}_w^e(1,3)}\right), \tag{3.26}$$

and

$$\alpha = \tan^{-1}\left(\frac{\mathbf{R}_w^e(3,1)}{\mathbf{R}_w^e(3,2)}\right). \tag{3.27}$$

The conventional Euler angles: pitch, roll and azimuth are obtained from elements of $\mathbf{R}_b^w$. They are given by

$$p = \sin^{-1}\left(\mathbf{R}_b^w(3,2)\right), \tag{3.28}$$

$$r = \tan^{-1}\left(\frac{\mathbf{R}_b^w(3,1)}{\mathbf{R}_b^w(3,3)}\right), \tag{3.29}$$

and

$$A = \tan^{-1}\left(\frac{\mathbf{R}_b^w(1,2)}{\mathbf{R}_b^w(2,2)}\right) - \alpha. \tag{3.30}$$

The mechanization equations from (3.10) to (3.30) are given in schematic form at Figure 3.1.

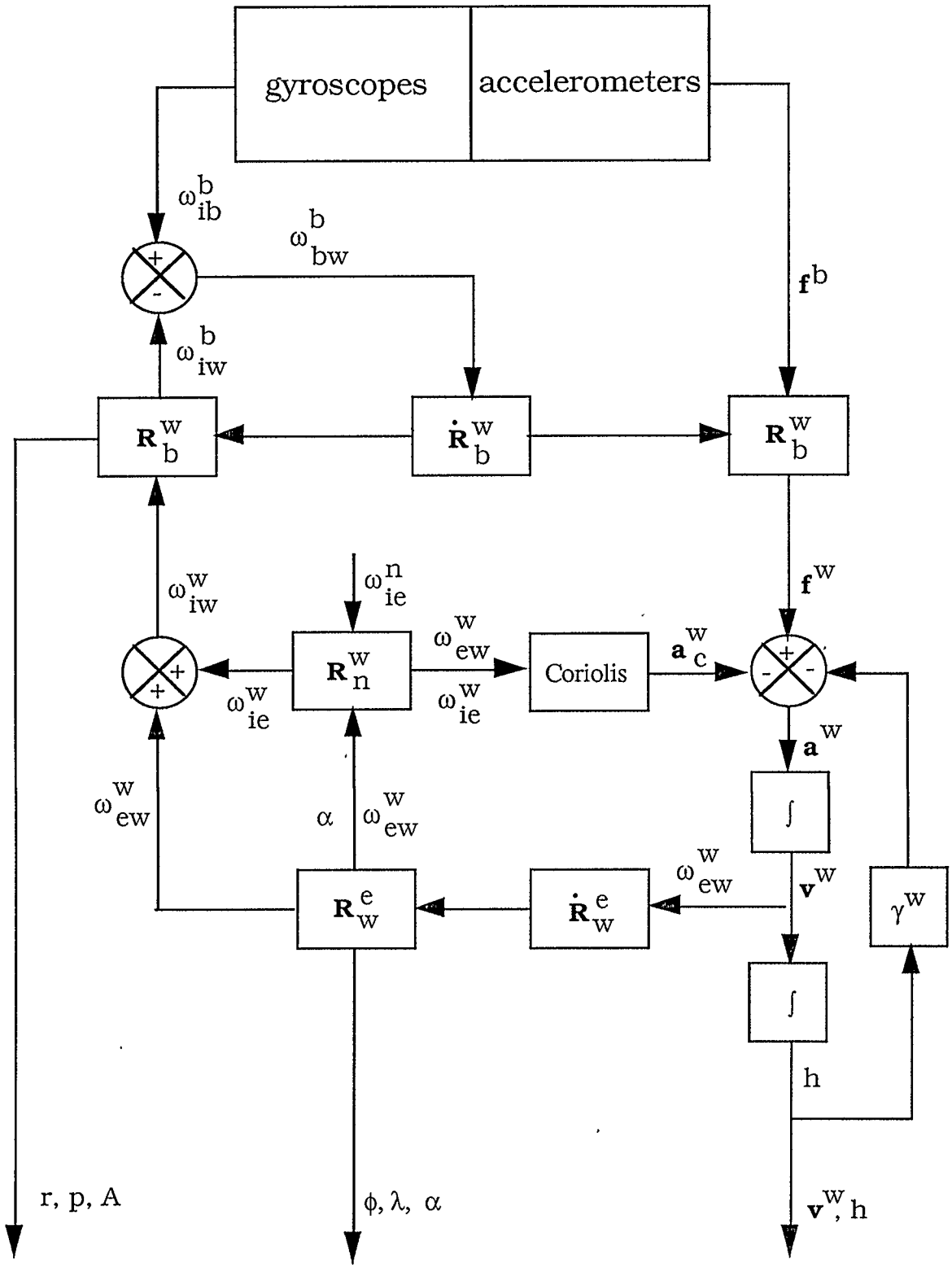

Fig 3.1: Flowchart of Strapdown Mechanization

3.3 Alignment

The navigation equations require knowledge of the initial Euler angles roll, pitch and azimuth, for the computation of the initial attitude matrix $\mathbf{R}_b^w$. These quantities are determined in the alignment process, at the beginning of the survey, when the INS is in stationary mode. First, coarse alignment is performed, obtaining approximate values for the attitude parameters. These approximate Euler angles are refined in fine alignment via a Kalman filter. In broad terms, the alignment principle is based on the fact that in static mode the gyroscopes sense only the earth rate while the accelerometers sense only gravity, therefore alignment involves gyro-compassing and self-levelling. Gyrocompassing is less accurate than self-levelling because of the weak nature of the earth-rate signal.

In gyro-compassing, the initial azimuth of the body system is computed, thus establishing local North. The initial azimuth is determined from the measured gyro rates by the equation

$$\omega_{ie}^{w} = \begin{pmatrix} \omega_e \sin A \cos\phi \\ \omega_e \cos A \cos\phi \\ \omega_e \sin\phi \end{pmatrix} = \mathbf{R}_b^w \, \omega_{ie}^{b} \quad , \tag{3.31}$$

which gives the initial azimuth as

$$A = \tan^{-1}\left(\frac{\omega_{ie}^{w}(1)}{\omega_{ie}^{w}(2)} \right) \quad . \tag{3.32}$$

In self-levelling, pitch and roll are computed using the accelerometer output. A strapdown system senses gravity components in the body axes of the mislevelled system. The velocity output of the mechanized navigation module, transformed to the body frame can be used to compute the roll and pitch, which in fact appear as errors in the level axes. The non-zero velocity output generated by the navigation module is caused by mislevellment given by roll and pitch. The roll r and pitch p are computed as:

$$r = \sin^{-1}\left(\frac{v_b^x}{\gamma\,\Delta t}\right), \tag{3.33}$$

$$p = -\sin^{-1}\left(\frac{v_b^y}{\gamma\,\Delta t}\right), \tag{3.34}$$

where Δt is the interval between resets.

The computed roll, pitch and azimuth are refined, together with gyro drifts and accelerometer biases, in the fine alignment using a Kalman filter that is updated with zero velocity updates in 10 seconds update intervals. After every update the Euler angles as well as the velocity and coordinates are reset. The typical alignment procedure takes about 10 minutes.

Chapter 4

Error Analysis

Error modelling is fundamental for dynamic parameter estimation from measurements. It describes the mathematical relationship between different error sources and is usually formulated in state space form. If external information is available, these errors can be estimated using different processing techniques. One of the most common processing techniques is Kalman filtering. The purpose of this chapter is to formulate a framework for GPS/INS dynamic parameter estimation using the state space approach.

In this chapter, the fundamental concept of dynamic systems modelling by state equations, is revieved first. Kalman filtering is introduced and filter equations are listed and discussed. Linearization of the non-linear dynamic systems equations is outlined next. Finally, the error models for both dynamic systems under consideration, i.e. GPS and INS, are given.

4.1 State Space Approach

Mathematical modelling of kinematic systems such as GPS and INS is usually done in the framework of linear dynamic systems. The

dynamic behaviour of such system can be described using state space representation. In this approach one reduces a system of higher order differential equations to a system of differential equations of first order. The set of n first order differential equations written in matrix form has the general explicit form:

$$\dot{\mathbf{x}} = \mathbf{F}(t)\mathbf{x}(t) + \mathbf{G}(t)\mathbf{w}(t) \ , \tag{4.1}$$

with initial conditions

$$\mathbf{x}\ (t_0) = \mathbf{x_0} \ ,$$

where	$\mathbf{x}$	is the state vector,
	$\dot{\mathbf{x}}$	is the time derivative of the state vector,
	$\mathbf{F}$	is the dynamics matrix,
	$\mathbf{w}$	is the random forcing function,
	$\mathbf{G}$	is the coefficient matrix of the random forcing functions,
and	$\mathbf{x_0}$	is the vector of initial values.

The state vector is a set of variables which suffice to describe the system behaviour completely. The choice of state variables is arbitrary in principle. In actuality, we are concerned only with the most convenient description of the system, in terms of observability and speed of computations. The physical properties are invariant with respect to the representation.

The above equation shows that the change of the state vector with time is composed of two parts, the quasi-deterministic part

governed by the dynamics matrix and the stochastic part determined by the forcing functions. The random forcing function is assumed to be uncorrelated in time and is thus treated as white noise. Given the state vector at time t_o, the state at any other time can be computed within a range given by the stochastic term of equation (4.1).

In general, the solution of a set of nonhomogeneous differential equations is not always possible. The solution of the homogeneous differential equation

$$\dot{\mathbf{x}} = \mathbf{F}(t)\mathbf{x}(t) \ , \tag{4.2}$$

is of the form

$$\mathbf{x}\ (t) = \Phi(t,t_o)\mathbf{x_o} \ , \tag{4.3}$$

where Φ is the transition matrix.

The particular solution of equation (4.1) is obtained by including the effect of the forcing functions in equation (4.1). The solution can be written in the general form

$$\mathbf{x}\ (t) = \Phi(t,t_o)\mathbf{x_o} + \int_{t_o}^{t} \Phi(\tau,t_o)\ \mathbf{G}(\tau)\ \mathbf{w}(\tau)d\tau \ , \tag{4.4}$$

known as the matrix superposition integral. It is characterized by the transition matrix, Φ , the vector of the initial values $\mathbf{x_o}$ and the random forcing function **Gw**.

The transition matrix obeys the conditions:

$$\dot{\Phi}(t,t_o) = \mathbf{F}(t)\Phi(t,t_o) \ , \tag{4.5}$$

$$\Phi(t_o,t_o)=\mathbf{I} \ , \tag{4.6}$$

where $\mathbf{I}$ is the identity matrix.

If $\mathbf{F}$ can be considered constant for the time interval Δt, the transition matrix can be derived analytically or numerically. Analytical methods include the method of inverse Laplace-transformation or eigenvalue decomposition. In practical applications the numerical approach is prefered, often using a simple approximation of the form

$$\Phi\ (t,t_o) = \mathbf{I} + \mathbf{F}\ \Delta t \ , \tag{4.7}$$

where $\mathbf{I}$ is the identity matrix and

$$\Delta t = t - t_o \ .$$

The total transition matrix between epoch o and k becomes the product Π of the intermediate transition matrices Φ_i

$$\Phi_{o,k} = \prod_{i=1}^{k} \Phi_i \ . \tag{4.8}$$

4.2 Kalman Filtering

Implementations of above system requires measurements. Measurements have errors cumulative in case of integration. These errors can be controled if external measurements are available. Such a

process is termed measurement update. Any measurement that can be expressed as a linear function of the state vector components can be used

$$\mathbf{l} = \mathbf{A}\,\mathbf{x} + \mathbf{e}\,, \tag{4.10}$$

where $\mathbf{l}$ is the vector of the measurements,

$\mathbf{A}$ is the design matrix,

and $\mathbf{e}$ is the vector of measurement noise.

The vector $\mathbf{e}$ is assumed to be a vector of random noise quantities with zero mean and covariance matrix $\mathbf{C}^e$.

Kalman filtering provides an optimal estimate of the system state at the current time, i.e. of the unknown elements of the state vector from all past and present information, provided the statistical properties of the system are reasonably well known. If both past and future measurements are used in post-mission mode, the estimation process is termed optimal smoothing. In this research only the filtering techniques are used. In the Kalman filter, the final state estimate is based on a combination of predicted states and actual measurements. It has the property of unbiasedness, minimum variance and consistency (Gelb, 1974).

The Kalman filter equations are given in detail in (Gelb,1974) and are listed below:

Prediction: $$\mathbf{x}_{k+1}(-) = \Phi_{k+1,k}\ \mathbf{x}_k\,, \tag{4.11}$$

$$\mathbf{C}^x(-) = \Phi_{k+1,k}\ \mathbf{C}^x\ \Phi^T_{k+1,k} + \mathbf{C}^w_{k+1,k}\ , \tag{4.12}$$

Update:

$$\mathbf{x}(+) = \mathbf{x}(-) + \mathbf{K}\{\ \mathbf{l} - \mathbf{A}\mathbf{x}(-)\}\ , \tag{4.13}$$

$$\mathbf{C}^x(+) = \{\ \mathbf{I} - \mathbf{KA}\ \}\mathbf{C}^x(-)\ , \tag{4.14}$$

$$\mathbf{K} = \mathbf{C}^x(-)\mathbf{A}^T\{\ \mathbf{A}\ \mathbf{C}^x(-)\mathbf{A}^T + \mathbf{C}^e\ \}^{-1}\ , \tag{4.15}$$

where $\mathbf{x}$ is the state vector,

Φ is the transition matrix,

$\mathbf{C}^x$ is the state covariance matrix,

$\mathbf{C}^w$ is the process noise covariance matrix,

$\mathbf{K}$ is the Kalman gain matrix,

$\mathbf{l}$ are the observations,

$\mathbf{A}$ is the design matrix,

and $\mathbf{C}^e$ is the measurement noise matrix.

The covariance matrix of the system noise $\mathbf{C}^w$ can be computed from the following equation:

$$\mathbf{C}^w = \int_0^{t_k - t_{k-1}} \mathbf{Q}(\tau)\ t_k d\tau\ , \tag{4.16}$$

where $\mathbf{Q}$ is the spectral density matrix of the noise.

The above equations express the updated state vector in terms of the predicted state and some external measurement vector. The new estimate, the measurement and the old estimate refer to the same instant. The observation information that was gathered up to the present moment is contained in state vector $\mathbf{x}$ and associated covariance matrix $\mathbf{C}^x$. Equations (4.11) to (4.15) are recursive, that is,

once all measurements at an epoch have been processed, the cycle starts again and the state is extrapolated to the next epoch. The off-diagonal terms of the covariance matrix express the statistical cross-correlation among the modelled states of the Kalman filter. These correlation terms determine the optimal Kalman gain, which in turn permits the optimal incorporation of external aiding measurements. In addition, the Kalman filter accounts for temporal correlation via the transition matrix Φ, computed from the dynamics matrix $\mathbf{F}$.

If the measurement noise covariance matrix is diagonal, i.e. if the measurements are uncorrelated with respect to one another, then they can be processed one at a time in scalar fashion. This eliminates the matrix inversion in equation (4.15), necessary for computation of the Kalman gain matrix $\mathbf{K}$. This matrix reduces to a vector, and thus results in a saving of computation time.

The standard Kalman filter algorithm may be numerically unstable in some applications (Bierman, 1977). This results in losing the positive-definiteness of the state vector covariance matrix. Alternate Kalman filter algorithms have been developed such as the Square Root Information Filter or U-D factorization filter. These have the advantages of preserving numerical accuracy and have almost the same speed as the standard Kalman filter algorithm. Practical investigations of the different methods for GPS/INS case show that there is no significant difference between different implementations (Czompo et al, 1990). Therefore in this research, the standard Kalman filter was implemented.

4.3 Linearization

The derivation of the Kalman filter equations is based on the assumption of linearity in the dynamics process (4.1) and observation model (4.10). In practice, there is a wide range of applications which contain nonlinear dynamics as well as nonlinear measurement relationships. It means that the basic equations (4.1) and (4.10) have to be written in the form

$$\frac{d\mathbf{x}}{dt} = \mathbf{f}(t,\mathbf{x}(t)) + \mathbf{u}(t) \ , \tag{4.17}$$

$$\mathbf{l} = \mathbf{h}(\mathbf{x}(t),t) + \mathbf{e} \ , \tag{4.18}$$

where **f** and **h** are known functions of time and state vector **x**.

In order to simplify this problem, both relationships can be expanded into Taylor series about some nominal vector $\tilde{\mathbf{x}}(t)$ in state space, which is close to $\mathbf{x}(t)$. The actual state vector $\mathbf{x}(t)$ can be written as

$$\mathbf{x}(t) = \tilde{\mathbf{x}}(t) + \Delta\mathbf{x}(t) \ . \tag{4.19}$$

Expanding the above equations into a Taylor series truncated after the first-order term and dropping the t inside the brackets,results in

$$\dot{\tilde{\mathbf{x}}} + \Delta\dot{\mathbf{x}} = \mathbf{f}(\dot{\tilde{\mathbf{x}}}) + \frac{\partial\mathbf{f}}{\partial\mathbf{x}}\Delta\mathbf{x} + \mathbf{u} \ , \tag{4.20}$$

$$\mathbf{l} = \mathbf{h}(\tilde{\mathbf{x}}) + \frac{\partial\mathbf{h}}{\partial\mathbf{x}}\Delta\mathbf{x} + \mathbf{e} \ , \tag{4.21}$$

where $\frac{\partial \mathbf{f}}{\partial \mathbf{x}}$ and $\frac{\partial \mathbf{h}}{\partial \mathbf{x}}$ are Jacobians of **f** and **h**, matrices of partial derivatives of **f** and **h** with respect to the components of state vector x, evaluated at point $\tilde{\mathbf{x}}$

$$\mathbf{F} = \frac{\partial \mathbf{f}}{\partial \mathbf{x}} = \begin{bmatrix} \frac{\partial f_1}{\partial x_1} & \cdots & \frac{\partial f_1}{\partial x_n} \\ \cdots & \cdots & \cdots \\ \frac{\partial f_n}{\partial x_1} & \cdots & \frac{\partial f_n}{\partial x_n} \end{bmatrix} \quad \mathbf{A} = \frac{\partial \mathbf{h}}{\partial \mathbf{x}} = \begin{bmatrix} \frac{\partial h_1}{\partial x_1} & \cdots & \frac{\partial h_1}{\partial x_n} \\ \cdots & \cdots & \cdots \\ \frac{\partial h_n}{\partial x_1} & \cdots & \frac{\partial h_n}{\partial x_n} \end{bmatrix} . \tag{4.22}$$

The nominal point is chosen to satisfy the equation

$$\dot{\tilde{\mathbf{x}}} = \mathbf{f}(\tilde{\mathbf{x}}) \ . \tag{4.23}$$

Substituting the equation (4.23) into the equation (4.20), the linear differential terms, involving only the perturbation quantities $\Delta\mathbf{x}$, emerge. The perturbation $\Delta\mathbf{x}$ of the state vector from some reference trajectory is commonly called the error state. This name is used in following, keeping in mind that it originates from the linearization process.

Equations(4.20) and (4.21) can be written in the form

$$\Delta\dot{\mathbf{x}} = \frac{\partial \mathbf{f}}{\partial \mathbf{x}} \Delta\mathbf{x} + \mathbf{u} \ , \tag{4.24}$$

$$\mathbf{l} - \mathbf{h}(\tilde{\mathbf{x}}) = \frac{\partial \mathbf{h}}{\partial \mathbf{x}} \Delta\mathbf{x} + \mathbf{e} \ . \tag{4.25}$$

The equations (4.24) and (4.25) have a structure typical for linear systems, therefore all equations of the linear Kalman filter (4.11 to 4.15) can be applied for the estimation of perturbations $\Delta\mathbf{x}$ from the reference trajectory determined by $\tilde{\mathbf{x}}$. If $\tilde{\mathbf{x}}$ is defined prior to processing the measurement data, the filter is called linearized Kalman filter (Gelb, 1974). In the extended Kalman filter, the equations are linearized about a trajectory, that is continuously updated with the state estimates resulting from the measurements. Throughout this research the extended Kalman filter is used.

Equation (4.24), describing the error state change, will be introduced for each dynamic system under consideration, that is for GPS and INS, in the following paragraphs.

4.4 INS Error State and Dynamics Matrix

The INS errors describe attitude, position, velocity and sensor errors. The error state vector, for the strapdown INS considered here, is

$$\mathbf{x} = \{ \varepsilon_N, \varepsilon_E, \varepsilon_U, \delta\phi, \delta\lambda, \delta h, \delta v_N, \delta v_E, \delta v_H, d_X, d_Y, d_Z, b_X, b_Y, b_Z \}^T, \tag{4.26}$$

where $\varepsilon_N, \varepsilon_E, \varepsilon_U$ are initial platform misalignments,

$\delta\phi, \delta\lambda, \delta h$ are errors in latitude, longitude and height,

$\delta v_N, \delta v_E, \delta v_H$ are errors in north, east, up velocities,

d_X, d_Y, d_Z are x, y, z residual gyro drifts in the body system,

and b_X, b_Y, b_Z are x, y, z residual accelerometers biases in the body system.

The error model for the strapdown system is well known and is given in detail in (Schmidt, 1978) or (Wong, 1988). Below, the final error equations are listed and their associated dynamics matrix is given.

4.4.1 Misalignments Error Equations

The misalignments, ε between body and local-level frame directly affect the angular rate of the body frame with respect to the local level frame. They are written in the form

$$\dot{\varepsilon} = \delta\omega_{nb}^{n} . \tag{4.27}$$

Differentiating equation (3.9) and using equations (3.10) to (3.20), the misalignment error equation can be expressed in the form

$$\dot{\varepsilon} = - \Omega_{in}^{n} \varepsilon - \delta\omega_{in}^{n} + \mathbf{R}_{b}^{n} \delta\mathbf{d} . \tag{4.28}$$

4.4.2 Position Error Equations

The error equations for the coordinate states are simply:

$$\delta\dot{\mathbf{r}}^{n} = \delta\mathbf{v}^{n} . \tag{4.29}$$

4.4.3 Velocity Error Equations

The velocity error equations are derived from the acceleration equation (3.22) as

$$\delta\dot{\mathbf{v}}^n = \mathbf{E}\mathbf{f}^n - (\Omega_{en}^n + 2\,\Omega_{ie}^n)\delta\mathbf{v}^n + (\delta\Omega_{en}^n + 2\,\delta\Omega_{ie}^n)\mathbf{v}^n + \mathbf{R}_b^n\,\delta\mathbf{b} - \frac{\partial\gamma}{\partial h}\,\delta h\,. \tag{4.30}$$

4.4.4 Gyro Drifts and Accelerometer Biases Error Equations

Gyro drifts and accelerometer biases are the errors remaining in the sensors after system calibration.The rates of change of the gyro drifts **d** and accelerometer biases **b** can be modeled by a first-order Gauss-Markov process, namely:

$$\dot{\mathbf{d}} = -\,\zeta\mathbf{d} + \mathbf{w}_d\,, \tag{4.31}$$

$$\dot{\mathbf{b}} = -\,\beta\mathbf{b} + \mathbf{w}_b\,, \tag{4.32}$$

where ζ, β are reciprocals of the correlation times of the respective processes,

and $\mathbf{w}_d, \mathbf{w}_b$ white noise of the respective processes.

The values for the correlation times as well as the white noise of the respective processes are obtained in calibration tests prior to the survey.

The INS dynamics matrix, describing the error rates as well as interrelation between different error sources, is derived from equations (4.26) to (4.32) and is given in Figure 4.1.

$$
\begin{matrix}
0 & -\omega\sin\phi & -\dot{\phi} & \omega\sin\phi & 0 & 0 & -\cos\phi & 0 & 0 & R_{12} & R_{22} & R_{23} & 0 & 0 & 0 \\
\omega\sin\phi & 0 & -\omega\cos\phi & 0 & 0 & 1 & 0 & 0 & 0 & R_{11} & R_{12} & R_{13} & 0 & 0 & 0 \\
-\dot{\phi} & \omega\cos\phi & 0 & -\omega\cos\phi & 0 & 0 & -\sin\phi & 0 & 0 & R_{31} & R_{32} & R_{33} & 0 & 0 & 0 \\
0 & 0 & 0 & 0 & 0 & 1 & 0 & 0 & 0 & 0 & 0 & 0 & 0 & 0 & 0 \\
0 & 0 & 0 & 0 & 0 & 0 & 1 & 0 & 0 & 0 & 0 & 0 & 0 & 0 & 0 \\
0 & -f_U/R_M & f_E/R_M & 0 & 0 & 0 & -\omega\sin 2\phi & 0 & -\dot{\phi}/R_M & 0 & 0 & 0 & R_{21}/R_M & R_{22}/R_M & R_{23}/R_M \\
f_U/R_E & 0 & -f_N/R_E & 0 & 0 & 2\omega\tan\phi & 0 & 0 & -2\omega/R_P & 0 & 0 & 0 & R_{11}/R_E & R_{22}/R_E & R_{13}/R_E \\
0 & 0 & 0 & 0 & 0 & 0 & 0 & 0 & 1 & 0 & 0 & 0 & 0 & 0 & 0 \\
-f_E & f_N & 0 & 0 & 0 & 2R_M\dot{\phi} & 2R_E\cos\phi & c & 0 & 0 & 0 & 0 & R_{31} & R_{32} & R_{33} \\
0 & 0 & 0 & 0 & 0 & 0 & 0 & 0 & 0 & -\zeta & 0 & 0 & 0 & 0 & 0 \\
0 & 0 & 0 & 0 & 0 & 0 & 0 & 0 & 0 & 0 & -\zeta & 0 & 0 & 0 & 0 \\
0 & 0 & 0 & 0 & 0 & 0 & 0 & 0 & 0 & 0 & 0 & -\zeta & 0 & 0 & 0 \\
0 & 0 & 0 & 0 & 0 & 0 & 0 & 0 & 0 & 0 & 0 & 0 & -\beta & 0 & 0 \\
0 & 0 & 0 & 0 & 0 & 0 & 0 & 0 & 0 & 0 & 0 & 0 & 0 & -\beta & 0 \\
0 & 0 & 0 & 0 & 0 & 0 & 0 & 0 & 0 & 0 & 0 & 0 & 0 & 0 & -\beta
\end{matrix}
$$

R_{ij} is the element in the ith row and j^{th} column of matrix $\mathbf{R}_b^n$

$c = 2\gamma + k$

Fig. 4.1: Dynamics matrix **F** of a 15-state INS Kalman Filter

4.5 GPS Error State and Dynamics Matrix

The GPS error model can be derived from the kinematic model describing the GPS vehicle trajectory (Schwarz et al, 1989). In this model the position **r** of the vehicle at consecutive times t_i and t_{i+1} is represented as

$$\mathbf{r}_{i+1} = \mathbf{r}_i + \dot{\mathbf{r}}_i \Delta t + \ddot{\mathbf{r}}_i \Delta t^2 + \ldots , \tag{4.33}$$

where $\Delta t = t_{i+1} - t_i$.

The series is truncated due to assumption made about the dynamics of the vehicle. In practice, either constant velocity or constant acceleration models are used (Schwarz et al, 1989). In this study the constant velocity model is used, that is

$$\mathbf{r}_{i+1} = \mathbf{r}_i + \dot{\mathbf{r}}_i \Delta t \ . \tag{4.34}$$

The error equations related to this model have the simple form

$$\delta\dot{\mathbf{r}} = \delta\mathbf{v} \ , \tag{4.35}$$

$$\delta\dot{\mathbf{v}} = 0 \ . \tag{4.36}$$

The above equation can be modified to take into account the disturbing accelerations which can be considered as stochastic zero

mean process, correlated over a certain time period T. These can be modeled as a first order Gauss-Markov process

$$\delta\dot{\mathbf{v}} = -\tau\mathbf{v} + \mathbf{w}\,, \tag{4.37}$$

where τ is the reciprocal of the correlation time T.

In the general case, besides dynamic process errors, error modeling should include the specific error sources affecting the observations. The GPS double difference observable, after resolution of ambiguities, is free of systematic errors, see equation (2.5). The GPS state error can then be expressed simply in terms of $\delta\mathbf{r}$, $\delta\mathbf{v}$ as

$$\mathbf{x} = \{\, \delta\phi,\ \delta\lambda,\ \delta h,\ \delta v_N,\ \delta v_E,\ \delta v_H \}^T\,. \tag{4.38}$$

One notes that the GPS state vector is thus a subset of the INS state vector where this subset consists of errors in position and velocity. Should other GPS observable be used, i.e. single difference, this error state must incorporate associated observable errors such as clock biases and drifts.

The GPS dynamics matrix $\mathbf{F}$ given by error equations (4.35) to (4.37) has the form

$$\mathbf{F} = \begin{bmatrix} 0 & 0 & 0 & 1/R_M & 0 & 0 \\ 0 & 0 & 0 & 0 & 1/R_E & 0 \\ 0 & 0 & 0 & 0 & 0 & 1 \\ 0 & 0 & 0 & \tau & 0 & 0 \\ 0 & 0 & 0 & 0 & \tau & 0 \\ 0 & 0 & 0 & 0 & 0 & \tau \end{bmatrix}\,. \tag{4.39}$$

The transition matrix Φ, can be easily derived, using equation (4.7), and can be found in explicit form in (Schwarz et al, 1989).

Chapter 5

GPS/INS Integration

Having introduced basic GPS and INS observation models in Chapters 2 and 3 as well as their dynamic error models in Chapter 4, the GPS/INS integration model will be examined in this chapter.

First, the complementary role of GPS and INS techniques is discussed and various GPS/INS integration configurations are briefly outlined. The carrier phase cycle slip correction and detection algorithm using INS position output is then developed. Finally, Kalman filter design, combining GPS and INS data, is presented and the lever arm correction is derived.

5.1 Complementary Role of GPS and INS

The goal of GPS/INS integration is to improve system performance over stand-alone GPS or INS systems. In brief, integration involves combining the advantages of individual systems while limiting their disadvantages. It results in a more versatile, accurate and reliable system but adds to the system cost and complexity. The trade-off between these factors has to be taken into account when designing such a system.

The significance of the pros and cons of the integrated versus the stand-alone system varies depending on the application. Generally, GPS provides highly accurate position, velocity and time data, and is unaffected by mission length or time since update. The main factor limiting the use of GPS in some situations is the requirement for line-of-sight between the receiver antenna and the satellites. In contrast, the INS is a self-contained measuring unit. It provides position, velocity and attitude at a high rate, but has time dependent error characteristics. These errors can be limited using GPS derived position and velocity to update the INS.

The integration process can be performed at different levels, i.e. hardware or software, and in different fashions depending on the specific situation. Hardware integration implies mutual aiding of the measuring processes in the systems. An example of this is GPS carrier loop aiding with INS velocity information. It is mainly used in high dynamic applications, eg, airborne navigation, for limiting the tracking loop bandwidth, filtering out the disturbing noise and achieving fast acquisition of the signal after loss of lock. Assembling a GPS receiver with an INS in one unit, enables volume, weight and power reduction, compared to separate units (Camberlain and Capit, 1990). Such hardware integrated units are used in a number of military applications (Camberlain and Capit, 1990) and are currently being evaluated for civil aviation. Another form of hardware integration is the torquing of the inertial platform based on INS error estimation with GPS. This design has the disadvantage however, that incorrect GPS

information would cause false torquing commands and therefore inaccurate navigation.

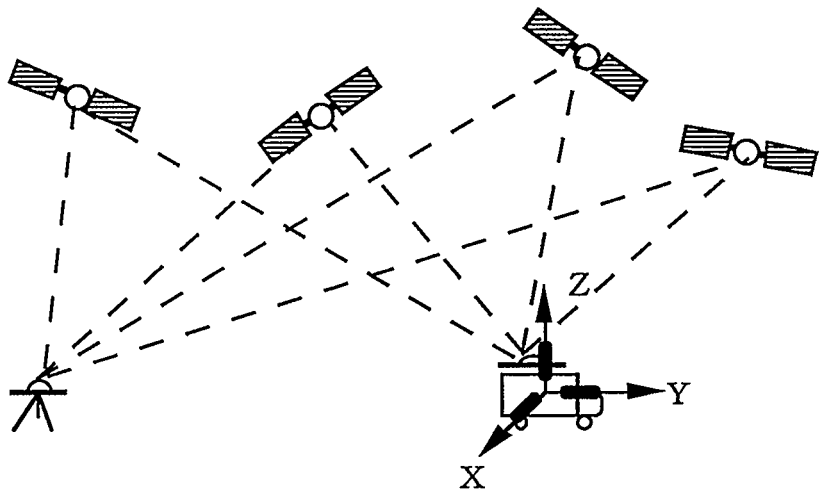

Fig. 5.1: Integrated GPS/INS Relative Positioning

Most GPS/INS system designs are integrated at the software level, without aiding at the measurement level. Software integration usually involves processing of separate streams of data from each independent sensor in central computer. The strapdown INS system is an ideal candidate for this type of integrated system. It simply outputs gyro and acceleration data to a computer, which then estimates navigation parameters without any feedback to the hardware. GPS and strapdown INS data can be combined in a computer in real time or in post-mission to get an optimal estimate of position, velocity and attitude. GPS data from one receiver, or two receivers operating in differential mode can be used, depending on applications and accuracy requirements. Results of integrating single receiver pseudorange and phase data with an INS, show that this method is suited for low-accuracy navigation applications (Wong et al, 1988). Higher accuracy

geodetic applications require the combination of an INS with differential GPS carrier phase measurements (Fig. 5.1). The following discussion is related to the integration of a strapdown system with single frequency receivers operating in a differential mode.

This hybrid system is particularly suited for trajectory determination, which requires the continuous determination of six degrees of freedom, usually represented by position and attitude. Low rate, high accuracy GPS position and velocity can be used to update the INS. The INS will then maintain, at high rate, highly accurate position and attitude between the GPS updates. On the other hand, redundant precise positional information from the INS can be used for cycle slip detection and correction, which is the limiting factor for high accuracy GPS performance in stand-alone mode. Thus integration of both positioning systems results in more reliable and more flexible system.

5.2 Cycle Slip Detection and Correction

GPS/INS integration provides a solution to the GPS carrier phase cycle slip problem. The algorithm for cycle slip detection and correction takes advantage of the GPS observable used, i.e. the double difference. It uses the fact, that double differences are dependent on receiver and satellite positions and ambiguity parameters, if residual atmospheric effects and measurement noise can be neglected, see equation (2.5). Since the change in the vehicle's position can be derived from the INS output, and the change in satellite position from

the broadcast ephemeris, it is possible to compute the double difference, $\nabla\Delta\Phi$. By monitoring the cycle differences, δ, between the computed and observed value of the double difference, it is possible to detect a cycle slip. It will show up as a discontinuity in the value of δ. The algorithm is shown in schematic form at Figure 5.2.

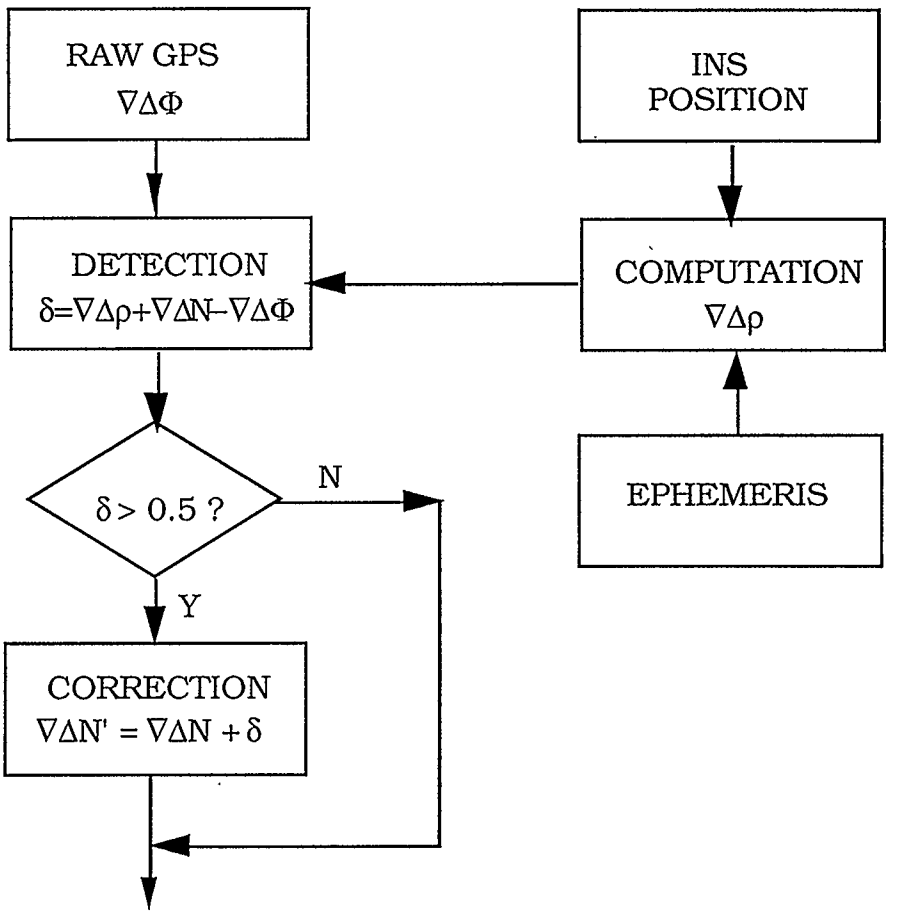

Fig. 5.2: Cycle Slip Detection and Correction Flowchart

The formula for cycle slip detection is easily derived from equation (2.5), and is of the form

$$\delta = -\nabla\Delta\Phi + (\nabla\Delta\rho + \nabla\Delta N) , \qquad (5.1)$$

where $\nabla\Delta\Phi$ is the observed carrier phase double difference,

$\nabla\Delta\rho$ is the computed range double difference,

and $\nabla\Delta N$ is the double difference ambiguity.

The double difference ambiguity, $\nabla\Delta N$, does not change from one epoch to the next if no cycle slips occur. Thus δ, expressed in cycles, is close to zero as long as cycle slip free data are processed. If it becomes larger than half a cycle, the cycle slip correction algorithm is activated. The bias ambiguity term is reset to a new value which is obtained by adding the integer number closest to δ to the previous value of the ambiguity. The implementation details of the algorithm and problems that might appear due to the inaccurate computation of δ are further discussed in Chapter 7.

5.3 Integration Strategies

Among the different estimation methods available for integration of GPS and INS data, the most commonly used is the Kalman filter approach. It uses the INS data for the determination of a reference trajectory while the GPS data are used for updating this trajectory. Although the problem of combining data from different sensors is straightforward in principle, it can lead to a violation of statistical assumptions underlying Kalman filter theory. They are based on the assumption of white noise of the dynamic system and measurement process. On the other hand, modelling the statistical properties of

these processes is not always possible. Therefore the design of the filter is always a compromise between theory and implementation.

The design of an optimal filter for GPS/INS integration has been the area of intensive research during last decade, see for instance (Tazartes and Mark, 1987). Early approaches to the problem were to use a Kalman filter with a common state vector. It was a global approach treating GPS/INS as one dynamic system. The two data streams were combined at the measurement level with a common state vector (Wong et al, 1988).

In recent years much research was done on decentralized Kalman filter methods (Carlson, 1988; Wei and Schwarz, 1990a). In this technique, a two-stage filter is employed. In a first step, the local systems process their own data to obtain a best local estimate. The results from the local Kalman filters are then used to update the master filter, which combines the information from the various local systems to produce the best global estimate of the master system (Wei and Schwarz, 1990a). The information that is passed from the local filters to the master filter distinguishes various decentralized Kalman filter designs.

In the rigorous approach, the fully decentralized filter, local Kalman filters provide the updated and predicted state vectors along with their respective covariance matrices. If the predicted state vector is neglected, the design is called a cascaded decentralized filter, because the output from one system is used as the measurement input to the next. This is a sub-optimal filter because the input is, in principle, correlated in time, and thus does not fulfil the fundamental

assumptions of Kalman filtering. The so-called Kalman filter with coloured noise has been developed to handle this situation and can be found in a number of textbooks, see for instance (Gelb, 1974). The next design, a sub-decentralized filter, is similar to a fully decentralized Kalman filter, but in addition, the results of the master filter are fed back to the local filters. Results for GPS/INS integration show that there is no significant difference between these filter designs (Wei and Schwarz, 1990a).

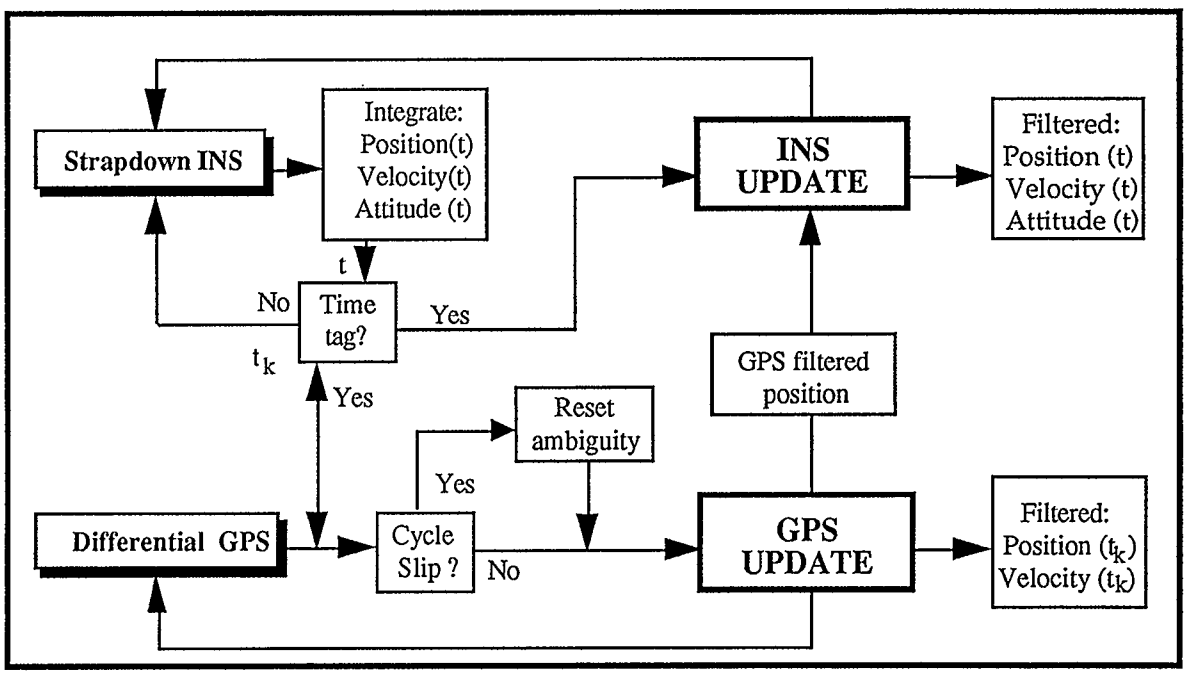

Fig. 5.3: GPS/INS Filter Flowchart

The cascaded decentralized filter has been chosen for this development. It has the advantage, that is very simple to implement and can be easily extended to process data from other sensors. In this concept two separate filters for GPS and INS are used. The INS state vector is given by equation (4.26) while the GPS state vector is given

by equation (4.38). The implementation of this idea is shown in Figure 5.3. The two filters are run independently and interact only occasionally. The GPS observations, corrected for cycle slips, are low rate update measurements for the local GPS filter. The output of GPS filter, position and velocity along with their covariance matrices, is a quasi-observable of the form given by equation (4.10) and is used to update the INS master filter. The observation vector **l** and the design matrix **A** have the simple form

$$\mathbf{l} = \begin{pmatrix} \mathbf{r} \\ \mathbf{v} \end{pmatrix} \quad \mathbf{A} = \begin{pmatrix} \mathbf{I} & \mathbf{0} \\ \mathbf{0} & \mathbf{I} \end{pmatrix} \quad . \tag{5.2}$$

The GPS position and velocity represent the measurement vector in equation (4.10) and are used to update the INS filter. Their covariance matrix, which is the covariance matrix of the GPS filter, is used as measurement noise covariance matrix $\mathbf{C}^e$ in equation (4.15). The INS filter estimates its errors in attitude, position and velocity at a high rate.They are used for computing the navigation parameters.

5.4 Offset Correction

The reference points of GPS and INS sensors usually do not coincide, see for instance Fig. 5.1. The GPS measurement point is the antenna centre. The centre of the INS is typically described as the centre of proof masses of accelerometers. In order to perform the integration, a common reference point has to be chosen. It is convenient to reference both systems to the INS centre. It requires

only the occasional transformation of the GPS derived position and velocity at a low rate.

The transformation of the GPS position, expressed in geographic coordinates, can be computed using a direction cosine matrix from the body to local level frame, which is computed in the mechanization module

$$\Delta \mathbf{r}^{n} = \mathbf{R}_{b}^{n}\, \mathbf{d} \,. \tag{5.3}$$

The vector **d**, the offset vector between INS centre and GPS antenna centre is expressed in terms of three Cartesian components in the body axes system of the INS. It is assumed to be constant and obtained before the survey.

The transformation of GPS velocity can be obtained by simple differentiation of equation (5.3) and by taking advantage of the fundamental differential equation (3.7)

$$\Delta \dot{\mathbf{r}}^{n} = \mathbf{R}_{b}^{n}\, \Omega_{nb}^{n}\, \mathbf{d} \,. \tag{5.4}$$

In practice, for small offsets, the velocity correction can be neglected.

Chapter 6

Implementation

Implementation of an integrated GPS/INS has been an important part of this research. The purpose of this chapter is to give the necessary background on the GPS/INS prototype and the GPS/INS software package. The system is described first, in terms of its suitability for field operations. This is followed by a general description of GPS/INS software. The computer program GPIN, developed for processing of GPS/INS data, is then presented in detail.

6.1 GPS/INS Prototype

The GPS/INS system consists of modified off the shelf components : an LTN-90-100 inertial strapdown system, two GPS receivers and a data acquisition system with a data collection computer. One GPS receiver is used at master station, while the second one is interfaced with a data acquisition system and LTN-90-100, that are used at rover station. The "rover" part of the system is schematically shown in Fig. 6.1. All individual components run on a direct current from 12 V batteries. An important part of the prototype is also a specially designed lever arm that is used for centering the

antenna over the control point. The whole system can easily be mounted and dismounted in a truck in about five minutes .

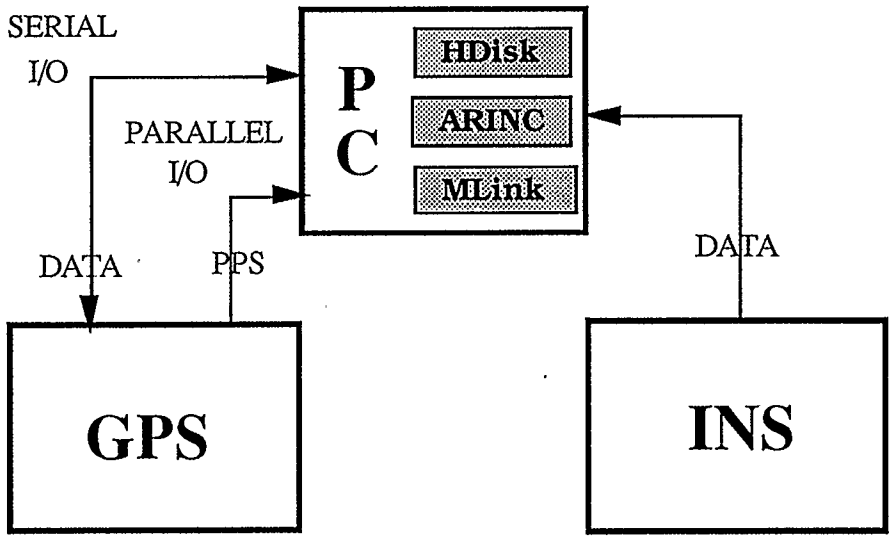

Fig. 6.1: GPS/INS Prototype Scheme

6.1.1 Strapdown Inertial System

The inertial hardware is an LTN-90-100 strapdown system (photo 6.1), which is primarily used in aircraft navigation and belongs to the 1 nm h^{-1} class of accuracy. It contains three 28 cm ring-laser gyros with a random drift of 0.02 dg h^{-1} and three torque restrained pendulous accelerometers (Litton,1984). The system runs also from standard aircraft 400 Hz 115 VAC or 28 VDC. Since LTN-90-100 was designed for use in an aircraft, modifications were made to adapt the system for land mode operation (Wong, 1988). The system is portable in principle, weighs 33 kg and has a power consumption of 130 W. It outputs two types of data - the integrated geographic coordinates and raw velocities at a 16 Hz rate, and acceleration and gyro rates at 64 Hz.

Photo 6.1: LTN 90-100 Strapdown System

Photo 6.2: GPS Receiver and Compaq 386

The acceleration and gyro rates are compensated for the coning, scaling and drift effects in the system. The second type of output, raw rate data is used in surveying applications, because of the limited precision of raw coordinates and velocities. The inertial data is output in the ARINC 429 format and recorded externally by the data acquisition system.

6.1.2 GPS Receiver

The GPS receiver is C/A code single frequency five channel Trimble 4000 SX receiver (photo 6.2). It outputs time, pseudorange, carrier phase and Doppler frequency at a maximum rate of 4 sec through an RS232 port. The GPS/INS data acquisition system is not dedicated to a particular type of receiver. The only requirement is data output in an accessible form through a standard communication port. The PPS - Pulse Per Second information is also needed for precise synchronization of the GPS receiver with external devices. Most of the commercially available receivers provide this information. Currently, work is under way of interfacing the LTN-90-100 with another type of receiver - the double frequency 12 channel Ashtech LD-XII.

6.1.3 Data Acquisition System

The main part of the data acquisition system is a computer with running logging software. The computer has dedicated boards: an ARINC interface to the INS unit and a Magnalink board. A portable

Compaq 386 with 100 Mb hard drive is used and it runs on 110 VAC so a DC/AC power converter has to be used in the field. Plans are made to purchase a 386 based portable computer running from 12 VDC. The ARINC 429 interface and data logging software was originally developed by Pulsearch Consolidated Ltd. in Calgary and later modified by the Department. The function of the ARINC interface is to enable the selective transfer of data at a 76800 baud rate from the inertial system to the computer. The Magnalink board is used for downloading the data from hard disk to a mass storage device, i.e. Magna Pac. It can store up to 2.2 Gb of data on a standard 8-mm video cassette.

GPS measurement data are transmitted to the computer through a serial port at a 9600 baud rate. The PPS (Pulse Per Second) information is transmitted through a parallel port. GPS and INS data are time tagged through the computer clock. Since the recorded computer time does not represent the actual time of measurement, it is refined in a post processing stage using the PPS output of the Trimble receiver and taking into account the transmission delays.

	Voltage [V]	Power [W]	Weight [kg]	Length [cm]	Width [cm]	Height [cm]
LTN-90-100	24 VDC	130	33	48	38	48
Trimble 4000 SX	12 VDC	50	27	75	50	25
Ashtech XII	12 VDC	16	4.5	31	21	11
Ruggedized PC	24 VDC	220	15	55	43	18.5
Compaq 386	110 VAC	350	10	20.5	21.5	18.5

Table 6.1: Physical Characteristic of GPS/INS Prototype Components

The physical characteristics of GPS/INS system components are summarized in Table 6.1.

6.1.4 GPS Antenna Lever Arm

In order to center the GPS antenna over the control point with centimetre accuracy, a special lever arm was designed and manufactured in the University workshop (photo 6.3). The antenna is mounted on a tribrach with optical plummet that is screwed to the lever arm. The arm can be swang out in two directions so that the operator can center over the point (photo 6.4). The centering takes about two to three minutes. During transport or during a run, the GPS antenna is kept in fixed position on the roof.

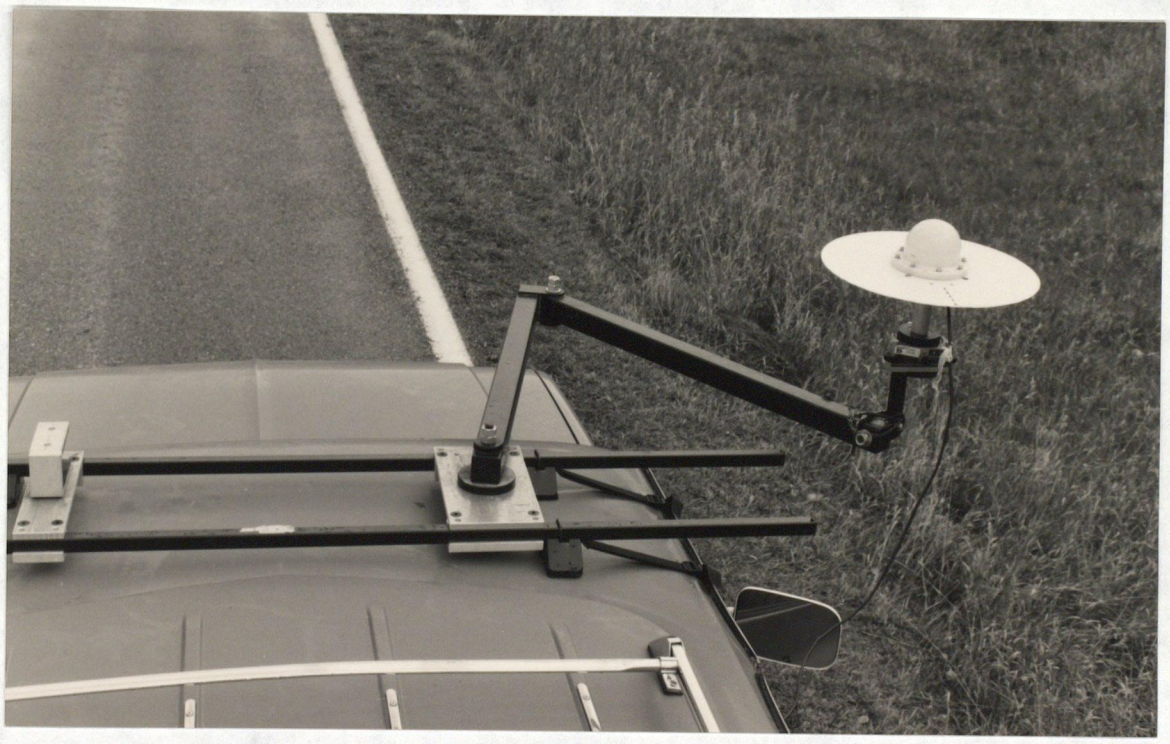

Photo 6.3: GPS Antenna Lever Arm

Photo 6.4: Centering the GPS Antenna over the Point

6.2 Attitude Parameters for Slope and Curvature

The INS yields the platform orientation referenced to the initial state by means of gyroscopes. The orientation parameters, i.e. roll, pitch and azimuth, relate the body coordinate system to the local-level system..

In case of a vehicle carrying an inertial system, orientation parameters can be used to determine the geometric parameters of the road; superelevation, slope, vertical and horizontal curvature. If the platform misalignments with respect to the road can be neglected, then superelevation is given by roll, while the slope of the road is given by pitch. This means, for an average vehicle speed of 70 km h^{-1}, that the INS can directly provide road parameters every 20 cm, giving a continuous profile of the road.

The vertical radius of curvature can be computed from the change in pitch, while the horizontal radius of curvature can be obtained from the change in azimuth

$$R_v = \frac{ds}{dp}, \qquad R_a = \frac{ds}{dA}, \tag{6.1}$$

where s is distance,

p is pitch,

A is azimuth,

and R_v, R_a are vertical and horizontal radius of curvature, respectively.

This is illustrated in Figs. 6.2a and 6.2b.

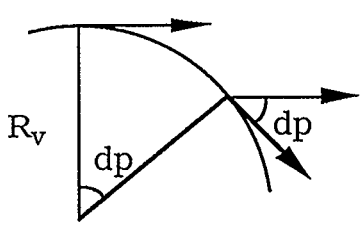

Fig. 6.2a: Radius of Vertical Curvature

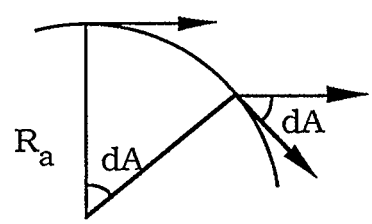

Fig. 6.2b: Radius of Horizontal Curvature

In route surveying, a scaled parameter is often used to define curvature, namely the degree of curvature (Davis et al,1981). The degree of curvature, D, is defined as the angle subtended by a 100 m arc (Fig. 6.3), so that

$$\frac{D}{100} = \frac{360^o}{2\pi R}, \tag{6.2}$$

and thus

$$D = \frac{36\,000}{2\pi R} = \frac{5729.578}{R} \quad . \tag{6.3}$$

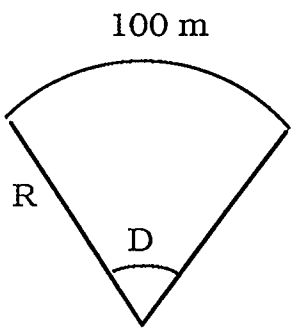

Fig. 6.3: Degree of Curve

6.3 Software Development

Based on the methodology discussed in Chapter 5, the post-mission program GPIN for GPS/INS integration has been developed. It is the major processing program of the GPS/INS system. The GPS and INS data have to be pre-processed to be input to the program, see Fig 6.4.

The programs UNSAT and UNEPH unlog GPS observation and ephemeris data to ASCII form. The function of the program TIMTAG is to compute the offset between GPS and INS times. It uses the PPS output of the GPS receiver that is recorded in GPS observation files. The program TRIMPRE pre-processes GPS data in a form acceptable for GPIN.

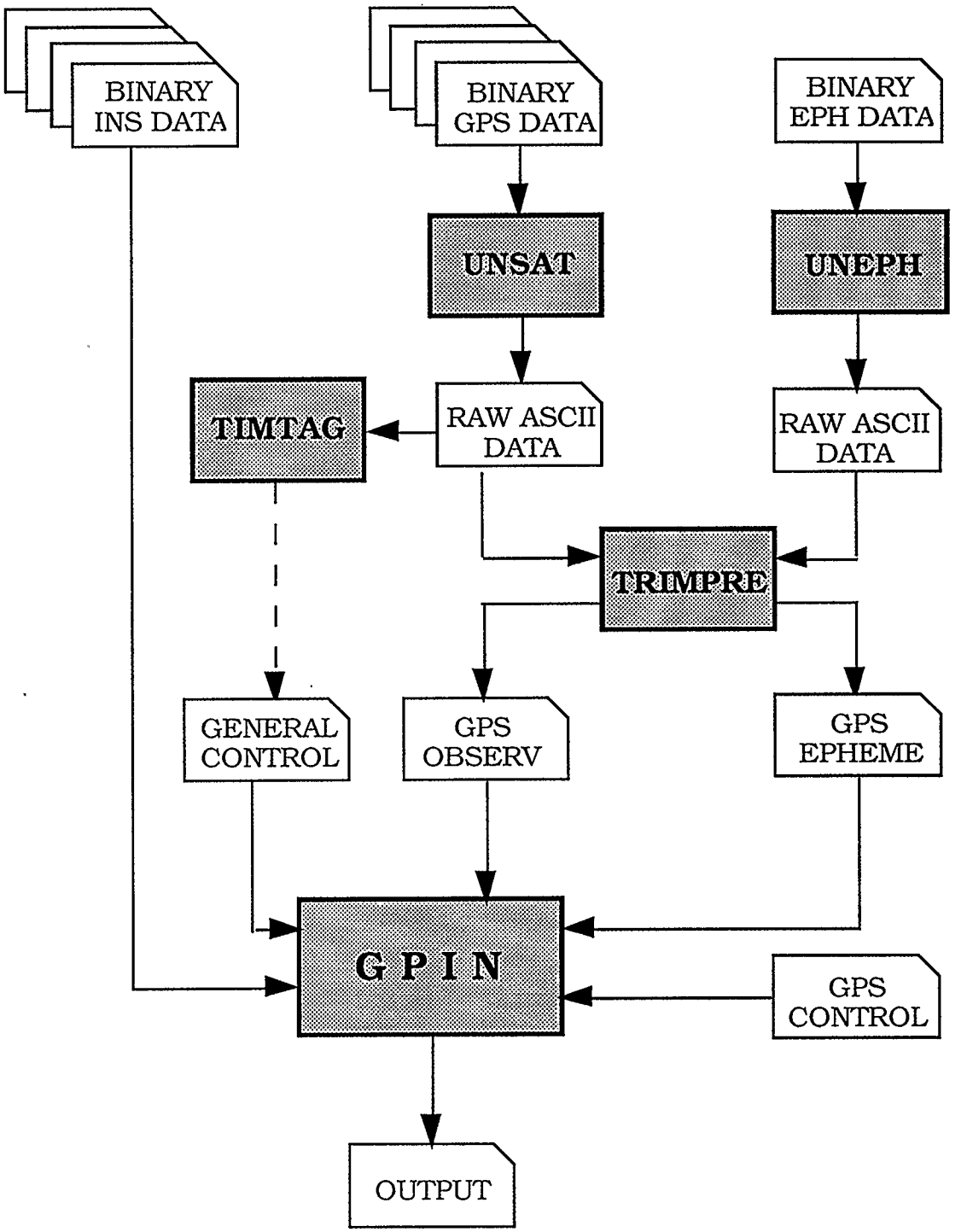

Fig. 6.4: GPS/INS Software Package Flowchart

The program GPIN needs control input files. The GENERAL CONTROL file contains initial parameters for INS Kalman filter as well as time of alignment. The GPS CONTROL file contains information necessary for initialization of the GPS processing part.

The program, GPIN, written in FORTRAN 77, runs on a Compaq 386 and needs about 550 K of RAM. Modules of the GPS kinematic software SEMIKIN of E.Cannon and LTN90 of R. Wong were modified and used in the GPIN program development. Since they had to be adapted for the specific task of GPS/INS integration a thorough understanding of the existing code was a prerequisite. Although the use of existing modules reduced the coding work, the amount of time needed for the integration software development was considerable. An effort was made to keep the program as flexible as possible so that data from other sensors can be accommodated. The program consists of two principal parts: a "static" part for processing static GPS/INS data at the beginning of the run (Fig. 6.5a), and a "kinematic" part for processing data during vehicle movement (Fig. 6.5b).

For static GPS, a batch least squares method is applied, in which the initial ambiguities are resolved. The estimated parameters, ambiguities and station coordinates are needed for starting the kinematic part.

The starting coordinates obtained from the GPS solution are input to the INS alignment. First the coarse alignment is performed, giving the approximate values for roll, pitch and azimuth of the system. These approximate Euler angles are refined during the ten minutes fine alignment.

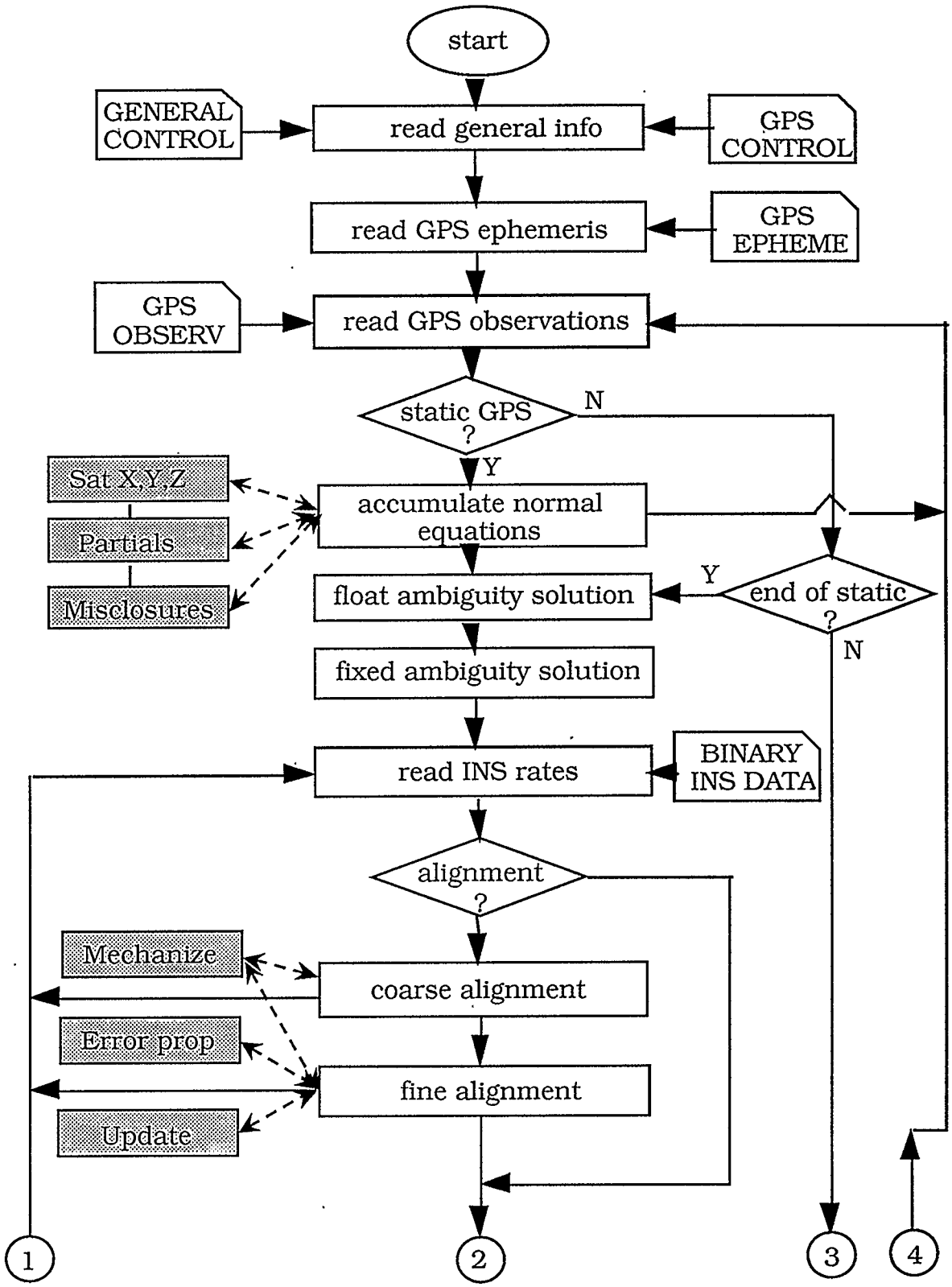

Fig. 6.5a: GPIN Program Flowchart- Static Part

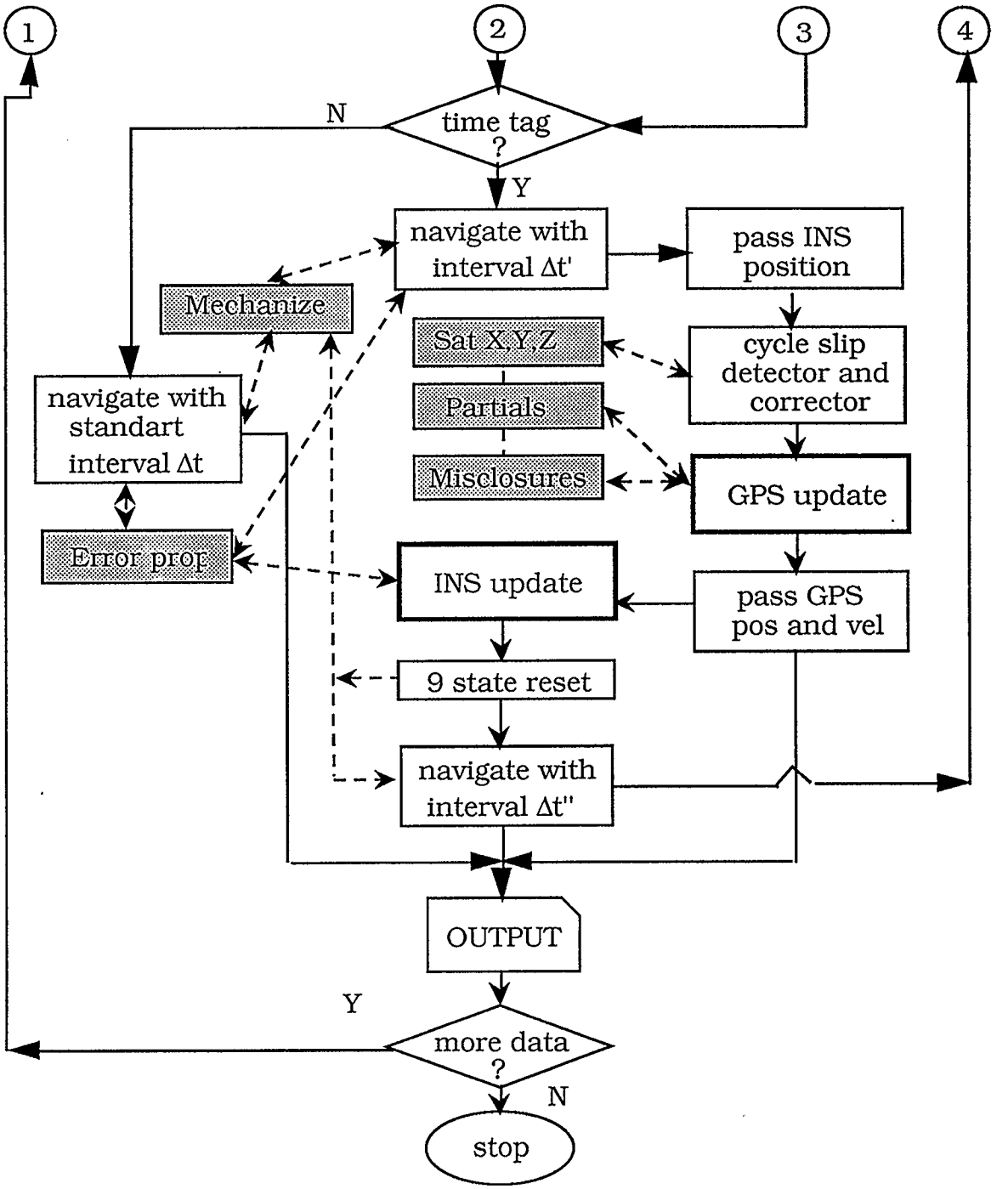

Fig. 6.5b: GPIN Program Flowchart- Dynamic Part

During dynamic positioning, two separate filters are applied to the GPS and INS measurements as discussed in Chapter 5. The INS measurements are continuously integrated in a mechanization module at a 64 Hz rate (LTN-90-100) to provide position, velocity and attitude of the system. When the GPS measurement matches the INS interval (Fig. 6.6) the integration is performed with interval $\Delta t'$, to compute the predicted INS position at the time of GPS measurement.

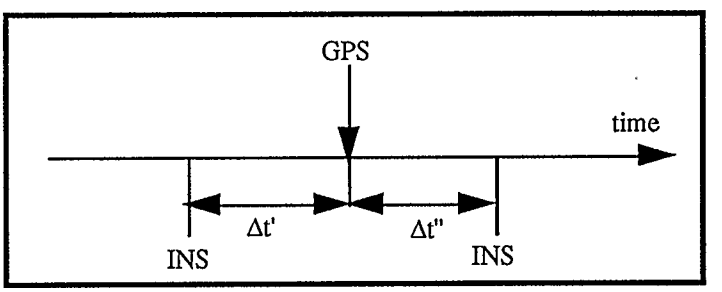

Fig. 6.6: Time Tagging of GPS and INS Measurements

This position is used for computation of the predicted double differences, which are compared with the observed carrier phase double differences. After passing the cycle slip detection and correction module, the phase double differences are used to update the GPS filter. In addition to the phase measurements, all other available GPS measurements, pseudo-range and phase rates, are used as updates. The determined position and velocity is then passed as update information for error estimation to the INS Kalman filter. The computed errors are used for a 9-state reset of attitude, position and velocity components of the INS state vector. Then the mechanization computations are continued with interval $\Delta t''$ until the end of the INS measurement interval, using corrected values of navigation

parameters. This step is important for a successful integration. Afterwards the new INS measurement record is read and the INS mechanization is performed with a standard interval cycle. The proper time-tagging of GPS and INS measurements, an underlying assumption of GPS/INS integration, is crucial for maintaining the accuracy of the system.

Chapter 7

Field Tests and Results

The results of theoretical and software developments should always be verified with real data, if possible. Field testing of the GPS/INS prototype has been an integral part of this research. This has provided the final check of system and software performance. The purpose of this chapter is to describe the field tests and results of data analysis performed with the use of the program GPIN.

First, a general description of field tests is given. This is followed by a more detailed description of tests which were carried out in 1989 and 1990. The results of position, slope and curvature determination are next analyzed in detail. In last section, bridging interval and cycle slip detection and correction algorithm are examined. Finally,the "ambiguity search" algorithm is proposed and tested.

7.1 Establishment of Test Network

A GPS test traverse was established on a stretch of Highway 40 in the Kananaskis region. An 8 km section located between the Trans Canada Highway and the University of Calgary Research Centre was

selected (Fig 7.1). This section has an adequate variation in slope and curvature for reasonable test of the system.

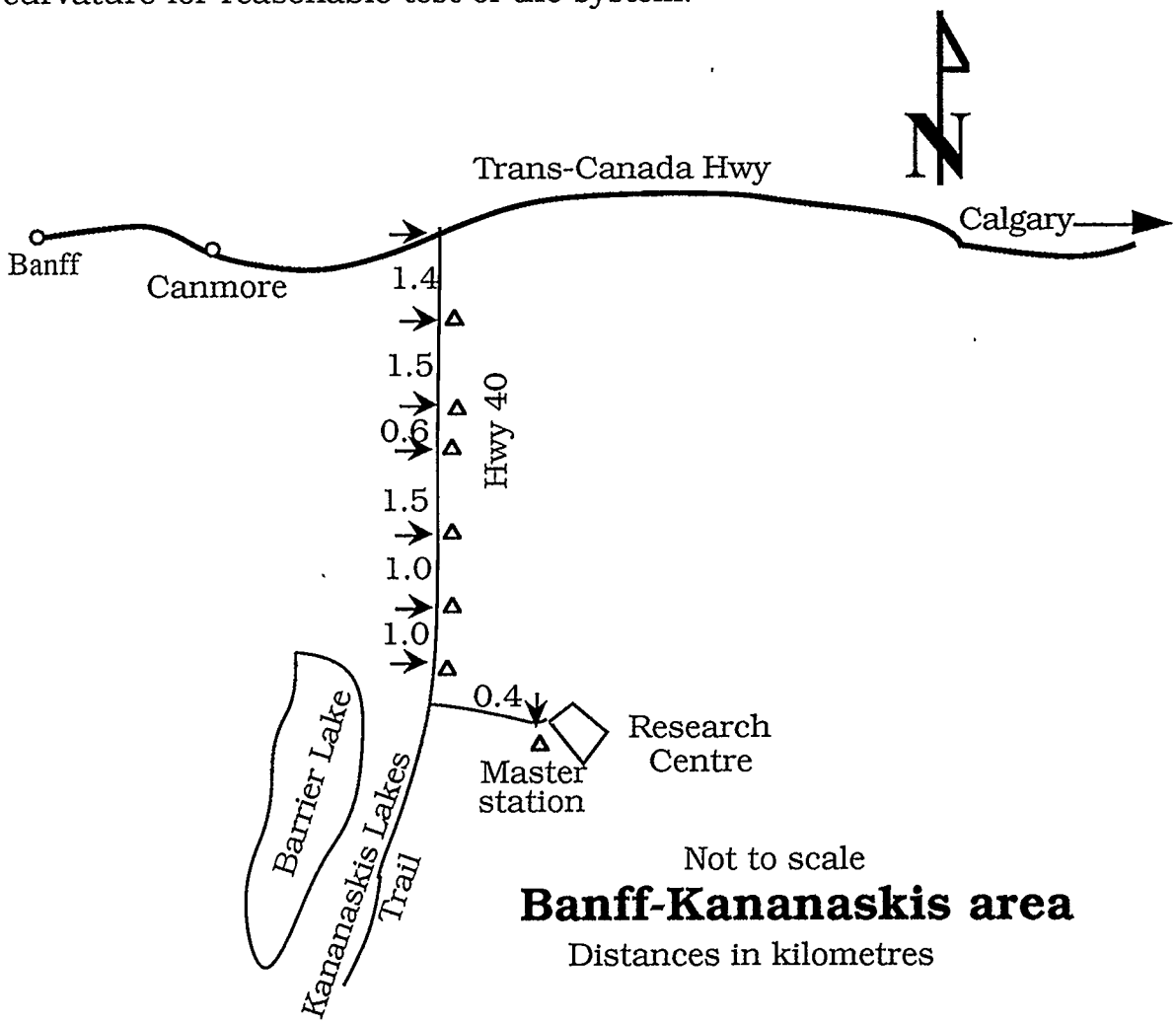

Fig. 7.1: Sketch of Field Test Area

The Department of Surveying Engineering had already established two stations in the traverse. In order to have points spaced at 1 km, six more points were needed. A monitor station at the U of C Research Centre was also necessary, so a total of seven stations were established. All points were monumented with brass caps on rebar so they would be permanent. All points in the traverse had to be surveyed

with respect to the monitor station. The GPS static differential technique was used for this as it is very accurate and relatively fast. Two Trimble 4000 SX GPS receivers were used, one located at the monitor station and the other at the station to be determined. At each station data was collected on five satellites for a period of two hours. The resulting accuracy between the master station and each point is 2 to 5 cm (1 σ). Since the established points were not directly accessible from the road, two offset points were established, one on each side of the road. They were marked by pins and then tied to the existing traverse.

7.2 General Description of Tests

The field tests were carried out during summer and fall 1989 and spring 1990. The field experiments of 1989 gave first hands-on experience with the equipment and with the data acquisition method. Much time was spent in the field and many lessons were learned at that time. Most problems were associated with the data acquisition system, namely the computer and data ARINC board, or with some auxiliary equipment like power generator at the master station. The equipment, was subject to harsh conditions in a truck, not only during the actual tests but also during transport from Calgary to the Kananaskis test field. The key to success was good planning, and knowledge of weak points of the system. This experience was gained in 1989 and a year later, another set of tests was performed with refined logging software. Improvements in the data logging software

mainly concerned the time tagging of GPS and INS data records. In 1990 the system reached fully operational status.

The offset between the antenna centre and the centre of the inertial system, determined in the body system of the INS, was measured before the test began. The measurement was done using a theodolite and tape. A simple geometric method of transfering the INS centre over the roof, was used. The X, Y, Z coordinates of the antenna centre were determined with 2-3 cm accuracy (1 σ).

During the field tests, the GPS/INS prototype was mounted in a truck, while a second GPS receiver was set up at the monitor station. The GPS/INS data in the truck and GPS data at master station were collected using personal computers. The GPS data rate was 0.25 Hz, while the INS rate was 64 Hz. The typical amount of data per hour of measurements is about 7 Mb at the rover and 0.5 Mb at the master station.

The first series of tests, in 1989, were performed in semi-kinematic mode to have a good assessment of the system's performance. It was achieved by stopping at known control points and comparing the system's output and ground truth values. In 1990 fully dynamic tests were carried out.

The semi-kinematic test procedure was as follows:

1. A 10 minute static survey and alignment was performed at the first control point with the GPS antenna centered over the point.
2. The antenna was put on the vehicle roof.
3. The truck was driven to the next control point at about 60km/h.

4. The antenna was centered over the next point using the lever-arm. At each point, static positioning was performed for 2-3 min. At the beginning and the end of the static measurements, a 10-sec INS zero velocity update was performed.

The GPS/INS data were processed using the program GPIN, described in chapter 6. The discussion of results is given in the following sections.

7.3 1989 Tests and Results

During the first test on June 16, 1989 data were recorded to check the survey procedure and the data acquisition hardware and software. After correcting the shortcomings, the second test was carried out on October 11 and 12.

In the first test, GPS/INS data were recorded on a 4 km section of the traverse. The whole traverse could not be surveyed due to a malfunction in one of the GPS receivers. Results of this test are presented only to demonstrate curvature determination since a survey plan of curvature was available for comparison. The survey took about half an hour.

The second series of tests was performed on the last 6 km of the traverse, due to intensive traffic. It gave the principal data set for the analysis. On October 11, the test lasted approximately 1 h during which six control points were visited. On the second day, the six points of the forward run were occupied along with 3 points of the reverse run, for a total time span of 1.5 h.

Several data problems and shortcomings were discovered during the post-processing phase. Separate processing of INS and GPS data showed that position results were shifted in time. However, results from both sets of data agreed with the coordinates at the control points. This implied that GPS and INS measurements were not properly time-tagged. After discussions with the receiver manufacturer, it was found that the time tags referred to UTC, not GPS time. The zero point of the two scales differed by 5 seconds in 1989. This explained the difference in the GPS and INS positions which corresponded to approximately five seconds. Another shortcoming of the time output was its insufficient accuracy (20 ms). Nevertheless, these data were processed using an approximate value of the time offset between the two systems and trying to find the best value from the analysis of multiple runs. The time tagging problem was corrected in the new version of the logging software that was used in later tests in 1990.

7.3.1 Position Accuracy

The data sets from the two days in October made it possible to examine the repeatability of results. Height and slope parameters have been investigated.

The positioning accuracy of the integrated system was first assessed by comparing the filtered position results to the control coordinates at the static points along the traverse. Figures 7.2 and 7.3 show the results for October 11 and 12 respectively.

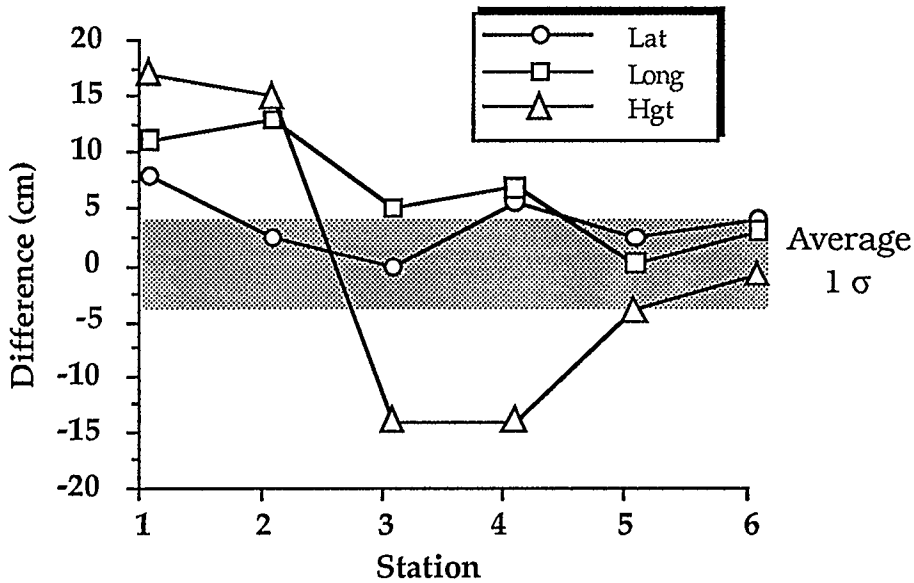

Fig. 7.2: Accuracy of the Integrated System at the Static Control Coordinates for October 11

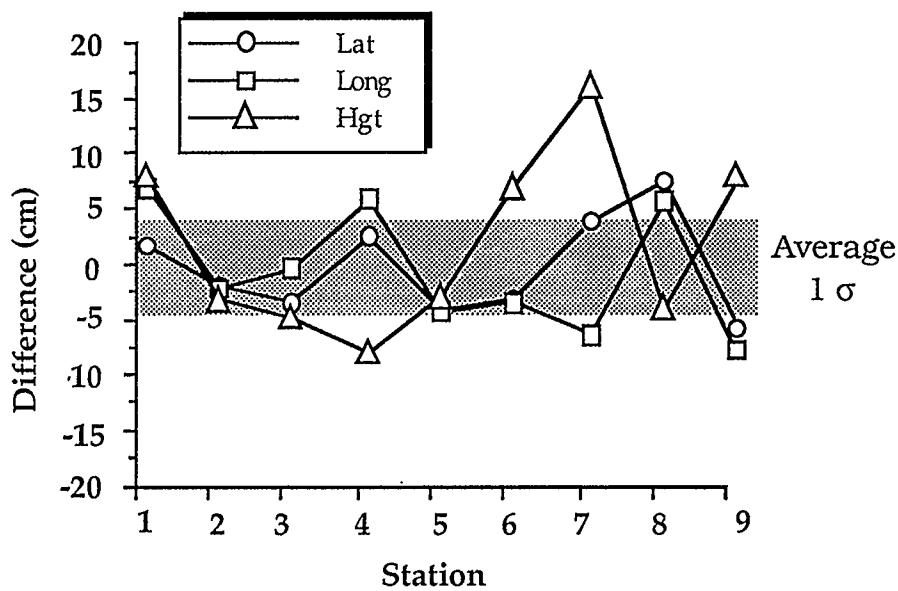

Fig. 7.3: Accuracy of the Integrated System at the Static Control Coordinates for October 12

Results are generally better than 10 cm except in height. The shaded areas show the average 1 σ coordinate error from the filter covariance

matrix and corrected for centering errors. They agree well with the RMS-values obtained from the direct computation. The results on October 11 are slightly worse due to the fact that only four satellites were used in the computations. The accuracy is fairly good and is close to the requirements given in Table 1.1 for a general survey system.

In order to assess the kinematic positioning accuracy of the system, the repeatability of the height results was used as a criterion. Fig. 7.4 shows a comparison of height profiles determined from the October 11 and 12 data. The rms height difference is ± 12.8 cm (1σ), and thus is well within the accuracy requirements shown in Table 1.1. This value includes interpolation as well as trajectory errors.

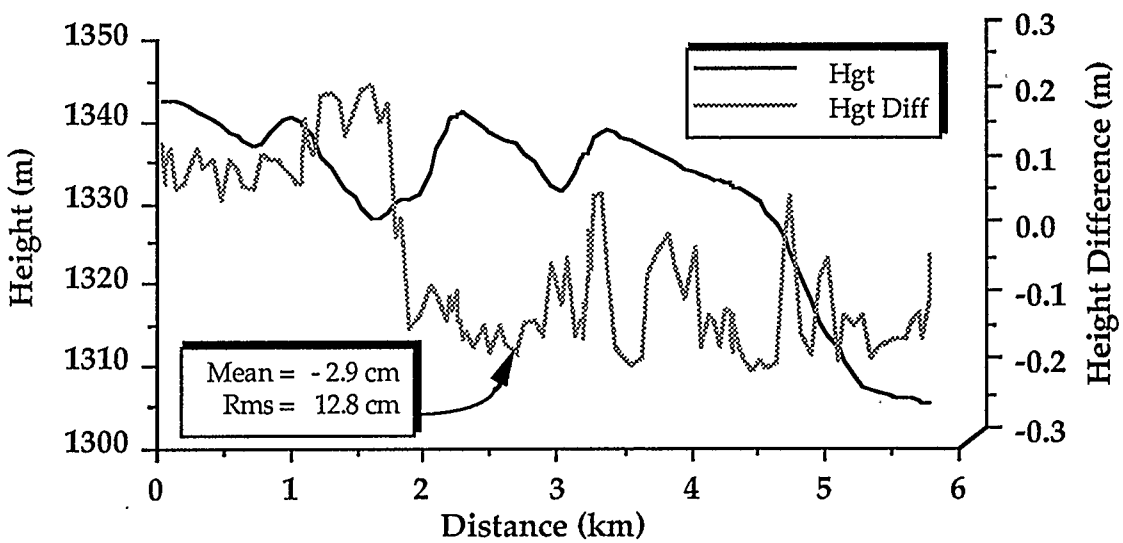

Fig. 7.4: Height Computed on October 11 and Difference in Computed Heights between October 11 and 12

Figure 7.5 shows the repeatability of slope determination for both days. In this case, the slope was computed from the height differences. The rms of the slope differences is ± 0.13% (1σ),

reflecting the high accuracy of the system. The agreement with the standard deviation obtained from the covariance matrix was again quite good. Theses values are well within the requirements of slope determination needed for the mobile system.

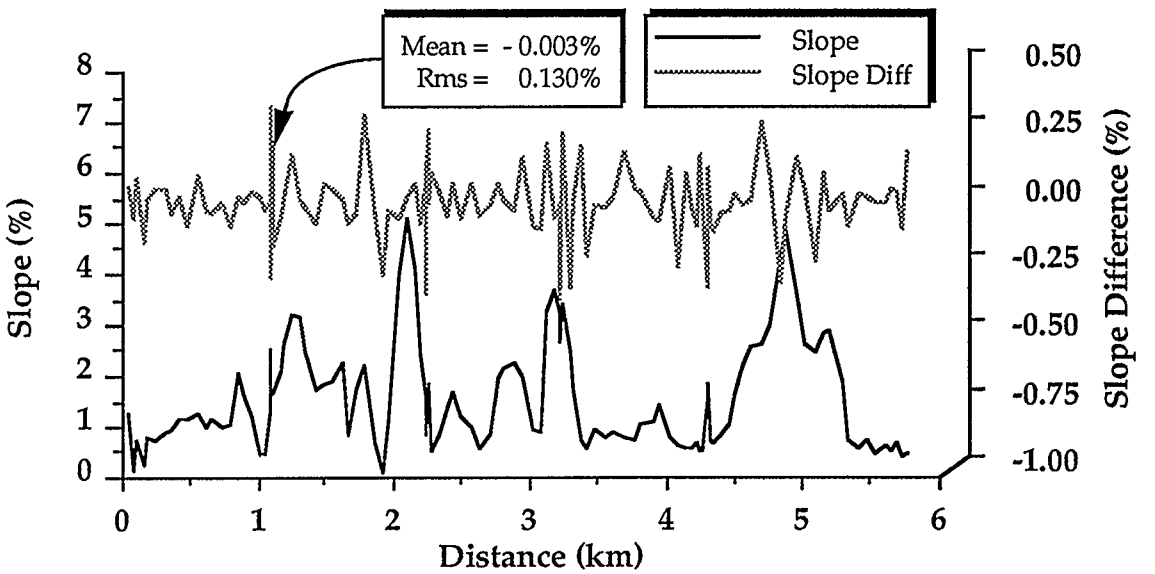

Fig. 7.5: Slope Computed on October 11 and Difference in Computed Slopes between October 11 and 12

7.3.2 Attitude Analysis

When analyzing attitude data, problems were encountered in the comparison of the road parameters determined from GPS/INS with the actual parameters taken from survey plans. Two kinds of plans were used for this purpose - the design plans acquired from Alberta Transportation and legal plans. None of these plans gave the full information needed for a detailed comparison. Design plans gave the vertical profile while legal plans gave horizontal information. In

addition, the GPS/INS position results were given in the WGS 84 reference system and this system cannot be directly related to the cadastral plan datum. Additional surveys were performed to tie the cadastral points to the control points. Nevertheless, the identification of curves was approximate as their characteristic points were taken from a map. In order to have insight into attitude determination by the system, the mean error of the attitude parameters was analysed.

Figs. 7.6 shows the slope of the road as computed from height differences. The plot agrees with the design plan although the actual slope (dashed lines) oscillates around the mean values, taken from the plan (solid lines). The deviations are up to 1% and reflect the detailed structure of the road as opposed to the general characteristics given in the design plan.

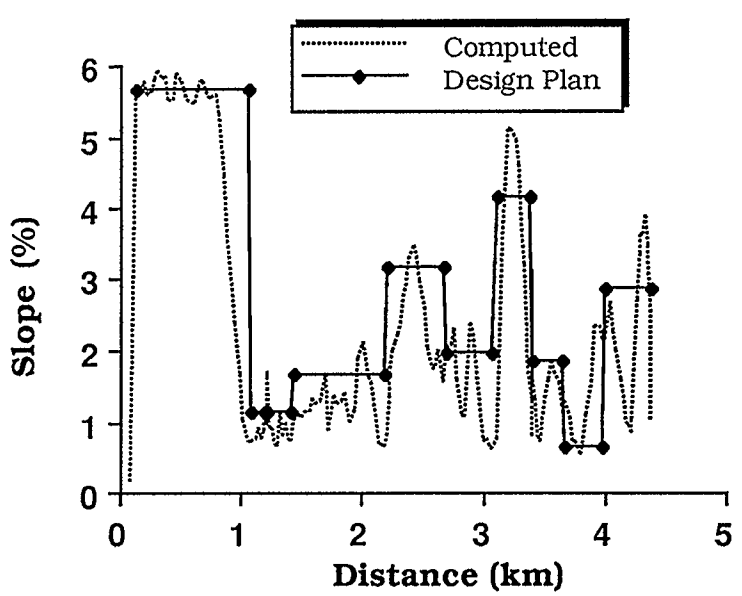

Fig. 7.6: Slope vs Distance

Figs. 7.7 to 7.12 show the attitude parameters of the system along with their standard deviations. The accuracy of roll and pitch is quite good, below 10 arc sec, which is sufficient for the determination of superelevation and vertical curvature of the road. The accuracy of the azimuth after alignment is only about 5 arc min, but improves with time due to coordinate updates.

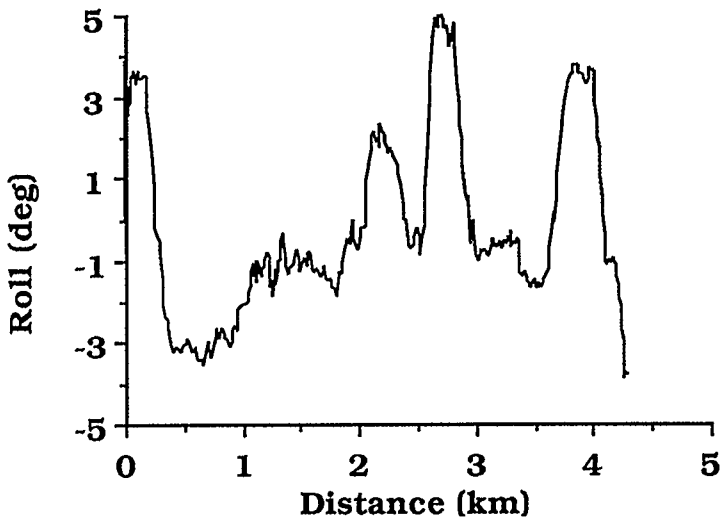

Fig. 7.7: Roll vs Distance

Fig. 7.8: Mean Error of Roll vs Distance

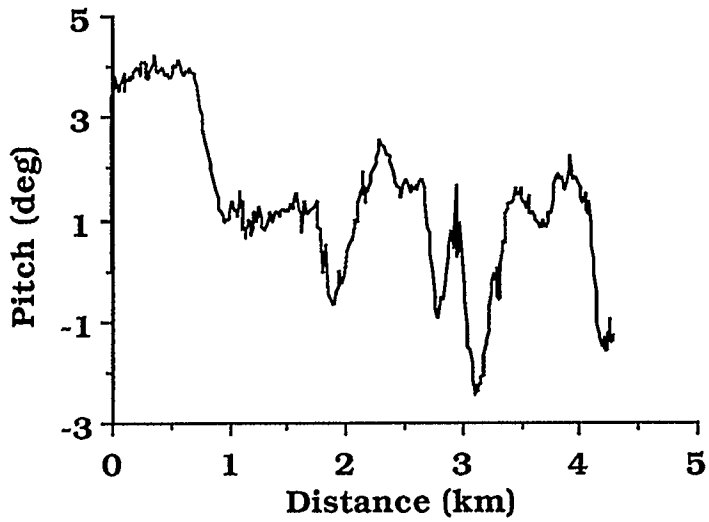

Fig. 7.9: Pitch vs Distance

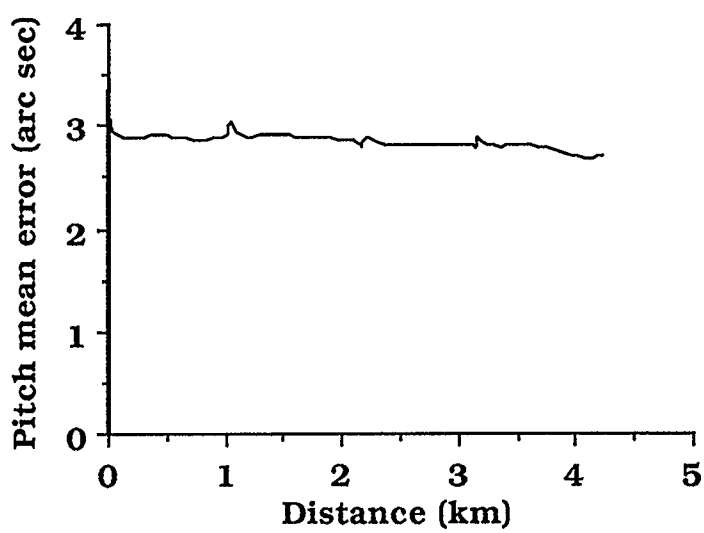

Fig. 7.10: Mean Error of Pitch vs Distance

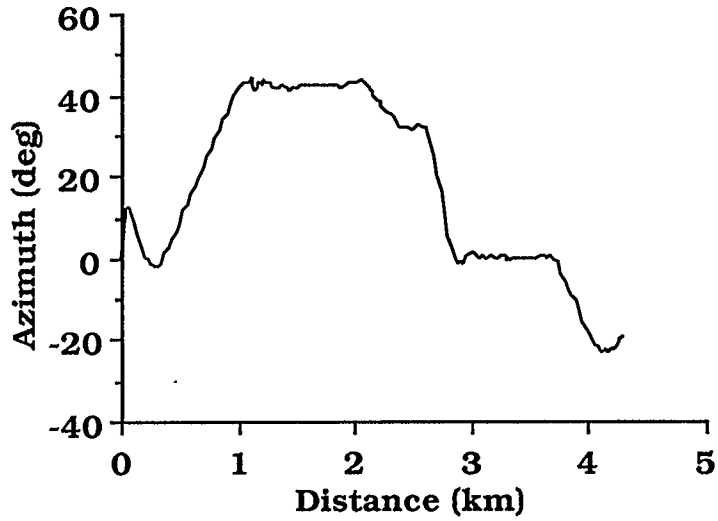

Fig. 7.11: Azimuth vs Distance

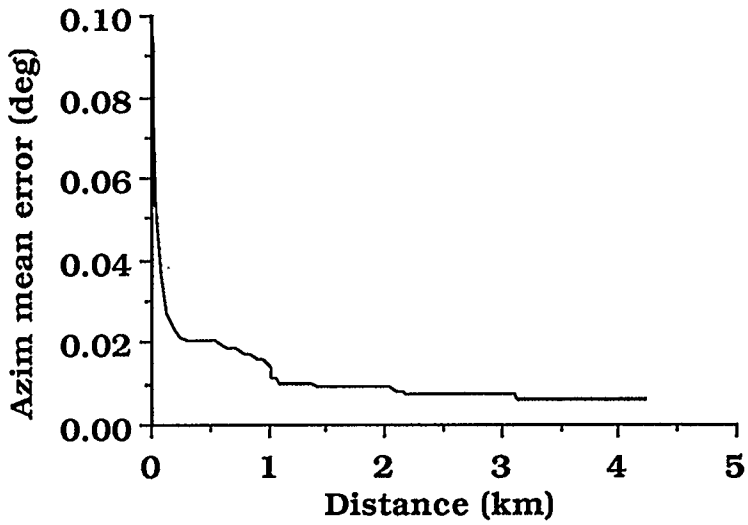

Fig. 7.12: Mean Error of Azimuth vs Distance

The attitude parameters can be used for the computation of road curvature. In this case only the parameters of horizontal curvature could be compared as there was no control information on vertical curvature and superelevation. Table 7.1 shows the comparison of

computed parameters with their actual values; where D_a^c is the computed value, and D_a^d is taken from the plan.

DISTANCE [km]	D_a^c [°]	D_a^d [°]
0.35	5.0	4.5
1.20	17.0	22.0
2.65	10.0	10.5
2.85	15.0	10.0

Table 7.1: Accuracy of Horizontal Curvature

The discrepancies between the computed and design values are due to differences between the actual vehicle trajectory and the theoretical centre of the road trajectory used in the plans. Also, the inexact identification of the beginning and the end of the curves and the fact that the parameters taken from the cadastral plan are related to right of way rather than to the actual road, may have contributed to the error.

All computed parameters satisfy the requirements given in Table 1.1. The position accuracy is well below the required 0.3 m. The accuracy of pitch and roll is good enough for vertical curvature and superelevation. The accuracy of the azimuth and of the derived horizontal curvature satisfies the given requirements. It is therefore likely that the discrepancies between derived parameters and control values are due to problems with the control values.

The results of the 1989 measurements were reported in (Lapucha et al, 1990). It was concluded that the system met the accuracy requirements of the the MHIS and that higher accuracies, as e.g. needed for a general survey system, are possible. The validation of this concept was the main goal of work performed in 1990. It was decided that further analysis would be limited to the positioning component. Positioning is of primary interest and a reliable analysis of curvature is not possible for a vehicle which can arbitrary change its trajectory.

7.4 1990 Tests and Results

Field tests of the GPS/INS system were carried out on May 3 and May 4, 1990 on the same Kananaskis traverse. Additional control information was available because the traverse was densified in June 1990 by a survey crew from Alberta Transportation who established intermediate points every 25 m. Points were surveyed using conventional techniques giving 10 cm accuracy in latitude, longitude and height. It gave an external check to assess the capabilities of the system in a fully dynamic mode.

Each day two runs were performed, the forward run in semi-kinematic mode as described before, and the backward run without stops. The first run represented an 'over-controlled' situation, where the GPS/INS was aided with ZUPT information and GPS static positioning. The second run represented real operational conditions.

The tests had three objectives:

- assessment of the general positioning accuracy of the system at static control points
- comparison of GPS/INS performance in ZUPT aided mode and in pure dynamic mode
- assessment of a potential accuracy degradation of the system with time, due to unknown errors

At the start of the forward run, a 10 minute period of static GPS and INS data were collected at the first control point of the traverse for initialization purposes, as was previously explained. The van was then driven at about 60 km h^{-1} to the subsequent point of the traverse. In the backward direction no stops were made. Five satellites were observed throughout the tests.

First, the overall positioning accuracy of the integrated system was assessed by comparing the filtered position results to the control coordinates at the static points along the traverse. Figures 7.13 and 7.14 show the results for May 3 and 4 respectively. Point 7 on these figures represents the first point of the traverse occupied at the end of backward run. Differences between the filtered GPS/INS and control coordinates are below 10 cm and are well within those defined for the MHIS in Table 1.1 and close to surveying system requirements. Part of the error, about 1-2 cm, is stemming from the inaccurate centering of the GPS antenna.

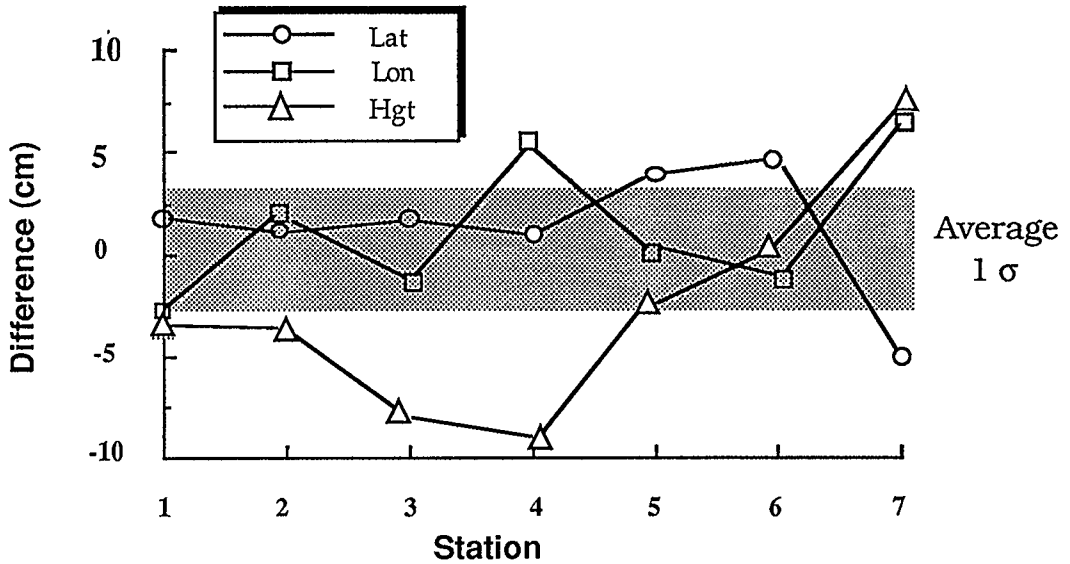

Fig. 7.13: Accuracy of the Integrated System at the Static Control Coordinates for May 3

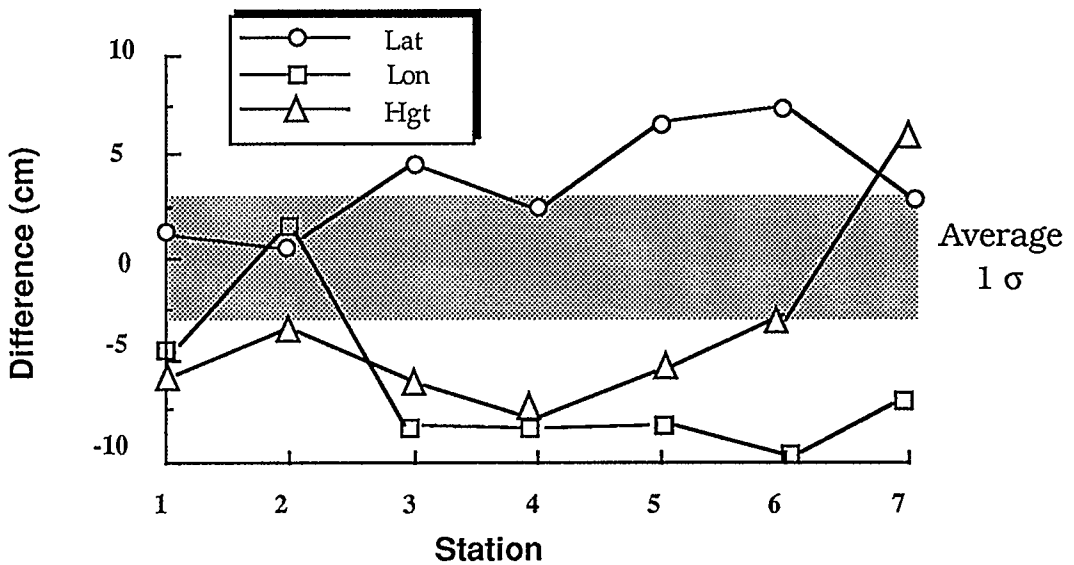

Fig. 7.14: Accuracy of the Integrated System at the Static Control Coordinates for May 4

In order to assess the interpolating accuracy of the system between GPS measurement epochs, the GPS/INS trajectory output was compared to the 'ground truth' heights, determined by the

conventional survey. Figures 7.15 and 7.16 show a comparison of the May 3 and 4 height profiles for the forward run with the heights surveyed by Alberta Transportation. The surveyed heights for the west side of the road, in backward direction, were not available. The rms height difference is ± 6.7 cm and ± 9.0 cm for May 3 and 4 respectively, and thus well within the accuracy requirements for the MHIS shown in Table 1.1. This value includes control heights errors as well as identification and trajectory errors. It also confirms earlier results from 1989, based on repeatibility analysis of heights from backward and forward runs.

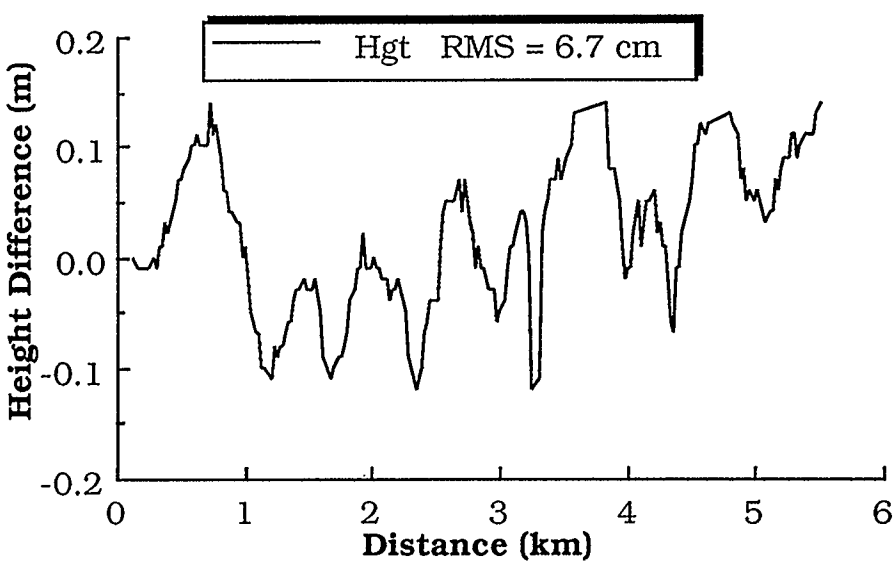

Fig. 7.15: Comparison of Height Profile for May 3

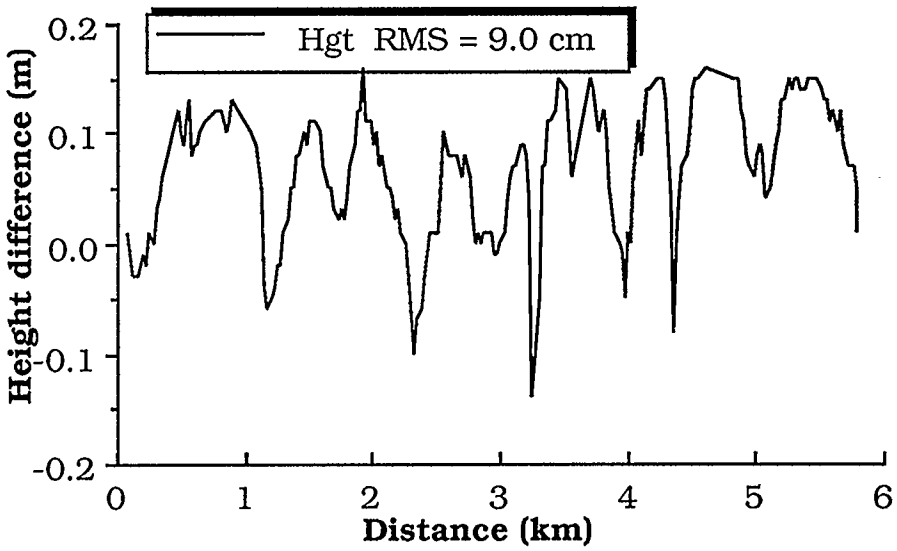

Fig. 7.16: Comparison of Height Profile for May 4

7.5 Testing of Bridging Interval and Cycle Slip Detection and Correction

7.5.1 Bridging Interval

Additional numerical tests were performed to assess the performance of the INS part of the system during potential loss of GPS lock, using May 4 data. Raw INS coordinates, integrated over different GPS update intervals, were compared to the GPS filtered coordinates. During these intervals, the INS filter was not updated, i.e. the system was working in free inertial mode. Figure 7.17 shows coordinate difference between the raw integrated INS position and the GPS filtered position computed for a four seconds interval, which is the standard interval of GPS measurements for the Trimble 4000SX receivers, using an external datalogging computer. Assuming that GPS

provides the true reference trajectory, which is not entirely true, the accuracy of the INS part of the system can be investigated. The position error is generally better than 10 cm, which corresponds to approximately half a cycle of the L1 wavelength. The results suggest that for a PDOP of 4 to 5 , which was typical for most of this run, the INS can be used for cycle slip detection and correction at the one cycle level. This is further discussed in section 7.5.2. It also confirms that the system interpolates the heights with the accuracy shown in Figs. 7.15 and 7.16. Fig. 7.17 shows the forward and backward run i.e. the backward run is starting at 6 km. The accuracy of the system in the forward and backward run is at the same level. This means that in a dynamic situation, the INS system is fully controlled by GPS.

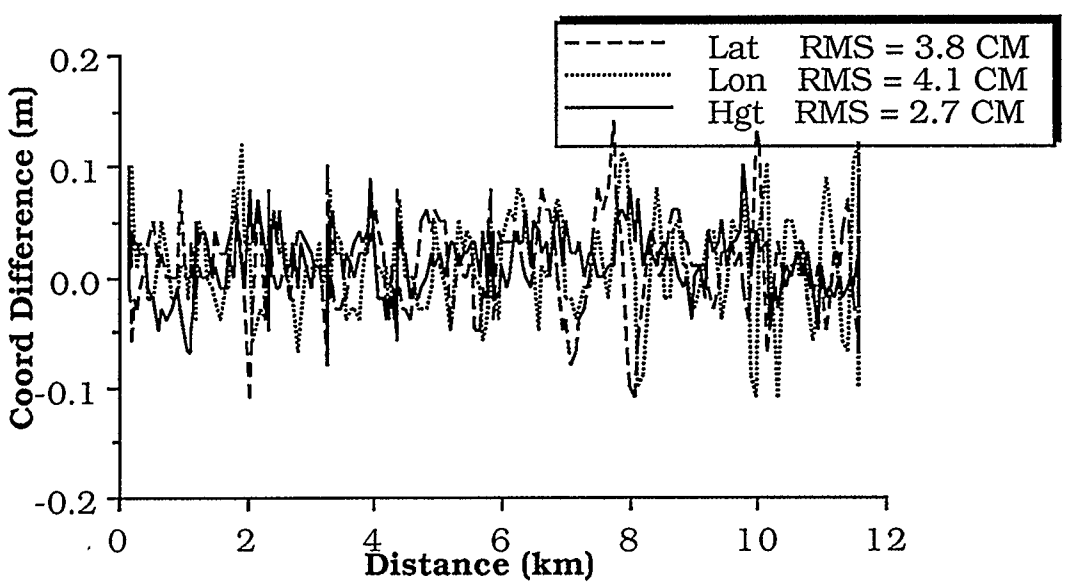

Fig. 7.17: Difference between INS Predicted and GPS Filtered Coordinates for a Four Seconds Interval

Additional computer runs were performed for different bridging intervals with different initial conditions for the INS master filter. The results are summarized in Fig. 7.18 which shows the RMS value of range differences between GPS and INS, as discussed before, for different intervals. The results suggest that the present bridging interval, which allows to recover the cycle slip on the L1 frequency is between 4 and 8 seconds. This is shorter than expected and indicates a possible imbalance in the statistical assumptions. In most cases, it should be sufficient, however to reacquisition the signal after the brief periods of total lock of loss, as could happen for instance when driving under an overpass.

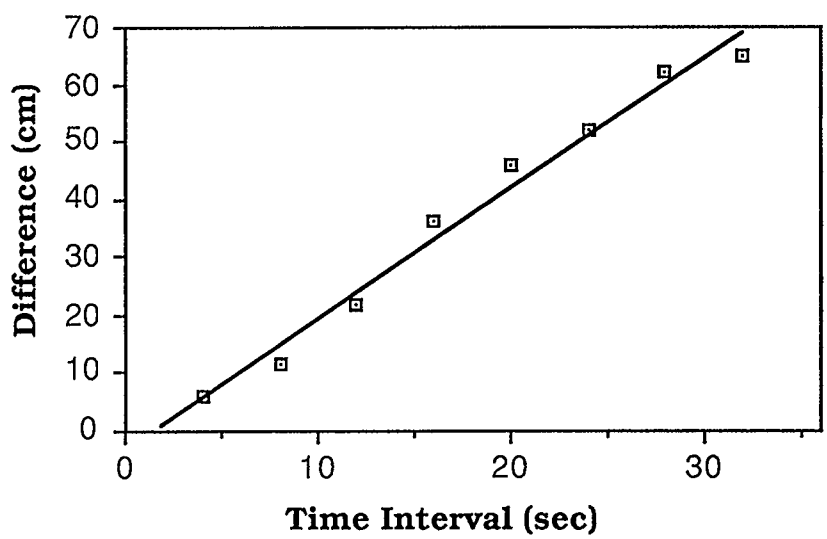

Fig. 7.18: RMS Position Error of Free-Mode INS vs Bridging Interval

It has been noticed that the results, especially for longer intervals, are very sensitive to the values of the spectral density matrices chosen. The "best" spectral densities for two different intervals are summarized in Table 7.2. They were obtained from test

runs. In both cases the spectral densities for velocity and bias error states are the same. The misalignment spectral densities differ, by three orders of magnitude. This is due to the fact that the error in the position update results in an azimuth error which decreases with the distance travelled. This effect does not show up in the standard filter because the same misalignment spectral densities are integrated using equation (4.16).Thus, these spectral densities should be optimized for the standard update interval. The sensitivity of the results to the statistical assumptions was generally not as critical for shorter intervals as it was for longer ones. This suggests that some additional investigations on optimal statistical assumptions for GPS/INS integration are necessary. It also indicates that different spectral densities might be necessary in GPS/INS integration as compared to pure inertial positioning.

State	Spectral density for 4 seconds interval	Spectral density for 32 seconds interval
$\varepsilon_N, \varepsilon_E, \varepsilon_U$	100.0 $arcsec^2/s$	0.1 $arcsec^2/s$
$\delta\phi, \delta\lambda, \delta h$	0	0
$\delta v_N, \delta v_E, \delta v_H$	$2.5 \cdot 10^{-7} m^2/s^3$	$2.5 \cdot 10^{-7} m^2/s^3$
$d_X, d_Y, d_Z,$	$1.4 \cdot 10^{-9} deg^2/h^3$	$1.4 \cdot 10^{-9} deg^2/h^3$
b_X, b_Y, b_Z	$1.4 \cdot 10^{-2} mgal^2/s$	$1.4 \cdot 10^{-2} mgal^2/s$

Table 7.2: Spectral Densities Chosen

7.5.2 Cycle Slip Detection and Correction

In order to test the GPS/INS cycle slip detection and correction capability, artificial cycle slips were generated in GPS phase data for certain satellites and at certain epochs in the May 4 data, which had generally good geometry (PDOP<5). The new GPS/INS data set was then processed with the program GPIN. Different cycle slips scenarios were tested. In general, it was found that the more satellites had cycle slips, the more difficulties can be expected in cycle slip fixing. Therefore, the most general case that cycle slips occur on all observed satellites, is presented. In all investigated cases "cycle slips" of 100, 200, 300, 400, 500 cycles were deliberately introduced at different epochs for the observed satellites 6, 9, 11, 12, 13 respectively. The problem of signal reacquisition is not considered in the following.

The results of the investigation are summarized in tables 7.3 and 7.4 for two extreme cases denoted as A and B. The integer numbers $[\delta]$, closest to δ as predicted from equation (5.1), represent the changes in double difference ambiguities $\nabla\Delta N$ predicted from the INS output. These are compared to the known values of the cycle slips generated. The accuracy of this prediction determines the performance of the algorithm. This accuracy is dependent on the error of the predicted INS position as well as satellite geometry. Of course, bad satellite geometry amplifies the error of the satellite ranges predicted from the INS position.

Case A, chosen at about 0.4 km of distance travelled, represents the typical situation for 90% of the data taken on May 4. In this case,

the predicted INS position is of sufficient accuracy for cycle slip correction. The difference between true GPS and INS predicted coordinates is 1 cm, 1 cm, 6 cm, for latitude, longitude and height, respectively. This translates into a total error smaller than 0.5 cycles in the computation of the predicted double difference range for the considered epoch, computed as difference in cycles between the known values of cycle slips and respective δ. The rounded $[\delta]$ gives the correct value of the cycle slip, and can be used for the computation of the new ambiguity $\nabla\Delta N'$.

Satellite Pair	$\nabla\Delta N$ [cycles]	δ [cycles]	$[\delta]$ [cycles]	$\nabla\Delta N'$ [cycles]	Error [cycles]
9-6	3484.00	-99.74	-100.00	3384.00	0
11-6	3686.00	-199.86	-200.00	3486.00	0
12-6	6663.00	-300.17	-300.00	6363.00	0
13-6	-7609.00	-400.24	-400.00	-8009.00	0

Table 7.3: Cycle Slip Detection and Correction - Case A

Case B represents one of the peaks in Fig. 7.17 and is chosen at about 1.8 km of distance travelled. There is no obvious reason for the peak, i.e. satellite geometry and system dynamics are about the same as for the rest of the trajectory. The difference between "cycle slip free" GPS and INS predicted coordinates is in this case -12 cm, 2 cm, 7 cm respectively. This transforms into the error larger than 0.5 cycle in some of the satellite range differences. Rounded $[\delta]$ give values which are out by one cycle as can be seen in the sixth column of Table 7.4. The INS error is increased by the rounding in this case. This

suggests that the corrections should be used without rounding for cycle slip correction.

Satellite Pair	$\nabla\Delta N$ [cycles]	δ [cycles]	$[\delta]$ [cycles]	$\nabla\Delta N'$ [cycles]	Error [cycles]
9-6	3384.00	-99.46	-99.00	3285.00	1
11-6	3486.00	-199.32	-199.00	3287.00	1
12-6	6363.00	-299.36	-299.00	6364.00	1
13-6	-8009.00	-400.19	-400.00	-8409.00	0

Table 7.4: Cycle Slip Detection and Correction - Case B

The errors in the prediction of δ affect computed GPS coordinates as almost constant biases for certain periods of time following the cycle slip. These biases in the coordinates are presented in Table 7.5 for each of the two cases A and B with and without rounding of δ, denoted as fixed and float.

Case	Latitude [cm]	Longitude [cm]	Height [cm]
A fixed	0	0	0
A float	-3	4	18
B fixed	12	10	34
B float	12	2	16

Table 7.5: Biases in Computed Coordinates

The fixed solution is usually very successful (first row of Table 7.5) but involves a risk (third row of Table 7.5) in case of incorrect

rounding. It is very important that the error in the prediction of δ remains below 0.5 cycle, which is in most cases true, as can be seen from Fig. 7.17. The float solution, although frequently less accurate than the fixed solution, is more reliable overall. It always produces reasonable results that are not affected by incorrect rounding. It has the disadvantage that INS position errors couple with GPS observation errors for the position determination.

The results above imply that a search for the best value of the ambiguities should be implemented using criteria such as the smallest distance between GPS coordinates and INS coordinates or the smallest height difference. A search algorithm using such criteria was developed and investigated in the final stage of research.

Assuming that the value of δ is accurate to 1 cycle, there are two possible integer numbers that can be estimated for each ambiguity. They are given in Table 7.6 in explicit form, as an example, for cases A and B. The asterisk '*' denotes the correct values which should be identified in the search.

Satellite Pair	CASE A		CASE B	
	1	2	1	2
9-6	3384.00*	3385.00	3285.00	3284.00*
11-6	3486.00*	3487.00	3287.00	3286.00*
12-6	6363.00*	6362.00	6064.00	6063.00*
13-6	-8009.00*	-8010.00	-8409.00*	-8410.00

Table 7.6: New Possible Ambiguities for Cases A and B

Given the fact that two integer values are possible for every unknown ambiguity, the number of combinations possible is

$$n = 2^{N-1} \quad . \tag{7.1}$$

where N-1 is number of double differences. Therefore in case of five satellites, a total of 16 combinations are possible as shown in Table 7.7.

Satellite Pair	* 1	2	3	4	5	6	7	8	9	10	11	12	13	14	** 15	16
9-6	1	1	1	1	1	1	1	1	2	2	2	2	2	2	2	2
11-6	1	1	1	1	2	2	2	2	1	1	1	1	2	2	2	2
12-6	1	1	2	2	1	1	2	2	1	1	2	2	1	1	2	2
13-6	1	2	1	2	1	2	1	2	1	2	1	2	1	2	1	2

Table 7.7: Combination Pattern for Five Satellites

The proper combination is indicated by '*' for case A and '**' for case B. The numbers 1 or 2 correspond to appropriate ambiguities from Table 7.6.

All possible combinations given in Table 7.7 were used to determine the best combination by the search algorithm implemented in the cycle slip detection and correction module. Each time, when a cycle slip was detected, the GPS Kalman filter was run through these sixteen alternatives, each time time with a different set of integer ambiguities. The resulting position obtained from the GPS Kalman filter were compared to the INS determined position to find the

minimal length of the difference vector. The criteria of minimal height difference was also investigated. The results of both computations are illustrated in Figures 7.19 and 7.20.

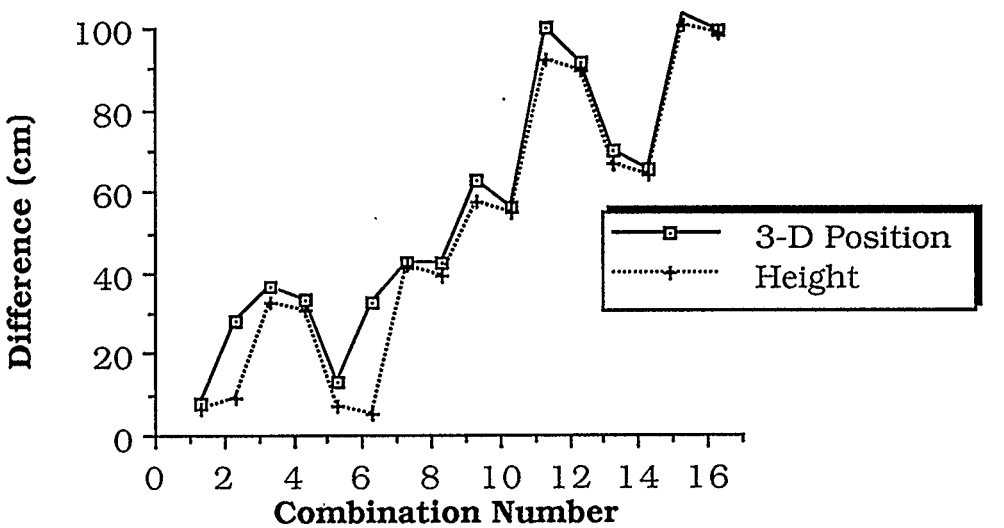

Fig. 7.19: Results of Ambiguity Search - Case A

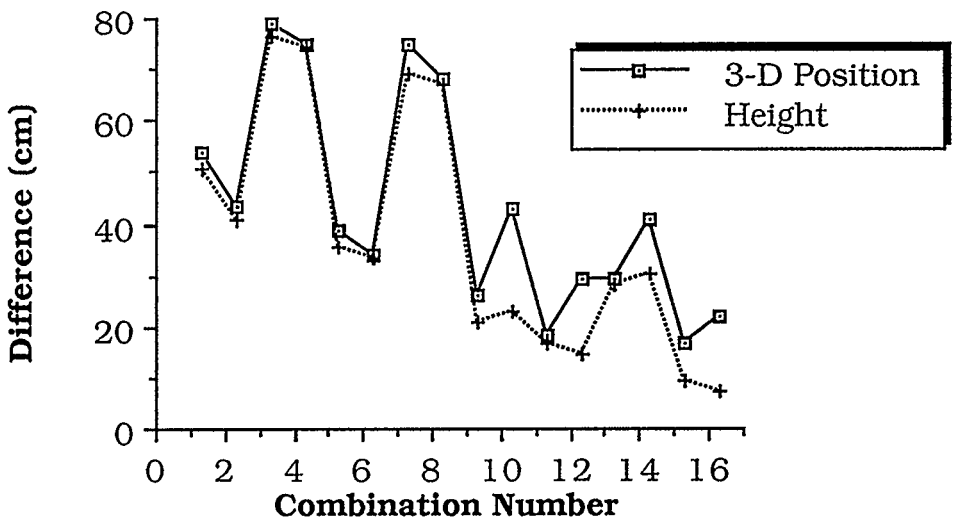

Fig. 7.20: Results of Ambiguity Search - Case B

In both cases A and B, the use of the "minimal distance" criterion identifies the correct results, i.e. combination patterns 1 and 15 for cases A and B respectively. The minimum difference was identified and is distinct for both cases, although this may be not as easy to see from the above figures, due to the scale. In case A, the minimum difference is 5.5 cm while the next smallest difference is 10.4 cm. In case B, it is 14.5 cm and 16.3 cm, respectively. The "minimal height difference" provided incorrect results in both cases as shown in Figures 7.19 and 7.20. Other criteria, such as a minimum trace of the updated state vector covariance matrix were also tested, however without success.

The above examples demonstrate the cycle slip correction and detection capability of the GPS/INS prototype system and the program GPIN. The best results were obtained with the "search algorithm" that enabled full resolution of the cycle slips. This is significant, because this is equivalent to "cycle slip free" results. Of course, the algorithm is sensitive to the geometry of satellites. The INS cannot solve the problem of bad satellite configuration. One should note, however, that in such a case any other algorithm, based for instance on statistical testing, will have the same problem.

The new values of ambiguities can also be determined using the "float solution", however the accuracy will in general deteriorate. In this case the solution is affected by the INS position error. In both cases the position results are well within accuracy requirements of the MHIS, given in Table 1.1.

Chapter 8

Conclusions and Recommendations

The main objective of this research, the development and testing of a prototype GPS/INS system for the positioning of the Mobile Highway Inventory System, has been met successfully. It has been also demonstrated that the system is more accurate than initially anticipated and can meet the more stringent accuracy requirements of highway surveying. The system, consisting of differential GPS and an inertial strapdown unit, has been extensively tested in the field and has reached operational status in the course of this research. It has been shown that the system is capable of sub-decimetre position accuracy in land mode operations. This is a significant result and opens new areas of applications for this technique.

The theoretical framework for combining the GPS and INS data is based on the theory of linear dynamic systems and the state space approach. Since both systems under consideration, the GPS and the INS, have nonlinear observation and dynamic models, linearization is necessary. The formulation of the GPS and INS state space models is given and provides the important link for GPS/INS Kalman filter development.

A software package for the processing of GPS/INS data has been developed. The program GPIN processes data by means of a decentralized Kalman filter, using the GPS determined coordinates and velocities as updates for the INS master filter. The program employs a cycle slip detection and correction algorithm, which uses the predicted INS coordinates for computation and correction of GPS double differences. The program has a modular structure that can be easily and quickly modified to accommodate data from new auxiliary measurement systems e.g. another satellite positioning system such as GLONASS.

The analysis of field data was based on a comparison with "ground truth" that was independently determined with sufficient accuracy. Position accuracy of the moving system has been assessed by stops at control points with known coordinates and by comparison with height profiles determined conventionally. Repeatability of the height profile has also been investigated. Results show that the positioning accuracy of the system is in the 5-10 cm range. Attitude parameters obtained from GPS/INS give very detailed information on the geometry of the road. The slope of the road can be obtained to better than 0.1% and curvatures to better than 0.1 degrees per 40 m. A comparison of horizontal curvature with the design values was somewhat inconclusive due to the problem with curve identification from as built plans. The accuracies that have been achieved are well within the specifications given for the Mobile Highway Inventory System (MHIS) for which the integrated system has been developed.

The system has also met the positioning requirements of a general survey system.

The cycle slip detection and correction capability of the GPS/INS system was tested using the GPS/INS data with simulated cycle slips. A new "ambiguity search" algorithm was proposed and initial testing was undertaken. It is based on the idea of finding the combination of the integer ambiguities that gives the minimal distance between the INS predicted and GPS determined positions. The development of a "ambiguity search" algorithm was necessary to solve the problem of differences between GPS and INS positions bigger than half a cycle but smaller than one cycle. The algorithm enabled full resolution of cycle slips for all the cases investigated which in general had good geometry.

In view of the results achieved, one can conclude, that the system may replace conventional techniques for a number of highway surveying problems at an accuracy level of 5 to 10 cm. The advantages are economic viability due to dramatically reduced time and a near-continuous data profile. The uniform output of the system is ideally suited for modern Geographic Information System and Digital Terrain Models. Moreover, the measurement procedure is safer than conventional techniques since it does not require physical presence of surveyors on the road. This is already a practical problem on highly frequented highways. The attitude output of the system cannot only be used for the determination of road parameters, but also for road inspection. Taking into account the high accuracy of roll and pitch, their abrupt changes could indicate frost heaves in the pavement. This

information could be used for planning the road maintenance schedule without the necessity of field inspections.

It is in the nature of scientific work, especially graduate research, that some questions are left open. In this case, the open problems concern both hardware implementation and modelling.

A real-time capability of the integrated GPS/INS would be major step in hardware development. It requires an efficient data link between GPS receivers operating in differential mode. It seems that present computer power is sufficient for processing data in real time and has enough space left for data logging operations. Additional study is necessary on the optimal choice of data to be transmitted.

Another attractive option is the use of P-code receivers, operating in differential mode and integrated with INS. The problem of longer bridging interval and ambiguity resolution would be easier to handle. By tracking both L1 and L2 frequencies, the wavelength of L1-L2 difference can be formed, which is about 86 cm. The predicted value of the ambiguity would have to be computed with the accuracy of about half of a cycle that is about 43 cm. This would mean that the present critical bridging interval would be significantly extended, or alternatively, lower quality inertial system could be used.

The incorporation of a simple sonar or laser device measuring the distance between the road surface and bottom of the truck could be another system modification of practical importance. It would enable the determination of relative inclination of the INS XY plane with respect to the road surface. This information would be used for correcting the slope determined by the system.

Currently, centering of the antenna over control points is tedious and cannot be done efficiently for production work. A general purpose road survey system would thus require the integration of a total station to have the capability to easily survey points not located on the highway. When designing such a system, a special calibration procedure for aligning the axes of the inertial system and the total station, should be developed.

Some additional tests are necessary to investigate the system performance for longer GPS differential baselines. The optimal occupying time for static initialization should also be examined both in simulations and practically in the field.

Other important recommendations concern problems that are outside of the author's expertise. In view of the future real-time capability of the system, interdisciplinary research effort should be put into the development of a Highway Mapping System. In such a hybrid system, GPS/INS would provide control information for digital imaging that would be done directly from the vehicle and analyzed in real time to produce a three dimensional digital terrain model. In fact it would be another step in the development of Automatic Vehicle Location and Navigation systems which use already existing digital maps for map matching.

Modelling work should be focused on the investigation and improvement of the accuracy of the INS prediction during GPS data gaps. Another form of Kalman filter, based on adaptive filtering, may be designed with additional state vector components.

Additional effort should be put into the investigation of ambiguity resolution for different cycle slip scenarios, especially if a further extension of the bridging interval is anticipated. The proposed "ambiguity search" algorithm is the first step to the solution of this problem. The INS will always provide redundant position information, which for short time intervals will usually be better than half a cycle. It can be the basis for employing some form of least-squares search for the best set of ambiguities that will give the best overall test statistics. Such algorithms have already been used in the static case and are presently being investigated for ambiguity resolution 'on the fly' using redundant satellite observations.

Another attractive option is to investigate the use of observations from emerging new satellite systems such as GLONASS and STARFIX. The redundant satellite observations, provided that they were of sufficient accuracy, would help to reduce masking problem with GPS. The integration of observations from these systems also opens new modelling problems that have not been investigated yet.

Certainly, these are some of the problems that will provide challenges in years to come.

References

Alberta Transportation (1983): " MHIS Operators Manual." Alberta Transportation, Edmonton, Alberta.

Bastos, L. and H. Landau (1988): "Fixing cycle slips in dual-frequency kinematic GPS-applications using Kalman filtering." *manuscripta geodaetica* , Vol 13, pp 249-256.

Baustert, G. , M.E. Cannon, E. Dorrer, G. Hein, H. Krauss, and K.P. Schwarz (1989): "A German - Canadian Experiment in Airborne INS-GPS Integration for Photogrammetric Applications." Proc. of the IAG Geodesy Symposia 102, Springler Verlag, New York.

Bierman, G. J. (1977): *"Factorization Methods for Discrete Sequential Estimation."* Academic Press, New York.

Beutler, G., I. Bauersima, W.Gurtner, M. Rothacher and T.Schildknecht (1987): "Evaluation of the Alaska Global Positioning System Campaign with the Bernese Software." *Journal of Gephysical Research*, Vol. 92, pp 1295-1303.

Bock, Y., S.A. Gourevitch, C.C. Counselman III, R.W. King and R.I. Abbot (1986): "Interferometric analysis of GPS phase observations." *manuscripta geodaetica* , Vol 11, pp 282-288.

Britting, K.R. (1971): *"Inertial Navigation Systems Analysis."* Wiley-Interscience, New York.

Camberlain, L. and B. Capit (1990): "ULISS G Fully Integrated, All-in-One and All-in-View Inertia/GPS Unit." Proc. of IEEE PLANS 90, Las Vegas, Nevada, March 20-23.

Cannon, M.E. (1987): "Kinematic Positioning Using GPS." MSc Thesis, Publ. # 20019, Dep. of Surveying Eng., The University of Calgary, Calgary.

Cannon, M. E. and K.P. Schwarz (1989): "GPS Semi-Kinematic Positioning Along a Well Controlled Traverse." Proc of Fifth International Geodetic Symposium on Satellite Positioning, Las Cruces, New Mexico, March 13-17.

Cannon M.E. (1990): "High Accuracy GPS Semi-Kinematic Positioning: Modelling and Results." *Navigation*, Vol 37, pp 53-64.

Cannon, M. E. and K.P. Schwarz (1990): "A Discussion of GPS/INS Integration for Airborne Photogrammetric Applications." KIS 90, Proc. of International Symposium on Kinematic Systems in Geodesy and Remote Sensing, Banff, Alberta, Sept. 10-13.

Carlson, N.A. (1988): "Federated Filter for Fault-Tolerant Integrated Navigation Systems." Proc. of IEEE PLANS 88, Las Vegas, Nevada, Nov. 29-Dec. 2.

Czompo J., D. Lapucha, Z. Liu, G. Lu, F. Sigouin-Allan and B. Townsend (1990): "Performance Analysis of Alternate Kalman Filter Algorithms." Unpublished seminar paper, Dep. of Surveying Eng., The University of Calgary, Calgary, April 25.

Davis, R.A., Foote F.S., Anderson J.A., Mikhail E.M.(1981): *"Surveying Theory and Practice."* Mc-Graw Hill, New York.

Forsberg R. (1990): "Experience with the ULISS-30 Inertial Survey System for Local Geodetic and Cadastral Network Control." KIS 90, Proc. of International Symposium on Kinematic Systems in Geodesy and Remote Sensing, Banff, Alberta, Sept. 10-13.

Frei, E. and G. Beutler (1989): "Some Considerations Concerning an Adaptive, Optimized Technique to Resolve the Initial Phase Ambiguities for Static and Kinematic GPS Surveying-Techniques." Proc. of Fifth International Geodetic Symposium on Satellite Positioning, Las Cruces, New Mexico, March 13-17.

Gelb, A. (ed.) (1974): *"Applied Optimal Estimation."* The M.I.T. Press, Cambridge, Massachusetts.

Giardina C.R, J. Heckathorn and D. Kransjanski (1981): "A Comparative Study of Strapdown Algorithms." *Navigation*, Vol 28, pp 101-106.

Goad, C.C. and L. Goodman (1974): "A modified Hopfield tropospheric refraction correction model." Presented at American Geophysical Union Annual Fall Meeting, San Francisco, California, Dec. 12-17.

Goad, C.C. (1985a): "Precise Relative Position Determination Using Global Positioning System Carrier Phase Measurements in a Non-Difference Mode." Proc. of First International Symposium on Precise Positioning with the GPS, Rockville, Maryland, April 15-19.

Goad, C.C. (1985b): "Precise Positioning with a Global Positioning System." Proc. Inertial Technology for Surveying and Geodesy. Publ. # 60005, Dep. of Surveying Eng., The University of Calgary, Calgary.

Goad, C.C. (1990a): "Determination of Precise Position on a Moving Vehicle with GPS." Proc. of IEEE PLANS 90, Las Vegas, Nevada, March 20-23.

Goad, C.C. (1990b): "Optimal Filtering of Psedoranges and Phases from Single Frequency GPS Receivers." *Navigation*, (in press).

Goldfarb, J. (1987): "An Aerotriangulation Using An INS-Differential-GPS." MSc Thesis, Publ. # 20022, Dep. of Surveying Eng., The University of Calgary, Calgary.

Hatch, R.(1982): "Synergism of GPS Code and Carrier Phase Measurements." Third International Geodetic Symposium on Satellite Doppler Positioning, Las Cruces, New Mexico, Feb. 16.

Hatch, R.(1990): "Instantaneous Ambiguity Resolution." KIS 90, Proc. of International Symposium on Kinematic Systems in Geodesy and Remote Sensing, Banff, Alberta, Sept. 10-13.

Hein, G.W., G.Baustert, B.Eissfeller, and H. Landau (1988): "High Precision Kinematic GPS Differential Positioning: Experiences, Results, Integration of GPS with a Ring Laser Strapdown Inertial System." Presented at the Int. ION GPS-88, Colorado Springs, Colorado, Sept. 19-23.

Heiskanen, W.A. and H. Moritz (1967): *"Physical Geodesy."* W.H. Freeman, San Francisco, London.

Hwang P. (1990): "Kinematic GPS: Resolving Integer Ambiguities on the Fly." Proc. of IEEE PLANS 90, Las Vegas, Nevada, March 20-23.

Knickmeyer, E.T. (1990): "Vector Gravimetry by Combination of Inertial and GPS Satellite Measurements." PhD Thesis, Dep. of Surveying Eng., University of Calgary, Calgary.

Lachapelle, G., W. Falkenberg, and M. Casey (1986): "Use of Phase Data for Accurate Differential GPS Kinematic Positioning." Proc. IEEE PLANS 86, Las Vegas, Nevada, Nov. 4-7.

Lachapelle, G., W. Falkenberg, J. Hagglund, D. Kinlyside, M. Casey, P. Kielland, M. Boudreau (1988): "Shipborne GPS Kinematic Positioning for Hydrographic Applications." *Navigation*, Vol 35, pp 73-88.

Lachapelle, G. and K.P. Schwarz(1989): "Kinematic Applications of GPS and GPS/INS Algorithms, Procedures, and Equipment Trends." Proc. of the IAG Geodesy Symposia 102, Springler Verlag, New York.

Lachapelle, G.(1990): "GPS Observables and Error Sources for Kinematic Positioning." KIS 90, Proc. of International Symposium on Kinematic Systems in Geodesy and Remote Sensing, Banff, Alberta, Sept. 10-13.

Lapucha D. (1990): "GPS/INS Trajectory Determination for Highway Surveying." KIS 90, Proc of International Symposium on Kinematic Systems in Geodesy and Remote Sensing, Banff, Alberta, Sept. 10-13.

Lapucha, D., K.P. Schwarz, M.E. Cannon, and H.E. Martell (1990): "The Use of INS/GPS in a Highway Survey System." Proc. of IEEE PLANS 90, Las Vegas, Nevada, March 20-23.

Lindlohr, W. and D. Wells (1985): "GPS Design Using Undifferenced Carrier Beat Phase Observations." *manuscripta geodaetica*, Vol 10, pp 255-295.

Loomis, P.V.W. (1989): "A Kinematic GPS Double-Differencing Algorithm." Proc. of Fifth International Geodetic Symposium on Satellite Positioning, Las Cruces, New Mexico, March 13-17.

Loomis, P.V.W. and G.J. Geier (1990): "Inertially Aided Lane Recapture after GPS Carrier Lock Loss." KIS 90, Proc. of International Symposium on Kinematic Systems in Geodesy and Remote Sensing, Banff, Alberta, Sept. 10-13.

Mader, G.(1986): "Dynamic Positioning Using GPS Carrier Phase Measurements." *manuscripta geodaetica*, Vol 11, pp 272-277.

Martell, H., M. Wei, K.P. Schwarz, W. Griffin and A. Peterson (1990): "Application of a Strapdown Inertial Surveyor for the Determination of Hoist Skip and Mine Shaft Trajectory." KIS 90, Proc. of International Symposium on Kinematic Systems in Geodesy and Remote Sensing, Banff, Alberta, Sept. 10-13.

Porter, T., E.H. Knickmeyer, and R.L. Wade (1990): "Pipeline Geometry Pigging-Application of Strapdown INS." Proc. of IEEE PLANS 90, Las Vegas, Nevada, March 20-23.

Remondi, B.W. (1984): "Using the Global Positioning System (GPS) Phase Observable for Relative Geodesy: Modelling, Processsing and Results." PhD dissertation, Center of Space Research, The University of Texas at Austin, Austin, Texas.

Remondi, B.W.(1985): "Performing Centimeter Accuracy Relative Surveys in Seconds Using GPS Carrier Phase." Proc. of First International Symposium on Precise Positioning with the GPS, Rockville, Maryland, April 15-19.

Remondi, B.W. (1988): "Kinematic and Pseudo-Kinematic GPS." Presented at the Int. ION GPS-88, Colorado Springs, Colorado, Sept. 19-23.

Savage, P.G. (1984): "Advances in Strapdown Sensors." *AGARD Lecture Series*, No. 133, Neuilly Sur Seine.

Schaffrin B. and E.W. Grafarend(1986): "Generating classes of equivalent linear models by nuisance parameter elimination-application to GPS observations." *manuscripta geodaetica* ,Vol 11, pp 262-271.

Schmidt, G.T. (1978): "Strapdown Inertial Systems - Theory and Applications." *AGARD Lecture Series* No. 95, Neuilly Sur Seine.

Schwarz, K.P. (1983): "Inertial Surveying and Geodesy." *Review of Geophysics and Space Physics*, Vol 21, pp 878-890.

Schwarz, K.P.(1987): "Geoid profiles from an integration of GPS satellite and inertial data." *Bolletino di geodesia e scienze affini*, Vol 46, pp 117-131.

Schwarz, K.P., M.E. Cannon, R.V.C. Wong (1989): "A Comparison of GPS Kinematic Models for the Determination of Position and Velocity Along a Trajectory." *manuscripta geodaetica*, Vol 14, pp 345-353.

Schwarz, K.P., E.H. Knickmeyer, and H. Martell (1990): "The Use of Strapdown Technology in Surveying." CISM Journal ACSGC Vol. 44, pp.29-37.

Tazartes, D.A. and J.G. Mark (1987): "Integration of GPS Receivers into Existing Inertial Navigation Systems." *Navigation*, Vol 35, pp 105-109.

Van Bronkhorst, A. (1978): "Strapdown System Algorithms." *AGARD Lecture Series* No. 95, Neuilly Sur Seine.

Vanicek, P. and E.J. Krakiwsky(1986): *"Geodesy -The Concepts."* North-Holland, Amsterdam.

Wei, M. and K.P. Schwarz (1990a): "Testing a Decentralized Filter for GPS/INS Integration." Proc. of IEEE PLANS 90, Las Vegas, Nevada, March 20-23.

Wei, M. and K.P. Schwarz (1990b): "A Strapdown Inertial Algorithm Using an Earth-Fixed Cartesian Frame." *Navigation*, Vol 37, pp153-167.

Wells,D.E., N. Beck, D. Delikaraoglou, A. Kleusberg, E.J. Krakiwsky, G. Lachapelle, R.B. Langley, M. Nakiboglu, K.P. Schwarz, J.M. Tranquilla, and P. Vanicek (1986): *"Guide to GPS Positioning"*. Canadian GPS Associates, Fredericton, New Brunswick.

Wong, R.V.C. (1982): "A Kalman Filter-Smoother for an Inertial Survey System of Local Level Type." MSc Thesis, Publ. # 20001, Dep. of Surveying Eng., The University of Calgary, Calgary.

Wong, R.V.C. (1988): "Development of a RLG Strapdown Inertial Survey System." PhD Thesis, Publ. # 20027, Dep. of Surveying Eng., The University of Calgary, Calgary.

Wong, R.V.C., K.P. Schwarz and M.E. Cannon: (1988) "High-Accuracy Kinematic Positioning by GPS-INS." *Navigation*, Vol 35, pp 275-287.